

**PROCESS OPTIMIZATION OF
A LIGNOCELLULOSIC MULTI-
PRODUCT BIOREFINERY**

Aristide Giuliano



UNIONE EUROPEA



*Ministero dell'Istruzione,
dell'Università e della Ricerca*



UNIVERSITÀ DEGLI
STUDI DI SALERNO

Department of Industrial Engineering

Ph.D. Course in Chemical Engineering

(XIV Cycle - New Series)

Thesis in Chemical Engineering

**PROCESS OPTIMIZATION OF A
LIGNOCELLULOSIC MULTI-PRODUCT
BIOREFINERY**

Supervisor

Prof. Diego Barletta

Ph.D. student

Aristide Giuliano

Scientific Referees

Prof. Massimo Poletto

Prof. Giancarlo Raiconi

Ph.D. Course Coordinator

Prof. Paolo Ciambelli

Articles on refereed journals:

- Giuliano, Poletto, Barletta; Process optimization of a multi-product biorefinery: the effect of biomass seasonality; Chemical Engineering Research and Design (2015) DOI: 10.1016/j.cherd.2015.12.011
- Giuliano, Cerulli, Poletto, Raiconi, Barletta; Flowsheet Optimization of a Multi-product Lignocellulosic Biorefinery. Part 1: MILP approach for a reference economic scenario (submitted to Industrial & Engineering Chemistry Research);
- Giuliano, Poletto, Barletta; Flowsheet Optimization of a Multi-product Lignocellulosic Biorefinery. Part 2: Effect of Reaction Yield and of Economic Parameters (submitted to Industrial & Engineering Chemistry Research);

Articles on book series:

- Giuliano, Cerulli, Poletto, Raiconi, Barletta; Optimization of a Multiproduct Lignocellulosic Biorefinery using a MILP Approximation; Computer Aided Chemical Engineering, 2014;
- Giuliano, Poletto, Barletta; Process Design of a multi-product Lignocellulosic Biorefinery; Computer Aided Chemical Engineering, 2015;

Summary

Articles on refereed journals:	III
Articles on book series:	III
Table captions.....	VI
Figure captions	IX
Abstract	XIV
1. Introduction.....	1
1.1 Biorefinery, Biofuels, Biochemicals	1
1.2 Process Synthesis methods	4
1.3 Process design and optimization of multi-product biorefineries	7
1.4 Biomass seasonality	9
2. Aim of the work	11
3. Superstructure.....	13
3.3 Hydrolysis and fermentation.....	18
3.3.1 Acid hydrolysis and levulinic acid production.....	18
3.3.2 Enzymatic hydrolysis.....	20
3.3.3 Hemicellulose dilute acid hydrolysis	21
3.3.4 Ethanol and succinic acid fermentations.....	22
3.4 Separation and purification.....	23
3.4.1 Levulinic acid purification	23
3.4.2 Ethanol purification	26
3.4.3 Succinic acid purification	28

3.5 Thermochemical conversion	29
3.6 Potential mass and heat integration of flowsheet	31
4. Mathematical modelling and optimization methodology	33
4.1 Mathematical modelling	33
4.2 Material balance constraints.....	34
4.3 Energy balance constraints.....	36
4.4 Heat integration	37
4.5 Reactor modelling	38
4.6 Equipment sizing.....	43
4.7 Capital costs	44
4.8 Total annual cost.....	45
4.9 Profitability	45
4.9 MILP solving method.....	46
4.10 Biomass seasonality.....	51
4.11 Biomass feedstocks.....	53
5. Results	55
5.1 Base case results	55
5.1.1 Process flowsheets, biomass allocation and product yield	55
5.1.2 Economic and profitability analysis.....	59
5.2 Base case results with reactor modelling	61
5.2.1 Base case: maximization of the NPV	62
5.2.2 Sensitivity analysis.....	64
5.2.2.1 Plant size.....	64

5.2.2.2 Products selling price.....	65
5.2.2.3 Discount rate.....	66
5.2.3 Maximization of the IRR	67
6 Results for biomass type and seasonality	73
6.1 Process flowsheets, biomass allocation and product yield	74
6.2 Economic and profitability analysis	84
7. Process synthesis of the biorefinery	89
7.1 1° iteration results	93
7.1 2° iteration results	95
7.2 3° iteration results	97
8. Conclusions	99
References	103
Abbreviations and symbols	114
ABBREVIATIONS.....	115
SYMBOLS	115
Appendix	118
Reactor modeling.....	119
Dilute acid hydrolysis with HCl (R1/R3) (Shen & Wyman 2012): ..	119
Dilute acid hydrolysis with H ₂ SO ₄ (R2/R4) (Girisuta et al. 2008): ..	120
Enzymatic hydrolysis (R5) (Kadam et al. 2004):.....	121
Acid hydrolysis of hemicellulose (R6) (Lee et al. 2000):	123
Ethanol fermentation (R8) (Leksawasdi et al. 2001):	124
Succinic acid fermentation (R9) (Song et al. 2008a):	128

Table captions

Table 3-1: *Pretreatment parameters for the optimization model.*

Table 3-2: *Equipment description of hydrolysis and fermentation section.*

Table 3-3: *Equipment description of separation and purification section.*

Table 3-4: *Product yields for the purification sections.*

Table 3-5: *Equipment description of thermochemical conversion section.*

Table 4-1: *Product yields for the reactors at fixed yields.*

Table 4-2: *Product yields for the reactors.*

Table 5-1: *Main parameters for the optimization model.*

Table 5-2: *Sensitivity results of the economic analysis on plant size and biochemicals selling price by maximizing the net present value*

Table 6-1: *Biomass price and composition (from Silvia-Fernandes et al, 2015a).*

Table 7-1: *Reactors yields used for RSTOIC block in Aspen Plus.*

Figure captions

Figure 1-1: *Representative diagrammatic framework of lignocellulosic biomass.*

Figure 3-1: *Superstructure of the multi-product lignocellulosic biorefinery (the dashed lines are exclusive).*

Figure 3-2: *Flowsheet for the pretreatment section.*

Figure 3-3: *Flowsheet for the hydrolysis and fermentation section.*

Figure 3-4: *Superstructure of enzyme production section (the dashed lines are exclusive).*

Figure 3-5: *Flowsheet for the separation and purification section of levulinic acid.*

Figure 3-6: *Flowsheet for the separation and purification section of ethanol.*

Figure 3-7: *Flowsheet for the separation and purification section of succinic acid.*

Figure 3-8: *Flowsheet for the thermochemical conversion of lignin.*

Figure 5-1: *Optimal process flowsheet of the biorefinery.*

Figure 5-2: *Biomass allocation for the lignocellulosic multi-product biorefinery.*

Figure 5-3: *Product yields for the lignocellulosic multi-product biorefinery. Black: levulinic acid yield; Mesh grey: ethanol yield; Striped grey: succinic acid yield; Grey: total yield.*

Figure 5-4: *Manufacturing cost distribution for the lignocellulosic biorefinery.*

Figure 5-5: *Capital cost distribution for the lignocellulosic biorefinery.*

Figure 5-6: *Optimal NPV flowsheets of biorefinery for base case and variants: a) base case; b) biomass feed rate 5 t/h (0.1 times the base case); c) levulinic acid selling price 7.50 \$/kg (+50% of the base case).*

Figure 5-7: *Objective function (net present value) and internal rate of return for each value of the discount rate. Net present value (●); internal rate of return (■).*

Figure 5-8: Biomass allocation (a) and product yields (b) for the base case by maximizing the net present value and the internal rate of return. Black: levulinic acid; dark grey: ethanol; light grey: succinic acid.

Figure 5-9: Capital cost for the lignocellulosic biorefinery by maximizing the net present value and the internal rate of return. Black: pretreatment section; dark grey: hydrolysis and fermentation section; light grey: separation and purification section; striped grey: thermochemical conversion section.

Figure 5-10: Cost distribution for the lignocellulosic biorefinery by maximizing the net present value and the internal rate of return. Black: raw material cost; dark grey: enzymes and reactants cost; light grey: utility cost; striped grey: other manufacturing cost.

Figure 5-11: Net present value for the lignocellulosic biorefinery by maximizing the net present value and the internal rate of return.

Figure 6-1: Optimal flowsheet using net present value as objective function. a) for eucalyptus; b) for wheat straw; c) for olive pruning.

Figure 6-2: Optimal flowsheet for the season-based biorefinery using net present value as objective function. a) case SB: three periods with a single biomass feedstock each; b) case SC: 1st period with eucalyptus, 2nd period with eucalyptus and wheat straw, 3rd period with eucalyptus and olive pruning.

Figure 6-3: Optimal flowsheet using internal rate of return as objective function. a) for eucalyptus; b) for olive pruning.

Figure 6-4: Biomass allocation (kg of biomass used to obtain a product / kg of biomass feed) using net present value as objective function. Black: biomass to levulinic acid; Grey: biomass to ethanol; Striped: biomass to succinic acid.

Figure 6-5: Product yields using the net present value as objective function. Black: levulinic acid yield; Grey: ethanol yield; Striped: succinic acid yield.

Figure 6-6: Product yields using the net present value as objective function for the case with a single biomass feedstock. Black: levulinic acid yield; Grey: ethanol yield; Striped: succinic acid yield.

Figure 6-7: Product yields using the net present value as objective function for 1st period with eucalyptus, 2nd period with eucalyptus and wheat straw, 3rd period with eucalyptus and olive pruning. Black: levulinic acid yield; Grey: ethanol yield; Striped: succinic acid yield.

Figure 6-8: Biomass allocation (kg of biomass used to obtain a product / kg of biomass feed) using the internal rate of return as objective function. Black: biomass to levulinic acid; Grey: biomass to ethanol; Striped: biomass to succinic acid.

Figure 6-9: Product yields using the internal rate of return as objective function. Black: levulinic acid yield; Grey: ethanol yield; Striped: succinic acid yield.

Figure 6-10: Product yields using the internal rate of return as objective function for the case with a single biomass feedstock. Black: levulinic acid yield; Grey: ethanol yield; Striped: succinic acid yield.

Figure 6-11: Product yields using the internal rate of return as objective function for 1st period with eucalyptus, 2nd period with eucalyptus and wheat straw, 3rd period with eucalyptus and olive pruning. Black: levulinic acid yield; Grey: ethanol yield; Striped: succinic acid yield.

Figure 6-12: Total investment cost using as objective function: net present value (black bar), internal rate of return (grey bar).

Figure 6-13: Total annual cost distribution using the net present value as objective function.

Figure 6-14: Net present value using as objective function: net present value (black bar), internal rate of return (grey bar).

Figure 6-15: Internal rate of return using as objective function: net present value (black bar), internal rate of return (grey bar).

Figure 7-1: Process optimization algorithm to obtain the optimal process design.

Figure 7-2: Optimal flowsheet for the base case of the multi-product biorefinery.

Figure 7-3: Product yields for the MILP model (dark bar) and for process simulation (light bar).

Figure 7-4: NPV obtained with the MILP model (dark bar) and with process simulation (light bar).

Figure 7-5: Biomass allocation for all iterations.

Figure 7-6: Optimal flowsheet for the second iteration by ampl.

Figure 7-7: Product yields for the MILP model (dark bar) and for process simulation (light bar) for the second iteration.

Figure 7-8: NPV obtained with the MILP model (dark bar) and with process simulation (light bar) for the second iteration.

Figure 7-9: Optimal flowsheet for the final process optimization.

Figure A-1: Product yields as a function of residence time in PF reactors operating: a) a dilute acid hydrolysis with HCl; b) a dilute acid hydrolysis with H₂SO₄; c) levulinic acid production with HCl; d) a levulinic acid production with H₂SO₄. Product legend: — — —, glucose; — — —, HMF; — — —, levulinic acid; •••••, xylose; - - - -, furfural; —••—, formic acid.

Figure A-2: Product yields in an enzymatic hydrolysis CST reactor. Product legend: — — —, glucose; — — —, xylose; - - - -.

Figure A-3: Product yields in a batch fermenter for ethanol production. Product legend: — — —, ethanol from glucose; —••—, ethanol from xylose; — — —, CO₂ from glucose; •••••, CO₂ from xylose.

Figure A-4: Product yields in a batch fermenter for succinic acid production. Product legend: — — —, succinic acid from glucose; — — —, succinic acid from xylose; — — —, acetic acid; •••••, lactic acid, —••—, formic acid.

Abstract

A methodology to reduce the complexity of the process optimization was applied to multiproduct biorefinery fed by lignocellulosic biomass. A process superstructure was built to consider alternative process pathways to levulinic acid, succinic acid and ethanol. A Mixed Integer Non-Linear Problem was obtained and transformed in a Mixed Integer Linear Problem by means of a discretization procedure of the non-linear variables. Rigorous design methods accounting for complete kinetics schemes for hydrolysis and fermentation reactors for the production of levulinic acid, succinic acid and ethanol were included in a biorefinery superstructure optimization. A discretization method was applied to obtain a MILP approximation of the resulting MINLP master problem. The optimal flowsheet of a biorefinery with hardwood feedstock, obtained by maximizing the Net Present Value, yields comparable biomass allocation to levulinic acid and succinic acid (more than 40% each) and the its balance to ethanol. A sensitivity analysis highlighted that the optimal flowsheet and the relevant technical and economic performances are significantly dependent on the economic scenario (chemical products selling price, discount rate) and on the plant scale. Finally, process optimization achieved by maximizing two different economic objective functions, Net Present Value and Internal Rate of Return, provided different optimal flowsheets and biomass allocation to chemical products. The effect of the change of the biomass type and composition on the plant was also considered. Results highlight that the composition of the biomass feedstock in terms of cellulose, hemicellulose and lignin has a significant effect on the biomass allocation to the three product production processes and on the relevant optimal flowsheet. Case studies with a combined use of different seasonal biomass types during the year were also studied to provide a methodology to find the optimal biorefinery flowsheet in real scenarios. In the season based scenario studied, product yield distribution and overall productivity of the plant varies during the different periods provided a constant biomass feed rate.

1.Introduction

1.1 Biorefinery, Biofuels, Biochemicals

The strong dependence of modern society on fossil fuels comes from the intensive use and consumption of petroleum derivatives which, combined with diminishing petroleum resources, causes environmental and political concerns. There is clear scientific evidence that emissions of greenhouse gases (carbon dioxide, methane and nitrous oxide), arising from fossil fuel combustion and land-use change as a result of human activities, are perturbing the Earth's climate (Solomon et al. 2007).

Concerning chemicals, their dependence on fossil resources is even stronger. The majority of chemical products are produced from oil refinery and almost 4% of oil is worldwide used for chemical and plastic production. In order to simultaneously reduce the dependence on oil and mitigate climate change in transport and chemical sectors, alternative production chains are necessary. It is increasingly recognized that there is not a single solution to these problems and that combined actions are needed, including changes in behavior, changes in vehicle technologies, expansion of public transport and introduction of innovative fuels and technologies. Recently, society began to recognize the opportunities offered by a future sustainable economy based on renewable sources and has been starting to finance R&D activities for its implementation. It is increasingly acknowledged globally that plant-based raw materials (i.e. biomass) have the potential to replace a large fraction of fossil resources as feedstocks for industrial productions, addressing both the energy and non-energy (i.e. chemicals and materials) sectors. At national, regional and global levels there are three main drivers for using biomass in

Chapter 1

biorefinery for production of bioenergy, biofuels and biochemicals (Cherubini & Strömman 2010).

Electricity and heat can be provided by a variety of renewable alternatives (wind, sun, water, biomass and so on), while biomass is very likely to be the only viable alternative to fossil resources for production of transportation fuels and chemicals, since it is the only C-rich material source available on the Earth, besides fossils. As a consequence, the sustainable biomass production is a crucial issue, especially concerning a possible fertile land competition with food and feed industries.

A biorefinery is a facility or network of facilities that integrates biomass conversion processes and equipment to produce transportation biofuels, power, and chemicals from biomass. This concept bears significant analogies with that of an oil refinery in which multiple fuels and other products are derived from oil. The progressive replacement of oil with biomass is a necessary breakthrough change to build a future biobased economy (Kamm et al. 2007) in which fossil carbon is replaced by renewable carbon in the role of both raw material and energy source. Second generation biorefineries using lignocellulosic biomass are among the most promising options, since they have many advantages from the energy and environmental standpoint (FitzPatrick et al. 2010)(Balat & Ayar 2005)(Menon & Rao 2012).

Lignocellulosics' are the most abundant source of unutilized biomass and their availability does not necessarily impact land use. Biomass in general consists of 40-50% cellulose, 25-30% hemicellulose and 15-20% lignin and other extractable components (Knauf & Moniruzzaman 2004). The effective utilization of all the three components would play a significant role in economic viability of the cellulose to biofuels/biochemicals process. In nature except in cotton bolls, cellulose fibres are embedded in a matrix of other structural biopolymers, primarily hemicellulose and lignin. Cellulose is a linear syndiotactic polymer of glucose linked together by β -(1/4)-glycosidic bonds whereas hemicellulose is a branched heteropolymer of D-xylose, L-arabinose, D-mannose, D-glucose, D-galactose and D-glucuronic acid. Lignin is composed of three major phenolic components, namely p-coumaryl alcohol, coniferyl alcohol and sinapyl alcohol. Lignin is a complex hydrophobic, cross-linked aromatic polymer that interferes with the hydrolysis process (Menon & Rao 2012). A representative diagrammatic framework of lignocellulosic biomass is illustrated in Fig. 1-1.

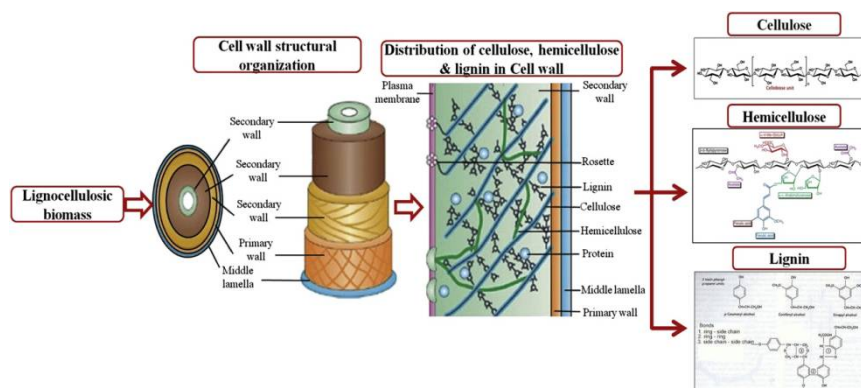


Figure 2-1: Representative diagrammatic framework of lignocellulosic biomass.

The high molecular weight and ordered tertiary structure make natural cellulose insoluble in water. Cellulose with low degree of polymerization will be more susceptible to cellulolytic enzymes. The isolation and derivatization/dissolution of cellulose are crucial steps in determining cellulose (Hallac & Ragauskas 2011). In general plant cell walls are subdivided as primary and secondary walls. The distribution of cellulose, hemicellulose and lignin varies considerably among these layers. The major impediments towards development of an economically viable technology for biodegradation of cellulose are the association with lignin and hemicellulose, crystallinity, degree of polymerization and surface area. During the biocatalytic valorization of lignocellulosic substrate, a residual fraction survives the attack. This fraction absorbs a significant amount of the original enzyme and restricts the use of these enzymes on added, fresh substrate (Arantes & Saddler 2011). Most potential cellulosic substrates for bioconversion are heavily lignified. Thus, most of the cellulose in nature is unsuitable for bioconversion unless effective and economically viable procedures (pretreatments) are developed to remove or modify lignin. The development and implementation of biorefinery processes is of utmost importance to meet the vision towards a sustainable economy based on bio-resources.

Efficient conversion of lignocellulosic materials to ethanol and value added biochemicals are still today a challenging proposition. In 2004, the National Renewable Energy Laboratory listed the 12 chemical compounds more easily obtainable from lignocellulosic biomass by industrial processes (T. Werpy. & G. Petersen. 2004). They are value-added chemicals or precursors of other chemicals in common use. However, the commercialization of conversion technologies has been hindered by several factors including unavailability of reliable feedstock supply systems, and

Chapter 1

non optimized conversion systems. For the latter issue, the optimization by process synthesis and integration can help to identify the most promising pathways and to increase the profitability of bio-based fuels and production of chemicals.

1.2 Process Synthesis methods

Rudd et al. (Rudd et al. 1973) proposed the term “synthesis”, over the past several decades, process synthesis has had a significant impact on the development, design and operation of (petro) chemical processes. Process synthesis can be considered as the cornerstone of the process design activity (Westerberg 2004), it provides a systematic way to identify the types of equipment, flowrates, operating/design conditions and optimal interconnections among different units that create the best total flowsheet. Traditionally, the synthesis problem can be described as follows: given a set of feedstocks and a set of desired final products with specifications, it is desirable to develop a systematic methodology with various objectives such as the highest yield, the highest energy efficiency or the most sustainable route for the generation of optimal configurations for transforming the raw materials to desired products.

Significant achievements have been made since the 1970s in the area of process synthesis for chemical processes, and, numerous synthesis frameworks, strategies and tools have been proposed (Westerberg 2004). Among the current process synthesis approaches that aims to be cost effective and energy efficient, three types of approaches can be found: heuristics based approaches that use specific process knowledge and experience, physical insights based approaches; superstructure optimization based approaches where mixed integer (non)linear programming are formulated and solved; and, hybrid approaches that combine aspects of the first two approaches in a hybrid scheme. The hierarchical decomposition based approach of Douglas (M. Douglas J. 1988) and pinch technology of Linnhoff (Linnhoff 1993) are examples of heuristics and physical insights based approaches.

At the base of the optimization process is the development of a superstructure of design alternatives, whether at a high level of abstraction or at a relatively detailed level of the units, the synthesis problem can be formulated in general terms as the mixed-integer optimization model:

$$\begin{cases} \min Z = C(x, y) \\ h(x) = 0 \\ g(x, y) \leq 0 \\ x \in X, y \in \{0,1\} \end{cases} \quad (1-1)$$

In which x is the vector of continuous variables representing flows, pressures, temperatures, while y is the vector of 0-1 variables to denote the potential existence of units. The equations $h(x) = 0$ are generally nonlinear and correspond material and heat balances, while the inequalities $g(x,y) \leq 0$, represent specifications or physical limits. As we have seen in the previous chapters it should be noted that for most of the applications in process synthesis, problem (MIP) has the special structure that the 0–1 variables appear linearly in the objective function and constraints. The reason for this is that in the objective 0–1 variables are commonly used to represent fixed charges, that is:

$$C(x, y) = c^T y + f(x) \quad (1-2)$$

While in the constraints they are used to represent logical conditions which normally can be expressed in linear form, that is:

$$g(x, y) = Cx + By - d \leq 0 \quad (1-3)$$

It is often not advisable to solve directly the nonlinear problem (MIP) for the case of a process flowsheet, but instead use a decomposition strategy. The other option is to avoid solving the MINLP by approximating this problem as an MILP through discretization.

In the case that nonlinearities are explicitly accounted for in problem (MIP), aside from the potentially large size of the MINLP model for the superstructure optimization of a process flowsheet, there are two other potential difficulties. The first is that when fixing the 0–1 variables for defining the corresponding NLP subproblem in a direct solution of the MINLP, one has to carry many redundant variables and equations that unnecessarily increase the dimensionality and complexity of this subproblem. The reason is that when some of the process units are not selected, the corresponding flow are fixed to zero, but yet the mass and heat balances of the “dry units” have to be converged. This usually introduces singularities that cause great difficulty in the convergence of the NLP. The second difficulty that arises from a direct solution of the MINLP is because

Chapter 1

the effects of nonconvexities are accentuated when flows take a value of zero (again effect of “dry units”). This may cause the NLP subproblem to converge to suboptimal solution or the master problem to “cut off” the optimal 0–1 combination. It is precisely these two difficulties that motivate the modelling/decomposition strategy described by Kocis and Grossmann (Kocis & Grossmann 1989).

Another optimization method is MILP approximation. In order to derive an MILP approximation to problem (MIP), we will partition the continuous variables x as follows:

$$x = \begin{bmatrix} z^d \\ x^c \end{bmatrix} \quad (1-4)$$

In which z^d is the vector of operating conditions that gives rise to the nonlinearities (e.g., pressures, temperatures, split fraction, conversions, etc.), and x^c is a vector of material, heat, and power flow variables that appear linearly. In this way, given a fixed value of z^d , the nonlinear equations reduce to a subset of linear equations, that is:

$$h(x) = 0 \Rightarrow Ex^c = e \quad (1-5)$$

In which the matrix of coefficients E and the right hand sides e are a function of z^d : $E(z^d)$, $e(z^d)$.

Since in general we would like to consider more than one fixed value for the variables z^d , we will require the introduction of the additional 0–1 variables y^d to represent the potential selection of the discrete operating conditions. In this way, the general form of the MILP approximation will be as follows:

$$\begin{cases} \min C = a_1^T y + a_2^T y^d + b^T \\ E_1 y^d + E_2 x^c = e \\ D_1 y + D_2 y^d + D_3 x^c \leq 0 \\ y, y^d = 0,1, x^c \geq 0 \end{cases} \quad (1-6)$$

While we have been able to eliminate the nonlinearities, it is clear that we have increased the number of discrete and continuous variables as well as the number of constraints. Also, in the general case the definition of the

matrix requires an prior evaluation or simulation of nonlinear models (Biegler L.T., Grossmann I.E. 1997).

MINLP solution algorithms based on generalized Bender decomposition (Floudas 1995), outer approximation (Duran & Grossmann 1986), extended cutting-plane methods (Westerlund et al. 1998) and branch-and-bound (Gupta, Omprakash K., Ravindran 1985) have been developed and improved over the last decades, and implemented in generic multi-purpose solvers (e.g. MINOS, DICOPT, BARON) integrated with commercial optimization software packages such as GAMS and AMPL (Trespalcios & Grossmann 2014). Several authors applied different methods for MINLP process optimization of biorefineries like disjunctive programming (Ponce-Ortega et al. 2012), DICOPT program (Zondervan et al. 2011), LINGO program (Gabriel & El-Halwagi 2013a).

In some cases optimization methods include iterative methods, interfacing the optimization software with technical computing software (e.g. MATLAB) (Geraili et al. 2014) and process simulation software (e.g. Aspen Plus) (Gabriel & El-Halwagi 2013a). In all these cases the authors identified the best process pathways among the available alternatives or the best end products to maximize a techno-economic objective function.

However, the large number of integer variables necessary for large superstructures and the need to have a reasonable computational time can make the MINLP extremely challenging, even for state-of-the-art optimization software (Bischi et al. 2014). Furthermore, the risk with most of the MINLP solvers is to find a local optimum instead of the global optimum, if the problem is non-convex. As a result, several approaches have been proposed to convert a MINLP into an approximated Mixed Integer Linear Problem (MILP). Such problem linearization is considerably advantageous because MILP convergence solution is guaranteed by extremely fast and effective commercially available MILP solvers (e.g., CPLEX, Gurobi, Xpress).

1.3 Process design and optimization of multi-product biorefineries

In general, the process systems design of biorefineries can be stated as follows: provided the aim of minimum costs and sustainable development (Poliakoff & Licence 2007), a systematic methodology is applied for the choice of optimal reaction routes and corresponding optimal flowsheet consisting of all the unit operations and the relevant design and operating conditions that are able to achieve a set of desired value-added products and

Chapter 1

fuels with specified flowrate, temperature and purity from a set of biomass derived feedstock with specified composition.

Several studies reported in the literature aimed at improving the process pathways to obtain more than a single product. Tippkötter et al. (Tippkötter et al. 2014) studied enzymatic hydrolysis of beech wood lignocellulose at high solid contents and its utilization as substrate for the production of biobutanol and dicarboxylic acids. Bioethanol and beta-lactam production was considered in the process design of Kim et al. (2014) (Kim et al. 2014). In this case SuperPro Designer was used to obtain the evaluation of the several process pathways.

The majority of existing biorefinery processes deal with the production of biofuels and bioethanol based on thermochemical and biochemical technologies. However, only few studies reported in the literature addressed the optimization of the biomass distribution among alternative pathways of a biorefinery co-producing alcohols (ethanol or butanol), high-value chemicals (succinic acid) and electricity (Zondervan et al. 2011), chemicals, like acetic acid (Luo et al. 2010) i-butene (Martín & Grossmann 2014) and 3-butadiene (Cheali et al. 2015). Significant improvements in the techno-economic feasibility can be also obtained by thermal conversion of the biomass components that cannot be easily converted by chemical or enzymatic processes (Cheali et al. 2014). Luo et al. (Luo et al. 2010) identified the best design of a multi-product lignocellulosic biorefinery producing ethanol, succinic acid, acetic acid and electricity.

Zhou et al. (Zhou et al. 2012) proposed a MILP model in which performance curves of process unit as a function of a single degree of freedom (an internal combustion engine, a boiler and an absorption chiller) were approximated with piecewise linear functions. The model is used to optimize the design of the cogeneration system while taking into account its lifetime operation and the investment cost. The total annual cost is then compared with that corresponding to a solution found by a simpler MILP model using linear performance curves. Problem linearization can be obtained also by variable discretization methods (Kalitventzeff 1991). In particular, for each non linear process variable, a vector of possible values of the variable was considered. The original variable was set equal to the sum of the product of each of these values and a binary variable. In the problem solution only one of these binary variables was allowed to be equal to 1. Mathematical programming was used by Scott et al. (Scott et al. 2013) in order to select alternative processes for bioethanol production from hardwood. Problem formulation led to a MINLP which was tackled by specific software. Moreover, a MILP formulation was also computed by

using a relaxation technique. Equations needed to relax the bi-linear product involve the introduction of new continuous variables.

Given a superstructure model developed to optimise the production process for levulinic acid, succinic acid and ethanol from biomass material, in this paper rigorous design methods accounting for complete kinetic schemes for the more accurate sizing of hydrolysis and fermentation reactors is considered. A discretization method is applied to use the results of the reactor design in the overall flowsheet optimization of the multiproduct biorefinery and to obtain a MILP approximation of a Mixed Integer Non Linear Programming master problem. These modifications on the superstructure optimization procedure allow a more reliable trade-off estimation between direct and investment cost. The resulting procedure can, therefore, be used to analyse the effects on the profitability of changes in the economic scenario due to long term uncertainty. For example, changes in the discount rate do play a significant role on the determination of Net Present Value by changing the significance of the investment cost. But also revenues and direct costs as subject to indeterminacy. In fact, the market of the top added value biochemicals is expected to rise. In particular, in the considered case of a biorefinery, the market price of succinic acid (Luo et al. 2010) and levulinic acid (Rackemann & Doherty 2011) price can have a significant influence on the economic feasibility of some of the innovative process routes considered and on their market growth potential. In order to address these issues, in this work a sensitivity analysis of some of the parameters of the economic scenario for the biochemical production is carried out.

1.4 Biomass seasonality

Furthermore, a significant replacement of fossil fuel refineries production with products from renewable feedstock biorefineries would require large amounts of lignocellulosic biomass. Therefore, the limited biomass availability and the challenging efficiency of the supply chain can be considered as one of the major barrier hindering the global development of biorefinery based processes (Balat 2011). In fact, the seasonal nature and the annual variability of the biomass supply may disfavour the use of several types of feedstocks due to logistic problems and economic unsustainability. More precisely, the discrete biomass supply due to its seasonality causes a challenging and costly management of the biomass storage in order to ensure a continuous supply for biorefineries (Yue et al. 2014). Moreover, the volatility of biomass cost and the dependence upon specific suppliers are factors threatening the economic stability of a biorefinery (Gnansounou & Dauriat 2010). The use of different biomass types over the year may overcome some of these constraints. On the other hand, different processing

Chapter 1

requirements of diverse biomass feedstocks may limit the biorefinery operational feasibility (Huang et al. 2009)(González-García et al. 2010). An enhanced flexibility of a biorefinery in terms of its ability to use multiple feedstocks can only be obtained by pursuing this objective since the initial stages of process design. Systematic process synthesis, linking process design methods and rigorous mixed integer programming, provides with powerful tools to attack this process optimization problem (Quaglia et al. 2012).

Recent studies revealed that in some regions (e.g. the United States) ethanol market is already saturated (Peplow 2014). Instead, promising opportunities are arising from the production of diverse bio-based chemicals and polymers (de Jong et al. 2012). In particular, a list of potential high added value chemicals that can be obtained from carbohydrates coming with biomass feedstock was reported to guide further scientific and technological efforts (T. Werpy. & G. Petersen. 2004)(FitzPatrick et al. 2010)(Bozell & Petersen 2010)(Menon & Rao 2012)(Sammons et al. 2008). As a result, a realistic scenario for sustainable biorefinery processes supplied with different seasonal lignocellulosic biomass types should include the production of added value biochemicals beside ethanol (Kokossis et al. 2015). In fact, papers in the literature addressed the optimization of the biomass feed partitioning among alternative pathways of a biorefinery co-producing alcohols, like ethanol or butanol (Zondervan et al. 2011), high-value chemicals, such as succinic acid (Giuliano et al. 2014), chemicals, like acetic acid (Luo et al. 2010), i-butene (Martín & Grossmann 2014) and 3-butadiene (Cheali et al. 2015). However, studies on process optimization of multiproduct biorefineries with seasonal multiple feedstocks are not available.

2. Aim of the work

The present work addresses the process flowsheet optimization of a multiproduct lignocellulosic biomass refinery by aiming at economic objective functions by means of mathematical programming methods. In particular, the co-production from a hardwood biomass feedstock of two of the top value added chemicals, levulinic acid and succinic acid (T. Werpy. & G. Petersen. 2004), as well as of ethanol is studied.

Given a superstructure model developed to optimise the production process for levulinic acid, succinic acid and ethanol from biomass material, in this paper rigorous design methods accounting for complete kinetic schemes for the more accurate sizing of hydrolysis and fermentation reactors is considered. A discretization method is applied to use the results of the reactor design in the overall flowsheet optimization of the multiproduct biorefinery and to obtain a MILP approximation of a Mixed Integer Non Linear Programming master problem. These modifications on the superstructure optimization procedure allow a more reliable trade-off estimation between direct and investment cost. The resulting procedure can, therefore, be used to analyse the effects on the profitability of changes in the economic scenario due to long term uncertainty. For example, changes in the discount rate do play a significant role on the determination of Net Present Value by changing the significance of the investment cost. But also revenues and direct costs are subject to indeterminacy. In fact, the market of the top added value biochemicals is expected to rise. In particular, in the considered case of a biorefinery, the market price of succinic acid (Luo et al. 2010) and levulinic acid (Rackemann & Doherty 2011) price can have a significant influence on the economic feasibility of some of the innovative process routes considered and on their market growth potential. In order to address

Chapter 2

these issues, in this work a sensitivity analysis of some of the parameters of the economic scenario for the biochemical production is carried out.

In the first part, the complex superstructure, as composed by alternative process routes to the three chemicals, is described in detail. Moreover, the corresponding mathematical model including shortcut methods for the process unit design is reported. The results for a base case economic scenario obtained by the solution of a Mixed Integer Linear Programming problem are discussed. In the second part of the paper, the model is enriched by rigorous design methods accounting for complete kinetic schemes for the more accurate sizing of hydrolysis and fermentation reactors. A discretization method is applied to use the results of the reactor design in the overall flowsheet optimization and to obtain a MILP approximation of a Mixed Integer Non Linear Programming master problem. Finally, a sensitivity analysis on the economic objective function and on the economic scenario is also addressed.

Two alternative economic objective functions (net present value and internal rate of return) were considered. The optimization analysis aimed at finding the optimal flowsheet, biomass allocation and product yield in several case studies involving a single feedstock and multiple feedstock biorefinery process.

However, studies on process optimization of multiproduct biorefineries with seasonal multiple feedstocks are not available.

The last part of the work aims at filling this gap. In particular, eucalyptus residues (EU), wheat straw (WS) and olive tree pruning (OP) were chosen as representative feedstock from Southern Europe (Silva-Fernandes, Duarte, Carvalheiro, Loureiro-Dias, et al. 2015). The seasonality of these biomass materials is partially complementary. In fact, EU is available throughout the year, WS is harvested in late spring/early summer, and OP is mainly available in winter and early spring. The storage costs of all these biomass materials are not expected to be significant since they have low moisture content. These features make these biomass materials good candidates for a multi-feedstock biorefinery under continuous operation throughout the year.

3. Superstructure

3.1 Superstructure

The most promising alternative processes at the industrial scale were selected and included in a complex process flowsheet to build the so-called superstructure of a biorefinery for the co-production of succinic acid, levulinic acid and ethanol. This work was based on a thorough survey of the literature concerning the available process pathways to obtain succinic acid, levulinic acid and ethanol. The biorefinery superstructure, built for this study consists of four sections (Figure 3-1):

- Pretreatment;
- Hydrolysis and fermentation;
- Separation and purification;
- Thermo-chemical conversion.

Each section is formed by alternative process pathways, each including several process stages operated in specific units. The main stages of the process are described in the following. Additional data concerning the process technology and main operating conditions assumed for the modelling of each stage are summarized in Tables 3-1, 3-4.

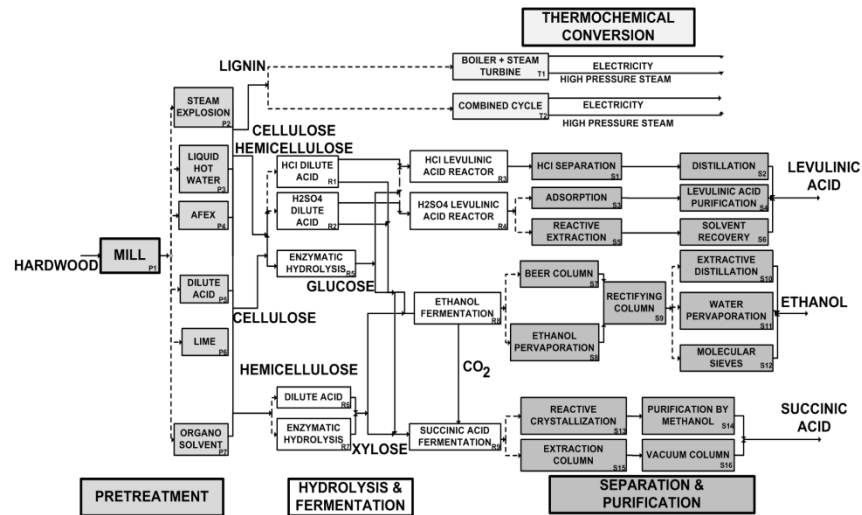


Figure 3-1: Superstructure of the multi-product lignocellulosic biorefinery (the dashed lines are exclusive).

3.2 Pretreatment

Biomass pretreatment generally consists of physical, chemical or thermochemical breakdown operation of the biomass to obtain the three main organic components of the lignocellulosic biomass: cellulose, hemicellulose and lignin. These components can be separated on the basis of their different solubility. Hemicellulose has the highest solubility, so it is the easiest to be separated (Huang et al. 2010). Using further treatments also cellulose and lignin can be separated (Zimbardi et al. 2002). Another option includes the possibility to send also the lignin to the reaction/fermentation section and then to obtain a lignin cake from the product purification section (Humbird & Aden 2009).

The first physical treatment considered in the superstructure was the preliminary size reduction process (mill P1). This is a common step independent of the subsequent pretreatment operation and its performances were fixed. Energy requirements were calculated as a function of the biomass flowrate and of the initial and final mean particle size according to Mani et al. (Mani et al. 2004).

The alternative pretreatment routes considered in this study were:

- Steam explosion (SE);
- Liquid hot water (LHW);

- Ammonia fiber explosion (AFEX);
- Dilute acid (DA);
- Lime;
- Organosolvent (OS);

Each route requires different operating conditions and heat duty for an effective pretreatment (Eggeman & Elander 2005).

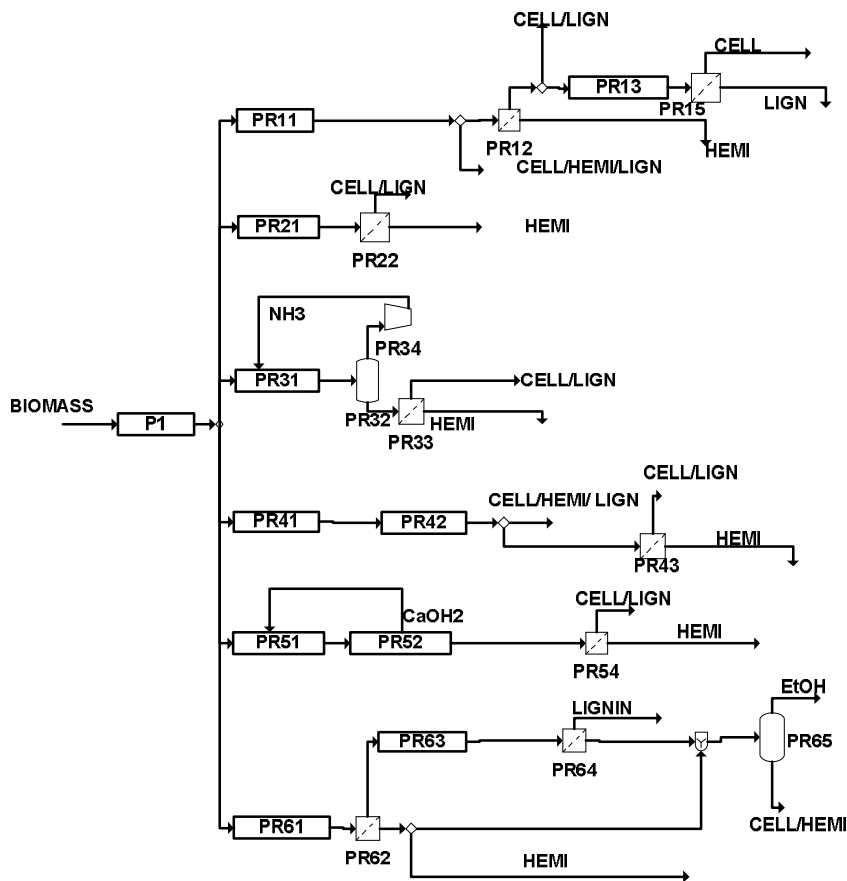


Figure 3-2: Flowsheet for the pretreatment section.

The steam explosion route (P2) was modelled assuming a steam explosion unit using medium pressure steam at 220°C with a residence time of 3 min (Zimbardi et al. 2002). After the steam explosion unit the superstructure includes a sequence of possible units to separate in a first step hemicellulose from lignin and cellulose and in a second step lignin from

Chapter 3

cellulose. As a result, the block corresponding to the steam explosion route can provide three alternative sets of outlet streams: 1) solubilised hemicellulose, solid cellulose and lignin stream; 2) solubilised hemicellulose stream and solid cellulose and lignin stream; 3) solubilised hemicellulose stream, solid cellulose stream, solid lignin stream.

The liquid hot water route (P3) was modelled assuming the use of a soaking unit using water at 190°C with a residence time of 15 min. After the soaking unit a possible solid liquid separation unit was considered (Mosier 2005). As a result, the block corresponding to the liquid hot water route can provide two alternative sets of outlet streams: 1) solubilised hemicellulose, solid cellulose and lignin stream; 2) solubilised hemicellulose stream and solid cellulose and lignin stream.

The AFEX route (P4) consists in a unit performing biomass soaking with ammonia at 90°C. Ammonia is then separated from the solubilised hemicellulose, solid cellulose and lignin stream by a flash unit and recycled to the AFEX unit after recompression (Gabriel & El-Halwagi 2013b).

The dilute acid route (P5) includes soaking unit operating at 160 °C with an H_2SO_4 solution. A subsequent acid neutralization stage with $\text{Ca}(\text{OH})_2$ is necessary. After the dilute acid treatment a possible solid liquid separation unit is considered (Humbird & Aden 2009). As a result, the block corresponding to the dilute acid route can provide two alternative sets of outlet streams: 1) solubilised hemicellulose, solid cellulose and lignin stream; 2) solubilised hemicellulose stream and solid cellulose and lignin stream.

The lime route (P6) includes a soaking unit operating at 120 °C using $\text{Ca}(\text{OH})_2$ at rates equal to 9% w/w of dry biomass. Recovery and recycle of $\text{Ca}(\text{OH})_2$ by addition of CO_2 and conversion to lime is considered (Chang et al. 1998). After the lime treatment a possible solid-liquid separation unit is also considered. As a result, the block corresponding to the lime route can provide two alternative sets of outlet streams: 1) solubilised hemicellulose, solid cellulose and lignin stream; 2) solubilised hemicellulose stream and solid cellulose and lignin stream.

The organosolvent route (P7) soaking unit operating at 180 °C and using an ethanol water solution 60 % w/w in ethanol. The residence time is 60 min. In the route, a distillation column is necessary to recover ethanol. A solvent make up is provided by an aqueous ethanol stream produced in the separation and purification section of the biorefinery (Pan et al. 2007).

Table 3-1: *Pretreatment parameters for the optimization model.*

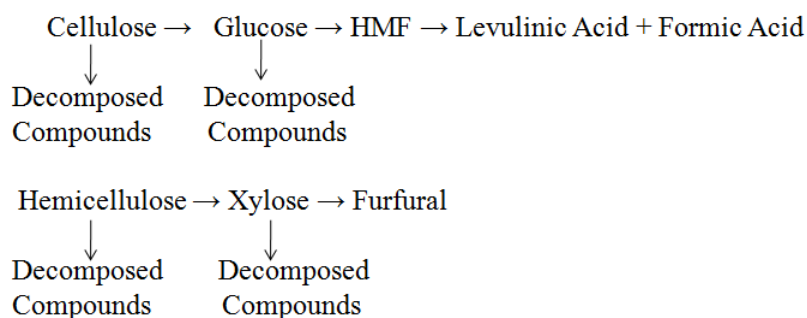
Pretreatment	Temperature (°C)	Residence time (min)	Concentration	Reference
Steam explosion	220 °C	3	/	Zimbardi et al., 2002
Liquid hot water	190 °C	15	/	Mosier et al., 2005
AFEX	90 °C	5	50%	Teymouri et al., 2004
Dilute acid	160 °C	10	1%wt H ₂ SO ₄	Humbird et al., 2011
Lime	120 °C	120	9% Ca(OH) ₂ w/w dry biomass	Chang et al., 1998
Organo solvent	180 °C	60	60% ethanol w/w dry biomass	Pan et al., 2006

The main operating conditions and yields to products assumed for all the pretreatment process routes are summarized in Table 3-1.

3.3 Hydrolysis and fermentation

3.3.1 Acid hydrolysis and levulinic acid production

Dilute acid hydrolysis (R1-R2) is used to obtain glucose and xylose from cellulose and hemicellulose, respectively, and to convert glucose to levulinic acid. The reaction network includes the formation of hydroxymethylfurfural (HMF) as an intermediate in the path from cellulose to levulinic acid and the conversion of xylose to furfural. Secondary parallel reactions can take place for cellulose, glucose and xylose to undesired decomposed compounds. The main reaction network is reported in the following:



Two different acid catalysts, H_2SO_4 and HCl , were considered (Rackemann & Doherty 2011). Acid hydrolysis is performed in a plug flow reactor at 150°C (Lee et al. 2000). Reaction network kinetics relevant to H_2SO_4 (Girisuta et al. 2008) (Lee et al. 2000) and HCl (Shen & Wyman 2012) were taken into account.

The outlet stream from the hydrolysis reactor is rich in intermediates (glucose and xylose) or in the final products (levulinic acid, formic acid and furfural) depending upon the residence time considered, with longer residence times in favour of final products. Therefore, if the conversion in the dilute acid reactor is insufficient, a second acid reactor (named levulinic acid reactor, R3) is used in series to produce more levulinic acid. Alternatively dilute levulinic acid stream from the hydrolysis reactor can also be subject to detoxification, carried out in an acid detoxification reactor, before being fed to fermentations in the ethanol or succinic acid routes.

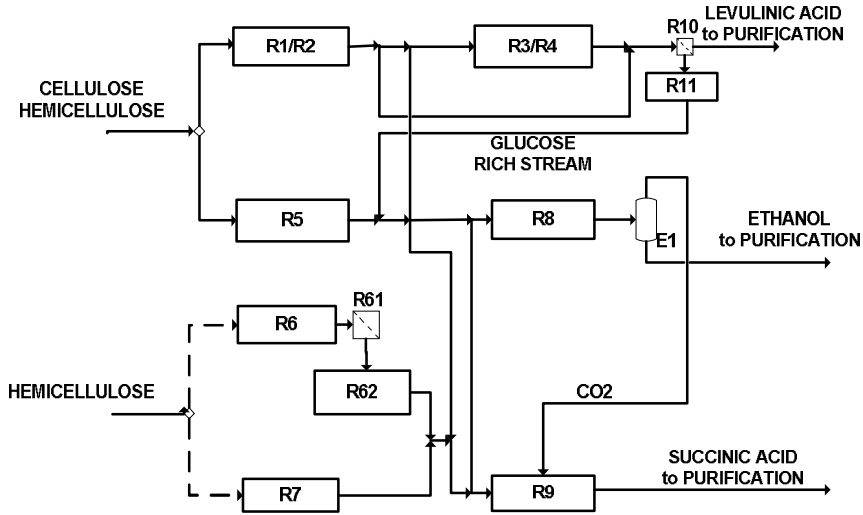


Figure 3-3: Flowsheet for the hydrolysis and fermentation section.

The levulinic acid reactor outlet stream is sent to an ultrafiltration filter to remove solid particles, oligomers and polymers (cellulose and hemicellulose) (Ramaswamy et al. 2013). Next, the filtered reaction liquor containing by products of the sugars hydrolysis and acid catalyst is conditioned by means of a detoxification stage (acid purification) if the sugars are sent to fermentation (Humbird & Aden 2009). Resulting wastewater is sent to dedicated treatment.

Table 3-2: *Equipment description of hydrolysis and fermentation section.*

Equipment	Action
R1	Acid hydrolysis reactor for cellulose and hemicellulose with HCl as catalyst
R2	Acid hydrolysis reactor for cellulose and hemicellulose with H ₂ SO ₄ as catalyst
R3	Levulinic acid reactor with HCl as catalyst
R4	Levulinic acid reactor with H ₂ SO ₄ as catalyst
R5	Enzymatic hydrolysis reactor for cellulose and hemicellulose
R6	Acid hydrolysis reactor for hemicellulose with H ₂ SO ₄ as catalyst
R7	Enzymatic hydrolysis reactor for hemicellulose
R8	Ethanol fermenter
R9	Succinic acid fermenter
R10	Solid separation
R11	Detoxification reactor for the glucose rich stream
R61	Solid separation
R62	Detoxification reactor for the xylose rich stream
E1	Flash to recover CO ₂ from ethanol fermenter

3.3.2 Enzymatic hydrolysis

Enzymatic hydrolysis (R5) is used to produce glucose and xylose from cellulose and hemicellulose using a continuous stirred-tank reactor by means of specific enzymes (Dimian & Bildea 2008). The superstructure includes two possible reactors. The first reactor can process either a mixed stream of

cellulose and hemicellulose or a stream of cellulose only. Enzymatic kinetics for this case was derived from Kadam et al. (Kadam et al. 2004). The second reactor (R7) can process a stream of hemicellulose only. The enzymatic kinetics for this case was taken from Flores-Sanchez et al. (Flores-Sánchez et al. 2013).

Two alternatives were considered to feed the enzymes to the enzymatic hydrolysis section. In one case the enzymes were bought from an external producer. In the second case, an on-site process section dedicated to produce cellulase enzymes (Humbird & Aden 2009) was considered. In this case part of the sugar-rich stream from the enzymatic reactor is recycled back to the enzyme production section. The two process alternatives are depicted in the flowsheet reported in Figure 3-4.

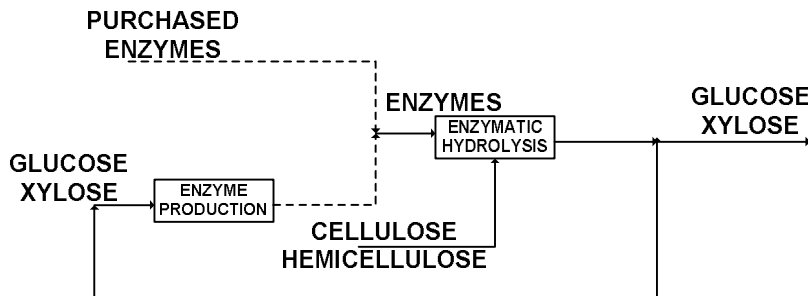
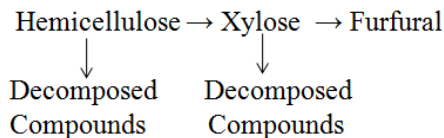


Figure 3-4: Superstructure of enzyme production section (the dashed lines are exclusive).

3.3.3 Hemicellulose dilute acid hydrolysis

Xylose can be also produced from hemicellulose by dilute acid hydrolysis (R6) in a plug flow reactor with H_2SO_4 as catalyst (Lee et al. 2000). The main reaction network is reported in the following:



After the hydrolysis, acid agents in the stream are neutralized in a detoxification stage to obtain higher pH as required for fermentations. The xylose-rich stream can be sent to either ethanol fermentation, or to succinic acid fermentation or partitioned between the two.

3.3.4 Ethanol and succinic acid fermentations

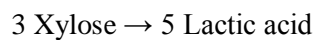
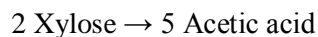
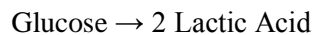
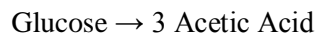
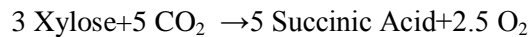
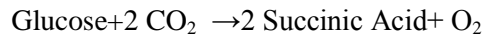
The streams of dissolved sugars produced by cellulose and hemicellulose by any of the hydrolysis routes are sent to fermentation stages.

Ethanol production (R8) takes place into batch fermenters in which sugars are converted into ethanol and CO₂ by specific microorganisms. *Zymomonas mobilis* strain ZM4(pZB5) turns out to be the best microorganism for the co-fermentation of C6 sugars and C5 sugars (Leksawasdi et al. 2001). Ethanol production reactions were:



The ethanol fermenter is composed by a batch reactors train in order to have a continuous production despite the required long residence time (Humbird & Aden 2009).

Succinic acid production is performed in a fermentation reactor (R9) fed with sugars solution and CO₂ provided from the ethanol fermenter. The reaction network considered (Luo et al. 2010) is the following:



These reactions require the microorganism *Mannheimia succiniciproducens* (MBEL55E). The chosen reaction kinetics are those reported by Song et al. (Song et al. 2008a).

Also the succinic acid fermenters for the same reason of ethanol fermenter is composed by a train of batch reactors.

3.4 Separation and purification

3.4.1 Levulinic acid purification

The purification section aims at obtaining 99 %wt levulinic acid. If HCl is the catalyst used for the acid hydrolysis the section consists in a separation stage (S1) of the HCl catalyst for its recovery and a subsequent separation stage (S2) of water by distillation (Shen & Wyman 2012). In particular the volatile HCl is recovered in the vapour stream of a flash stage (LA1) (Rackemann & Doherty 2011) that is recycled back. The resulting liquid stream made of levulinic acid, furfural, formic acid, water and other decomposed compounds is separated by a distillation column (C15) where the levulinic acid is recovered as a bottom product because it is the heavier compound with a boiling temperature of 246°C at atmospheric pressure. If H₂SO₄ is the catalyst used in the acid hydrolysis, two alternative purification processes are possible:

- chromatographic separation (S3) of H₂SO₄ and subsequent separation (S4) of water by distillation (Farone et al. 2000);
- reactive solvent extraction (S5) of organic compounds with subsequent distillation (S6) on the resulting streams to recover solvent and H₂SO₄ (O'Brien et al. 2000).

Table 3-3: *Equipment description of separation and purification section.*

Equipment	Action
C11, C12, C13	Distillation column train to recover pentanol
C14	Distillation column to purify levulinic acid
C15	Distillation column to purify levulinic acid
C21	Beer column
C22	Rectifying column
C23	Distillation column with ethylene glycolis as a solvent
C24	Distillation column to recover ethylene glycolis

Chapter 3

C31	Methanol distillation column
C32	Vacuum distillation column
CC11	Chromatographic column to purify levulinic acid
CR11	Reactive solvent extraction column to purify levulinic acid
CR31	Reactive solvent extraction column to purify succinic acid
CY31, CY32, CY33	Succinic acid crystallizers
E1	Flash to recover CO ₂ from ethanol fermenter
E2	Solids separation
E3	Pervaporation membrane for the beer stream
E4	Molecular sieves
E5	Pervaporation membrane for the azeotropic stream
LA1	Flash to recover HCl
LA2	Flash to recover H ₂ SO ₄
LA3	Reactor to convert levulinic acid to Pentyl levulinate
SA1	Reactor
SA2	Flash to separate steam
SA3	Membrane to recover the succinic acid crystals
SA4	Succinic acid purification by methanol
SA5	Flash to recover methanol

SA6	Flash to purify succinic acid
SA7	Thermal cracking

The first process route consists in a chromatographic column (CC11) with an adsorbent anionic resin used to separate H_2SO_4 from the aqueous solution and all the other organic compounds (Farone et al. 2000). Since this kind of chromatographic column needs a regeneration cycle, four columns in parallel were considered. The resulting aqueous solution of levulinic acid and a very small quantity of H_2SO_4 , formic acid and furfural is sent to a distillation column (C14). The bottom product is 99% wt levulinic acid.

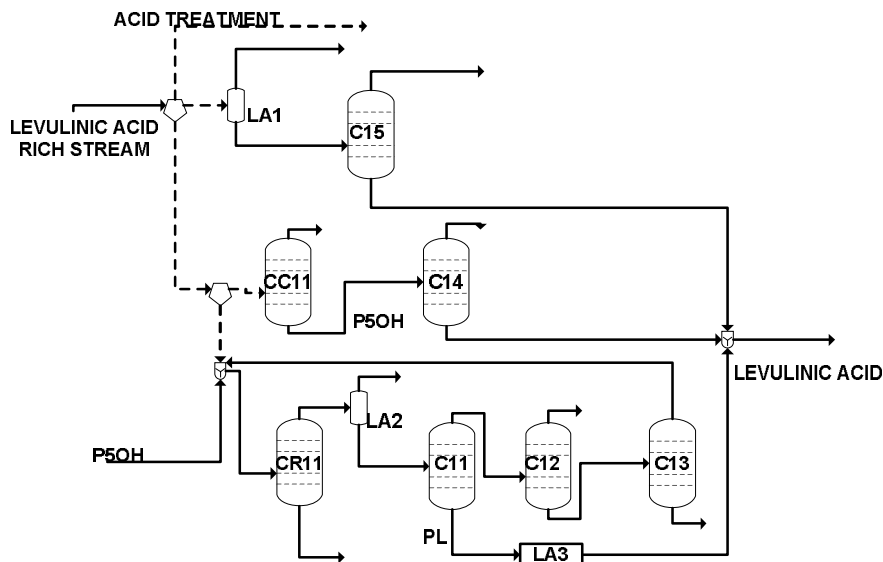


Figure 3-5: Flowsheet for the separation and purification section of levulinic acid.

The second process pathway consists in a reactive solvent extraction column (CR11) with pentanol solvent. Pentyl levulinate is obtained from the levulinic acid reactive extraction while the aqueous solution of H_2SO_4 is recovered in the raffinate stream. A distillation column will recover the acid catalyst from this latter stream. The extract stream containing mainly organic species (pentyl levulinate, furfural, pentanol and decomposed compounds) is sent to a flash unit (LA2) removing water and then to a train of distillation columns (C11, C12, C13). Pentyl levulinate is obtained from the bottom of

the first column (C11) and it is sent to a reactor (LA3) for the conversion to levulinic acid (Kamm et al. 2007). The top stream of the first column is sent to two additional distillation columns (C12, C13) to recover pentanol (Ayoub 2008).

3.4.2 Ethanol purification

The first separation unit is a flash to recover the CO₂ produced in the ethanol fermentation to be sent to the succinic acid fermenter. A ultrafiltration unit is used to remove both solid particles and non hydrolysed oligomers and polymers from cellulose and hemicellulose (Ramaswamy et al. 2013).

Ethanol purification up to 99 %wt can be carried out by either conventional unit operations, such as distillation and extractive distillation, or innovative technologies, such as pervaporation membranes and molecular sieves.

Table 3-4: Product yields for the purification sections.

Equipment	Main product yield (% wt)	References
Chromatographic column to purify levulinic acid	95	(Farone et al. 2000)
Distillation column to purify levulinic acid	95	(Farone et al. 2000)(Shen & Wyman 2012)
Reactive solvent extraction column and distillation column to purify levulinic acid	84	(Ayoub 2008)
Distillation columns to ethanol	99	(Dimian & Bildea 2008)
Pervaporation membranes to ethanol	95	(O'Brien et al. 2000)(Alvarez et al. 2008)
Distillation column with entrainer	95	(Errico et al. 2013)
Molecular sieves to ethanol	90	(Kwiatkowski et al. 2006)
Reactive crystallization of succinic acid	99	(Yedur et al. 2001)
Extraction and distillation column to purify succinic acid	90	(Song et al. 2007)

The first purification step up to 77 %wt of ethanol can be performed by either a beer column (S7) (Dimian & Bildea 2008) or a pervaporation membrane (S8) (O'Brien et al. 2000). A rectifying column (S9) achieves ethanol azeotropic composition(92.5 %wt) (Dimian & Bildea 2008).

Final purification step can be carried out by three alternative processes:

- extractive distillation (S10),
- molecular sieve unit (S11),
- pervaporation membranes (S12).

In particular, extractive distillation requires two columns and uses ethylene glycol as entrainer. The first column provides pure ethanol as distillate and a mixture as bottom product, that is sent to the second column, where the ethylene glycol is recovered as bottom product and water as distillate (Errico et al. 2013).

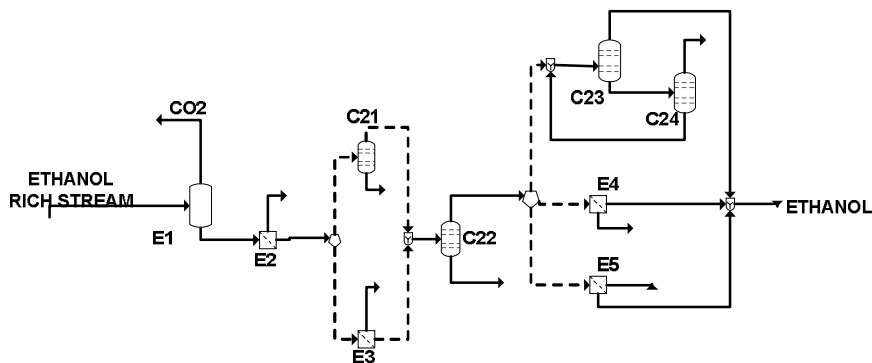


Figure 3-6: Flowsheet for the separation and purification section of ethanol.

Molecular sieves consist in zeolites adsorption units able to purify ethanol up to 99% wt (Kwiatkowski et al. 2006). Since molecular sieves need regeneration, two units in parallel were considered to alternate adsorption and regeneration.

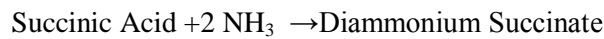
Pervaporation membranes are used to dehydrate the azeotropic water-ethanol mixture by water permeation (Alvarez et al. 2008). The main process parameter is the downstream pressure (of the permeate phase). A downstream pressure of 0.133 kPa was considered.

3.4.3 Succinic acid purification

The purification of succinic acid can be carried out alternately by:

- reactive crystallization (S13) and purification (S14) with methanol (Yedur et al. 2001);
- solvent extraction (S15) combined with distillation (S16) and a crystallization (Song et al. 2007).

The first purification process requires a reactor (SA1) to convert succinic acid to diammonium succinate by means of the following reaction:



A crystallizing unit (CY31) is used to obtain succinic acid as a solid precipitate product by the reaction:



Methanol solvent is used in order to purify the liquor with succinic acid crystals. In fact, all residual organic compounds are dissolved in the methanol-phase and pure succinic acid is obtained. Residual succinic acid in the organic phase is also recovered by further crystallization (CY32). Methanol is recovered by distillation (C31). A thermal cracking (SA7) allows the recovery and recycle of ammonia and ammonium sulfate (Yedur et al. 2001).

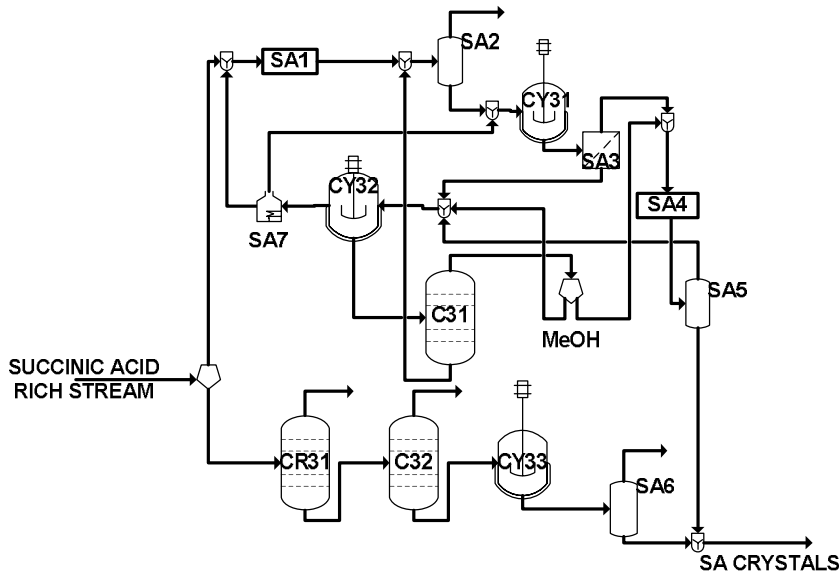


Figure 3-7: Flowsheet for the separation and purification section of succinic acid.

The alternative purification process of succinic acid consists of three units (Song et al. 2007):

- a reactive extraction column (CR31) with octanol solvent to remove by-product acids from the fermentation broth;
- a vacuum distillation column (C32) to eliminate residual volatile carboxylic acids such as acetic, formic and lactic acids. This operation is used to facilitate the subsequent crystallization;
- a crystallizer (CY33) to obtain 99%wt pure succinic acid crystals(Huh et al. 2006).

3.5 Thermochemical conversion

In the lignin section, the thermochemical conversion of the lignin-rich stream allows to produce high pressure steam and electricity. The lignin stream, coming either from the pretreatment section or from the separation section, is sent to two alternative process pathways:

- lignin gasification (T1) coupled with a combined cycle;

Chapter 3

- lignin combustion (T2) coupled with a Rankine cycle.

In the first case, an Integrated Gasification Combined Cycle is considered. In particular, the raw syngas from the gasification reactor is sent to a gas cleaning section and then to a gas turbine (Hamelinck et al. 2005). Both high pressure steam produced by heat recovery from the gasifier and flue gas at the exit of the gas turbine are sent to the heat recovery steam generator (HRSG). Resulting steam is sent to three steam turbines to produce electricity and intermediate and low pressure steam (Aden et al. 2002).

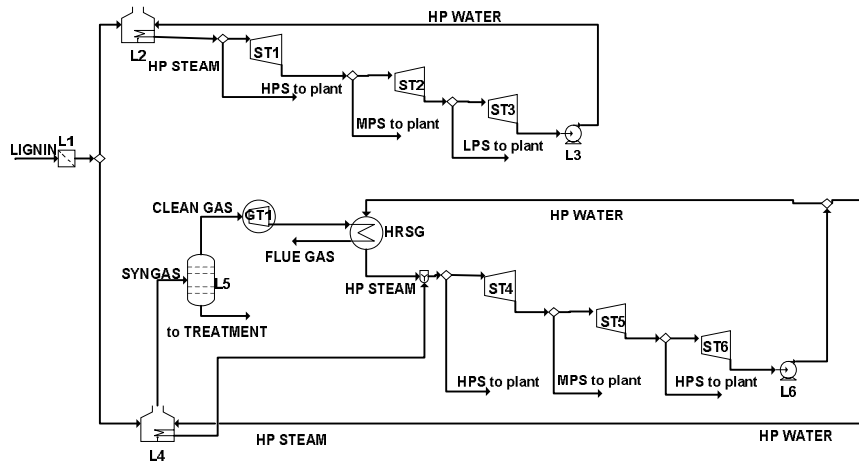


Figure 3-8: Flowsheet for the thermochemical conversion of lignin.

In the case of lignin combustion high pressure steam is produced in the boiler and is sent to steam turbine train at three pressure levels (Humbird & Aden 2009).

Table 3-5: *Equipment description of thermochemical conversion section.*

Equipment	Action
GT1	Gas turbine for the combined cycle
L1	Solids separation
L2	Furnace for lignin
L3	High pressure pump for lignin combustion pathway
L4	Gasifier
L5	Gas cleaning
L6	High pressure pump for combined cycle pathway
ST1, ST2, ST3	Steam turbines for lignin combustion pathway
ST4, ST5, ST6	Steam turbines for combined cycle pathway

3.6 Potential mass and heat integration of flowsheet

The biorefinery superstructure described above offers potential mass and heat integration opportunities between different pathways. In particular, intermediate by-products could be used as feedstocks for other process units for the alternative main products. Main mass integration options are represented by:

the CO₂ produced by the ethanol fermentation (R8) can be used as a feed stream for the succinic acid fermentation (R9);

the sugar by-products of the acid hydrolysis (R1-R2) to levulinic acid can be used as feed for the fermentation units (R8-R9);

steam produced from thermo-chemical processes (T1-T2) can be used for steam explosion pretreatment (P2);

Chapter 3

ethanol from the fermentation process and purification can be used as a solvent for organosolvent pretreatment (P7);

organic residues from fermentations and thermochemical section can be used into anaerobic digestion as substrates. The produced biogas can be used into the lignin gasifier or combustor mixed with air for air preheating by combustion (Humbird & Aden 2009).

Heat integration is required for the economic feasibility of a lignocellulosic biorefinery (Cardona & Sanchez 2007). In fact, energy-intensive processes, such as distillation columns and pretreatment processes, can be integrated with steam generation from thermochemical processes of solid residues (lignin-rich stream). Therefore, heat integration is also addressed in the present work as detailed in section 3.3.

4. Mathematical modelling and optimization methodology

4.1 Mathematical modelling

From the standpoint of the mathematical description, the optimization problem of the process superstructure described in the previous section consists in:

- mass and energy balance equations;
- inherent constraints relevant to process conditions;
- design equations for the process unit sizing;
- heat integration equations;
- capital cost and operating cost equations;
- economic objective function.

In particular, the main process inherent constraints concern the exploitation of mass and energy integration opportunities described in section 2.5 to minimise the use of additional reactants and energy utilities. For example, the CO₂ needed for the succinic acid fermentation is provided by the by-product stream of the ethanol fermentation only.

4.2 Material balance constraints

Several kinds of material balance equations are considered in the superstructure model.

The set of balance equations on splitters balances is given by (Biegler L.T., Grossmann I.E. 1997):

$$\begin{aligned}
 F_i^k &= \sum_{j=1}^{n_j} F_{i,j}^{k,IN} \mu_j^k && \text{for } k = 1, \dots, n_k - 1 \\
 F_i^{IN} &= \sum_{j=1}^{n_j} F_{i,j}^{k,IN} && \text{for } k = 1, \dots, n_k - 1 \\
 F_i^{IN} &= \sum_{k=1}^{n_k} F_i^k && (4-1) \\
 \sum_{j=1}^{n_j} y_j^k &\leq 1 && \text{for } k = 1, \dots, n_k - 1 \\
 F_{i,j}^{k,IN} &\leq y_j^k \text{ UB} && \text{for } j = 1, \dots, n_j; k = 1, \dots, n_k - 1 \\
 y_j^k &\in \{0, 1\}
 \end{aligned}$$

where F_i^k is the component i mass flowrate of the outlet stream k ; F_i^{IN} is the component i mass flowrate of the inlet stream; μ_j^k are the n_j discrete values of the split fraction for the stream k ; $F_{i,j}^{k,IN}$ are the n_j inlet flowrate variables deriving from the disaggregation of the inlet flowrate F_i^{IN} , n_k is the number of outlet streams, y_j^k are binary variables for the selection of outlet stream flowrates, UB is the upper bound for the flowrates (Biegler L.T., Grossmann I.E. 1997). When the splitter can feed more than one outlet stream, corresponding to the case in which several parallel pathways are possible, the μ_j^k discrete values are real numbers between 0 and 1. Differently, when the splitter can feed only one outlet stream, corresponding to only one of the process pathways, the μ_j^k discrete values reduce to the two

integer values 0 and 1. This material balance formulation yield linear constraints for the continuous variables and the binary

The set of balance equations of mixer are:

$$F_i^{OUT} = \sum_{k=1}^{n_k} F_i^k \quad (4-2)$$

where F_i^k is the component i mass flowrate of the inlet stream k ; F_i^{OUT} is the component i mass flowrate of the outlet stream.

For reactors in which the reactant j is converted to product i we have:

$$F_i^{OUT} = F_j^{IN} \eta_{i,j}(T, P, c, pH) + F_i^{IN} \quad (4-3)$$

where F_i^{OUT} is the product i outlet flowrate, F_j^{IN} is the reactant j inlet flowrate, F_i^{IN} is the product i inlet flowrate, $\eta_{i,j}(T, P, c, pH)$ is the yield to product j of reactant i . The yield is a function of temperature T , pressure P , catalysts concentration c , potential of hydrogen pH.

For separation units we have:

$$F_i^k = F_i^{IN} \zeta_{i,k}(T, P) \quad (4-4)$$

where F_i^k is the component i mass flowrate of the outlet stream k , F_i^{IN} is the component i inlet flowrate, $\zeta_{i,k}(T, P)$ is the fractional recovery of component i in the outlet stream k . This recovery is a function of temperature T and pressure P .

The following constraint was used to ensure that the CO_2 produced by ethanol fermentation is sufficient as reactant for the succinic acid fermentation, as mentioned in section 2.9:

$$F_{CO_2}^{EtOH, fer} \geq F_{CO_2}^{SA, fer} \quad (4-5)$$

Chapter 4

where $F_{CO_2}^{EtOH,fer}$ is the CO₂ outlet flow rate from ethanol fermenter, $F_{CO_2}^{SA,fer}$ is the CO₂inlet flow rate to succinic acid fermenter.

4.3 Energy balance constraints

Energy balances are also needed in order to estimate the steam and the thermal energy required by the process.

For each process unit the following general stationary energy balance equation applies:

$$\sum_{i=1}^{n_i} F_i^{IN} \Delta H_i^{IN} + Q_{GEN} + Q_{EXT} = \sum_{i=1}^{n_i} F_i^{OUT} \Delta H_i^{OUT} \quad (4-6)$$

Where Q_{GEN} is generated heat power during the process and Q_{EXT} is the external heat duty, ΔH_i^{IN} and ΔH_i^{OUT} are the specific enthalpies of component i at the inlet and at the outlet conditions, respectively.

For the reboilers and the condensers of the distillation columns, the heat duty was estimated, by means of the simplified relations proposed by Biegler et al.(Biegler L.T., Grossmann I.E. 1997). On the hypotheses of constant molar fluxes and saturated liquid feed the rising vapour stream is equal to the sum of the liquid reflux stream, L , and the liquid distillate stream, D , therefore:

$$Q_{EXT} = (L + D) \sum_{i=1}^{n_i} x_{B,i} \lambda_i \quad (4-7)$$

for reboilers, and:

$$Q_{EXT} = -(L + D) \sum_{i=1}^{n_i} x_{D,i} \lambda_i \quad (4-8)$$

for condensers.

where, $x_{B,i}$ and $x_{D,i}$ are the molar fraction of the bottom and of the distillate respectively and λ_i is the latent heat of the component i . In eq. 4-6 to 4-8, cp and λ are considered constant with temperature.

For the mixer units, energy balances were not considered since it was always assumed the same temperature for all inlet streams and also the heat of mixing was neglected. In order to obtain the same temperature for all the inlet streams before mixing, heat exchangers were used to make the temperature difference vanish.

Energy balances on transformation units producing electricity, as steam or gas turbines were carried out in a simplified manner as:

$$E = \eta_{ISO}\eta_{MEC}(\Delta H^{IN} - \Delta H^{OUT})F \quad (4-9)$$

Where E is the electricity generated by the turbine, η_{ISO} and η_{MEC} are isentropic efficiencies and mechanical efficiencies of turbine, ΔH^{IN} and ΔH^{OUT} are inlet and outlet specific enthalpies of stream F.

4.4 Heat integration

The minimization objective on the use of external energy utilities in the whole biorefinery plant was addressed by using heat integration methods according to the pinch analysis. Using the heat duties Q_{EXT} from the solution of eqs 4-6 to 4-8 calculated on all the plant equipment units, the pinch theory was applied in order to minimize the required hot and cold external utilities (Linnhoff & Hindmarsh 1983). Since the inlet and outlet stream temperatures of each heat exchangers are fixed according to the process requirements, a linear problem was obtained to derive the heat duty of external hot and cold utilities:

Chapter 4

$$\begin{aligned}
 CP_k &= \frac{Q_{EXT,k}}{T_k^{OUT} - T_k^{IN}} && \text{for } k = 1, \dots, n_h \\
 Q_j &= \sum_{k=1}^{n_h} CP_k \omega_k v_{j,k} (T_j - T_{j+1}) && \text{for } j = 1, \dots, n_{int} \\
 \bar{Q}_j &= \bar{Q}_{j-1} - Q_{j-1} && \text{for } j = 1, \dots, n_{int} \\
 Q_{HOT} &\geq -(\bar{Q}_{j-1} - Q_{j-1}) && \text{for } j = 1, \dots, n_{int} \\
 Q_{COLD} &= \bar{Q}_{n_{int}} + Q_{HOT} && (4-10)
 \end{aligned}$$

where CP_k is the heat capacity flowrate of the stream through the heat exchanger k , T_k^{IN} and T_k^{OUT} are the temperatures of the inlet and outlet stream, respectively, $Q_{EXT,k}$ is the heat duty of the exchanger k , n_h is the number of heat exchangers, n_{int} is the number of subintervals, T_j and T_{j+1} are the temperature bounds of the subinterval j belonging to the overall temperature range of the heat exchanger network, Q_j is the heat duty exchanged in ΔT_j , \bar{Q}_j is a heat duty auxiliary variable and it represent the heat necessary to heat all cold stream from T_j to $T_{n_{int}}$. Q_{HOT} and Q_{COLD} are the required heat duty of hot and cold utilities, respectively. Finally, ω_k is equal to 1 for a hot stream and to -1 for a cold stream; $v_{j,l}$ is equal to 1 or to 0 if the temperature subinterval $[T_{j+1}, T_j]$ is included or not in the heat exchanger temperature range $[\omega_k T_k^{OUT}, \omega_k T_k^{IN}]$.

4.5 Reactor modelling

For reactors the eq. 4-6 was considered. In the first part of the work values were assumed for each hydrolysis reactor and fermentation reactor according to available literature data. These values are reported in Table 4-1.

Table 4-1: Product yields for the reactors at fixed yields.

Reactor	Temp. (°C)	Residence time	Yield (kg _{product} /kg _{reactant})	Reactor kind and references
Reactor to convert cellulose/glucose to levulinic acid with H ₂ SO ₄ as catalyst	150	20 min	Glucose: 30% Xylose: 10% Levulinic acid: 25%	PFR (Girisuta et al. 2007)
Reactor to convert cellulose/glucose to levulinic acid HCl as catalyst	150	10 min	Glucose: 15% Xylose: 8% Levulinic acid: 12%	PFR (Shen & Wyman 2012)
Enzymatic reactor to produce glucose and xylose	45	65 h	Glucose: 50% Xylose: 65%	CSTR (Kadam et al. 2004)(Flores-Sánchez et al. 2013)
Reactor to convert hemicellulose to xylose	150	70 min	Xylose: 40%	PFR (Lee et al. 2000)
Fermenter to produce ethanol	30	12 h	Ethanol: 47%	Batch (Leksawadi et al. 2001)
Fermenter to produce succinic acid	40	6 h	Succinic acid: 37%	Batch (Song et al. 2008b)

In the second part of the work the hydrolysis and fermentation reactors were modelled by rigorous methods accounting for relevant kinetic schemes to address a more accurate design of the reactors. Constant volume and temperature were assumed for all the reactors. In particular, plug flow reactors for the dilute acid hydrolysis and the levulinic acid reaction were modelled by the following molar balance equations:

Chapter 4

$$\frac{dc_i}{d\tau} = \sum_{j=1}^{n_r} v_{i,j} r_j(c_i, c_k) \quad \text{for } i = 1, \dots, n_{comp}$$

$$I.C. \tau = 0 \quad c_i = c_{i0} \quad (4-11)$$

where τ is the residence time in the reactor, c_i and c_k are the molar concentration of component i and k , respectively, r_j is the reaction rate of component i in reaction j , $v_{i,j}$ is the stoichiometric coefficient for component i in reaction j , assuming negative value if component i is a reactant and positive values if the component i is a product, c_{i0} is the initial concentration of component i , n_{comp} is the number of components and n_r is the number of reactions.

Batch reactors for ethanol and succinic acid fermentation were modelled by the following mass balance equations:

$$\frac{dw_i}{d\tau} = \sum_{j=1}^{n_r} v_{i,j} \psi_{i,j} R_j(w_i, w_k) \quad \text{for } i = 1, \dots, n_{comp} \quad (4-12)$$

$$I.C. \tau = 0 \quad w_i = w_{i0}$$

where τ is the batch time in the reactor, w_i and w_k are the mass concentration of component I and k , respectively, R_j is the reaction rate of component i in reaction j , $v_{i,j}$ is the stoichiometric coefficient for component i in reaction j , assuming negative value if component i is a reactant and positive values if the component i is a product, $\psi_{i,j}$ is the ratio between the molecular weight of component i and the molecular weight of the component on which the reaction rate R_j is calculated w_{i0} is the initial mass concentration of component i , n_{comp} is the number of components and n_r is the number of reactions.

The resulting set of ordinary differential equations 4-11 and 4-12 was solved either analytically or numerically. In particular, when the reaction rates were linear functions of concentrations, analytical solutions were derived. Instead, when the reaction rates were non linear functions of concentrations, the set of ODEs was numerically solved by a variable order solver based on the numerical differentiation formulas, namely the *ode15s* function available in MATLAB®.

Table 4-2: Product yields for the reactors.

Reactor	Temp. (°C)	Residence time	Yield (kg _{product} /kg _{reactant})	Reactor kind and references
Reactor to convert cellulose/glucose to levulinic acid with H ₂ SO ₄ as catalyst	150	0-120 min	Glucose: 0-30% Xylose: 0-60% Levulinic acid: 0-55%	PFR (Girisuta et al. 2007)
Reactor to convert cellulose/glucose to levulinic acid HCl as catalyst	150	0-50 min	Glucose: 0-15% Xylose: 0-30% Levulinic acid: 0-35%	PFR (Shen & Wyman 2012)
Enzymatic reactor to produce glucose and xylose	45	0-72 h	Glucose: 0-70% Xylose: 0-60%	CSTR (Kadam et al. 2004)(Flores-Sánchez et al. 2013)
Reactor to convert hemicellulose to xylose	150	0-120 min	Xylose : 0-70%	PFR (Lee et al. 2000)
Fermenter to produce ethanol	30	0-30 h	Ethanol: 47%	Batch (Leksawadi et al. 2001)
Fermenter to produce succinic acid	40	0-15 h	Succinic acid: 0-47%	Batch (Song et al. 2008b)

Continuous stirred tank reactors for enzymatic hydrolysis were modelled by the following mass balance equations:

$$w_i = w_{i0} + \tau \sum_{j=1}^{n_r} v_{i,j} \psi_{i,j} R_j(w_i, w_k) \quad \text{for } i = 1, \dots, n_{comp} \quad (4-13)$$

Chapter 4

In this case a set of algebraic non-linear equations was obtained. Its solution was numerically sought by an unconstrained non-linear optimization, the Nelder-Mead simplex algorithm, namely the *fminsearch* function available in MATLAB®.

The kinetic networks considered for each reactor and the references to the relevant kinetic model adopted are reported in Table 4-2.

Once the relevant balance equations, Equation 4-11, 4-12 or 4-13 are solved for the relevant reactors, concentration-time profiles are available and, thus, it is possible to derive the overall product yield defined as the ratio between the converted mass of product p and the initial mass of reactant r , provided the normalization of stoichiometric coefficients:

$$\eta_p(\tau) = \frac{w_p(\tau) - w_{p0}}{w_{r0}} \quad \text{for } p = 1, \dots, n_{comp} \quad (4-14)$$

The volume of PFR and CSTR, V , was calculated as:

$$V = \frac{F\tau}{\rho} \quad (4-15)$$

where F is the stream mass flow rate, and ρ is the stream average density.

Batch reactors for fermentation were sized taking into account the required batch time for reaction and the time for cleaning, filling and emptying of vessels, t_{cfe} . A train of reactor was considered to ensure a continuous product flowrate. Accordingly the volume of each batch reactor, V , was estimated as:

$$V = \frac{F(\tau + t_{cfe})}{\rho N_u} \quad (4-16)$$

The number of units, N_u , and the volume of batch units was estimated by minimizing the capital cost. The resulting number of units for fermentation was six. The results in terms of product yield as a function of residence time according to Equation 4-14 obtained by solving the set of equations 4-11 for PFR, the set of equations 4-12 for batch reactors and the set of equations 4-13 for CSTR are reported in the appendix. In particular, Figure A-1 reports the space-time profile of product yields for the dilute acid hydrolysis of cellulose and hemicellulose with HCl catalyst (Figure A-1a) and with H₂SO₄ catalyst (Figure A-1b) in PF reactors. Figure A1c-2d report the batch-

time profile of product yields for the levulinic acid PF reactors converting glucose with HCl catalyst (Figure A1c) and with H₂SO₄ catalyst (Figure A1d). Figure A2 reports the yield vs residence time operating conditions for the enzymatic hydrolysis in CSTR converting cellulose and hemicellulose. Figures A3, A-4 report the batch time profile of product yields for the fermentation of glucose and xylose. In particular, Figure A-3 refers to ethanol fermentation and Figure A-4 to succinic acid fermentation.

4.6 Equipment sizing

All process vessel operated in continuous mode as plug flow reactors for acid hydrolysis and continuous stirred tank reactors for enzymatic hydrolysis. Their volumes were derived from the residence time values required to obtain the desired yield to product values. Therefore, linear equations relating volume, residence time and volumetric flow rate were used. The number and the volume of batch units was estimated by considering batch-product removal times. Assumed residence time values are reported in Table 4-2.

The shortcut method proposed by Biegler et al. (Biegler L.T., Grossmann I.E. 1997) was used for the sizing of the distillation columns. For these units the tray number, the reflux ratio and the molar vapor flow rate going upwards into the column are the main variables necessary to evaluate costing of the columns.

Despite heat integration was applied to minimize the use of external utilities, a heat exchanger network based on the coupling of hot and cold process streams was not derived for the sake of simplicity. Therefore, the number of heat exchangers was assumed equal to the number required without heat integration. This assumption underestimates the number of units with respect to the heat integration case. Heat exchanger areas were evaluated by using linear equations, assuming overall heat transfer coefficients, U_k , as a function of the type (phase, organic or inorganic species) of exchanging streams and mean temperature differences ΔT constants (40°C) for all heat exchangers, since the stream coupling are unknown:

$$A_k = \frac{Q_{EXT,k}}{U_k \Delta T} \quad (4-17)$$

Chapter 4

As a result of the above described assumptions, the sizes of all the pieces of equipment (including distillation columns and heat exchangers) resulted linearly proportional to the stream mass flow rate or to the heat flow rate.

4.7 Capital costs

Capital costs of equipment were estimated by power law of capacities of the specific unit to account for the real scale:

$$CC_k = CC_{k,0} \left(\frac{S_k}{S_{k,0}} \right)^{m_k} \quad (4-18)$$

Where $CC_{k,0}$ is the capital cost of the equipment item k with the base capacity or size $S_{k,0}$, and CC_k is the capital cost the equipment item k with the real capacity or size S_k , m_k is the sizing exponent for the kind of unit k . The main relevant economic data for the equipment cost were retrieved from the work of Hamelinck et al. (Hamelinck et al. 2005) on the techno-economic performance of lignocellulosic biorefineries producing bioethanol. The capital costs of the purification equipment units were calculated separately. A piecewise linearization of eq. 4-18 was performed in order to obtain a linear correlation between capital costs and unit capacity or size. Chemical Engineering Plant Cost Index (CEPCI) was applied to update to the year of the analysis the equipment cost estimated years ago:

$$ECC_k = CC_k \frac{CEPCI_{2014}}{CEPCI_{ref}} \quad (4-19)$$

Where ECC_k is direct capital cost in the year of interest for the analysis, $CEPCI_{2014}$ and $CEPCI_{ref}$ are Chemical Engineering Plant Cost Index in 2014 and in the costing reference year, respectively.

The total project investment cost (TIC) was calculated by adding to the bare module cost ECC and the auxiliary costs. The latter were assumed as proportional to ECC by means of specific factors as follows :

$$TIC = \sum_{k \in Eqp} ECC_k (1 + K_k) \quad (4-20)$$

where K_k is a cost factor accounting for equipment purchase, installation, instrumentation and controls, piping, electrical systems, buildings including services, engineering, construction, legal and contractors fees, project contingency, land and working capital. Values of K_k were set to those suggested by Biegler et al. (Biegler L.T., Grossmann I.E. 1997).

4.8 Total annual cost

The total annual cost (TAC) of the process is the sum of operational cost (OPC) and feedstock purchasing cost (FSC):

$$TAC = OPC + FSC \quad (4-21)$$

The operational cost (OPC) includes the maintenance and labour cost (MLC), process utility (steam) cost ($STMC$), natural gas cost (NGC), and power cost (PWC):

$$OPC = MLC + STMC + NGC + PWC \quad (4-22)$$

The cost of maintenance and labour MLC is evaluated as proportional to the total investment cost (TIC) by a specified cost factor f_c :

$$MLC = f_c TIC \quad (4-23)$$

Relevant prices of utilities were obtained from Humbird et al. (Humbird & Aden 2009).

4.9 Profitability

The process revenues come from the sales of levulinic acid, ethanol, succinic acid and electricity at market price (updated to september 2014). As a result, the revenues are given by:

$$\text{Rev} = \sum_{p=1}^{n_p} F_p p_p \quad (4-24)$$

Chapter 4

where F_p is the mass production rate of product p , p_p is the unit market price (\$/kg) of product p (Wang et al. 2013), n_p is the number of products. The market prices are given in Table 5-1.

Given the life span of the project, t_{ls} , and made the hypothesis that the plant construction takes 3, the cash flow for the year i is defined as:

$$CF_i = -f_iTIC + g_iWC + (Rev - TAC)(1 - t) + DPt \quad (4-25)$$

Where f_i is the fraction of TIC spent during year i , describing the investment distribution over the years, WC is the working capital, t is the tax rate and DP is the depreciation, g_i is a parameter equal to -1 for $i = 3$ (the year before the plant start-up), 1 for $i = t_{ls}$, 0 for all other values of i . In particular, a straight-line depreciation for ten years was assumed.

Two economic objective functions based on the cash flow analysis were considered. The first was the Net Present Value defined as:

$$NPV = \sum_{i=0}^{t_{ls}} \frac{CF_i}{(1+r)^i} \quad (4-26)$$

Where CF_i is the cash flow for the year i , r is the annual discount rate.

4.9 MILP solving method

The mathematical description, the optimization problem of the process superstructure described in the previous section consists in:

- mass and energy balance equations;
- inherent constraints relevant to process conditions;
- design equations for the process unit sizing;
- heat integration equations;
- capital cost and operating cost equations;
- economic objective function.

All the equations and inequalities are described in detail in the part 1 of the paper (Giuliano, Cerulli, et al. 2016). The economic objective function considered in the base case is still the Net Present Value.

A significant improvement of the mathematical model of the superstructure in the present work regards the inclusion of the results of the rigorous reactor modelling described in section 3 in the mass balance equations of reactors:

$$F_p^{OUT} = F_r^{IN} \eta_p(\tau) + F_p^{IN} \quad (4-27)$$

where F_p^{OUT} is the product p outlet flowrate, F_r^{IN} is the reactant r inlet flowrate, F_p^{IN} is the product p inlet flowrate, $\eta_p(\tau)$ is the product p yield obtained by equation 4-14. In this formulation the mass balance equation 4-27 is non-linear, due to the term given by the product of F_r^{IN} and of $\eta_p(\tau)$, in which this latter is also a non linear function of τ . Moreover, also the reactor design equations 4-15 and 4-16, are non linear due to the presence of the product of F and τ .

As a consequence, the resulting optimization mathematical model is a Mixed Integer Non Linear Problem (MINLP) with the integer variables for the selection of alternative technologies:

$$\begin{cases} \max z = c(x^L, x^N, y) \\ h(x^L, x^N, y) = 0 \\ g(x^L, x^N, y) \leq 0 \\ x^L, x^N \in R^+, y \in \{0, 1\} \end{cases} \quad (4-28)$$

where z is the economic objective function, x^L is the vector of continuous linear variables corresponding to the mass flowrates and heat duties, x^N is the vector of continuous non-linear variables representing the reactor variables, residence times and product yields, y is the vector of binary variables necessary for the logics of decisions.

The equality constraints $h(x^L, x^N, y) = 0$ represent mass and energy balances constraints and cost related constraints. The inequality constraints

Chapter 4

$g(x^L, x^N, y) \leq 0$ are related to design specifications (i.e., capacity limits and upper and lower bounds on process variables, etc.).

As a result, the problem statement reported in Equation 4-28 can be rearranged as follows:

$$\begin{cases} \max z = a(x^N)x^L + by \\ A(x^N)x^L + By = 0 \\ C(x^N)x^L + Dy \leq 0 \\ x^L, x^N \in R^+, y \in \{0, 1\} \end{cases} \quad (4-29)$$

Where $a(x^N)$ is a vector of non linear functions of the continuous variables x^N , $A(x^N)$ and $C(x^N)$ are matrices of non linear functions of the continuous variables x^N , b is a vector of coefficients, B and D are matrices of coefficients.

The search of the optimal solution of a MINLP problem might be very difficult to address. As a result, a variable discretization method was applied to linearize the problem (Kalitventzeff 1991). In particular, for each non linear variable x^N (residence time and process yield), a vector of possible values ζ_i of the variable was considered. The original variable was set equal to the sum of the product of each of these values and a binary variable. In the problem solution only one of these binary variables was allowed to be equal to 1. This transformation can be expressed in mathematical terms as follows:

$$\begin{aligned}
 x_j^N &= \sum_{i=1}^{n_j} \zeta_{j,i} y_{j,i}^d \\
 a_j(x_j^N) &= \sum_{i=1}^{n_j} a_j(\zeta_{j,i}) y_{j,i}^d = \sum_{i=1}^{n_j} \alpha_{j,i} y_{j,i}^d \\
 x_k^L &= \sum_{i=1}^{n_j} x_{k,i}^L \\
 x_{k,i}^L &\leq y_{j,i}^d UB \\
 a_j(x_j^N) x_k^L &= \sum_{i=1}^{n_j} \alpha_{j,i} x_{k,i}^L \\
 \sum_{i=1}^{n_j} y_{j,i}^d &= 1 \\
 y_{j,i}^d &\in \{0, 1\}
 \end{aligned} \tag{4-30}$$

where $\zeta_{j,i}$ are the discrete values assumed for the non-linear variable x_j^N , n_j is the number of discrete values assumed for the non linear variable x_j^N , $y_{j,i}^d$ are the binary variables of the discretization, $\alpha_{j,i}$ are the discrete values of the function $a_j(x_j^N)$, $x_{k,i}^L$ are additional linear variables, UB is the upper bound.

As an example of the application of this discretization formulation we can consider the mass balance equation on a reactor:

$$F_p^{OUT} = F_r^{IN} \eta_p(\tau) \tag{4-31}$$

For the sake of simplicity, this equation differs from Equation 4-27 only for the absence of the term related to the presence of the product component in the inlet stream. By applying the discretization of Equation 4-30), we have:

Chapter 4

$$\begin{aligned}
 \tau &= \sum_{i=1}^{n_d} \bar{\tau}_i y_i^d \\
 \eta_p(\tau) &= \sum_{i=1}^{n_d} \eta_p(\bar{\tau}_i) y_i^d = \sum_{i=1}^{n_d} \bar{\eta}_{p,i} y_i^d \\
 F_p^{OUT} &= \sum_{i=1}^{n_d} F_{r,i}^{IN} \bar{\eta}_{p,i} \\
 F_r^{IN} &= \sum_{i=1}^{n_d} F_{r,i}^{IN} \\
 \sum_{i=1}^{n_d} y_i^d &\leq 1 \\
 F_{r,i}^{IN} &\leq y_i^d \text{ UB} \\
 y_i^d &\in \{0, 1\}
 \end{aligned} \tag{4-32}$$

where $\bar{\tau}_i$ are the discrete values assumed for τ , n_d is the number of discrete values, y_i^d are the binary variables of the discretization, $\bar{\eta}_{p,i}$ are the discrete values of the function $\eta_p(\tau)$, $F_{r,i}^{IN}$ are additional linear variables. The discrete values for $\bar{\tau}_i$ and $\bar{\eta}_{p,i}$ were derived from the functions reported in Figures from A-1 to A-4.

This transformation allowed obtaining a mixed linear problem (MILP) as an approximation of the initial MINLP problem:

$$\begin{cases}
 \max z = \alpha x^L + \beta y + \gamma y^d \\
 Ax^L + By + Ey^d + \delta = 0 \\
 \Gamma x^L + \Delta y + Hy^d + \varepsilon \leq 0 \\
 x^L \in R^+ \quad y, y^d \in \{0, 1\}
 \end{cases} \tag{4-33}$$

where $\alpha, \beta, \gamma, \delta, \varepsilon$ are vectors of coefficients, $A, B, \Gamma, \Delta, E, H$ are matrices of coefficients.

On the one hand, this simplification allowed using more efficient solution methods for MILP optimization problems. On the other hand, a significant

increase of the number of binary variables and real variables was determined. In fact, for each non-linear variable x^N a set of several binary variables y^d (typically 10) was introduced by the discretization procedure.

4.10 Biomass seasonality

Approximate design equations were used to estimate the characteristic size or capacity of the process equipment units. In particular, non-linear correlations between the yield to products and the residence times of the hydrolysis and the fermentation reactors were derived by separately solving complete model equations including material balances, reactor design equations and kinetic equations. In case the resulting systems include ordinary differential equations, these were numerically solved by MATLAB computing tools. Further details on these models and their solution can be found elsewhere (Giuliano, Poletto, et al. 2016). The sizing of distillation columns was performed by the shortcut methods based on the Fenske, Underwood and Gilliland equations as reported by Biegler et al. (Biegler L.T., Grossmann I.E. 1997). The sizing of the units for the biomass pretreatment and for the thermo-chemical conversion of lignin was not addressed in detail. In fact, the sizes of the process equipment are linearly dependent on mass flow rate or energy and, therefore, the capital costs of these units were directly estimated by means of the correlations with the mass flow rate of the feed or the generated power suggested by Hamelinck et al. (Hamelinck et al. 2005).

In addition to the case of a biorefinery with a single biomass feedstock, a study of the combined use of different seasonal biomass types during the year is also presented. On this purpose, we assumed that each of the three biomass types was available for four months in a year. This problem was modelled by replicating mass and energy balances and design constraints for the three biomass kinds. In fact, for each of the three periods of the year different mass and energy balances apply depending on the used biomass feedstock. This resulted in a significant increase of the number of variables, equations and inequalities (roughly by a factor of three). As a result, design constraints for each piece of equipment provided with three different values for the unit size corresponding to each of the three biomass kinds treated. Thus, the largest size value was considered in order to use the same unit for the three biomass kinds over different periods of the year. Of course, this choice leads to a certain overdesign of the units for their use in some periods of the year, but it is necessary to ensure the plant flexibility with the biomass feedstock. This approach was mathematically formulated by a new set of inequality constraints as follows:

Chapter 4

$$\begin{cases} S_j \geq S_{j,EU} \\ S_j \geq S_{j,WS} \\ S_j \geq S_{j,OP} \end{cases} \quad (4-34)$$

where S_j is the size of equipment j , $S_{j,EU}$ is the size of equipment j for the case relative to the use of eucalyptus only, $S_{j,WS}$ is the size of equipment j for the case relative to the use of wheat straw, $S_{j,OP}$ is the size of equipment j for the case relative to the use of olive pruning.

Heat integration was addressed according to the pinch analysis to minimize the energy exchanged by utilities. In particular, process synthesis and heat integration were carried out simultaneously assuming variable flow rates and fixed temperatures for the heat exchangers (Yee et al. 1990). Heat exchanger areas were evaluated assuming relevant global heat transfer coefficients and constant mean temperature differences for all the network units.

Capital costs were calculated by power law correlations as a function of the unit capacity or the feed flow rate and relevant sizing factors:

$$CC_k = CC_{k,0} \left(\frac{S_k}{S_{k,0}} \right)^{m_k} \quad (4-35)$$

where $CC_{k,0}$ is the capital cost of the unit k with base size $S_{k,0}$, CC_k is the capital cost of the unit k , with size S_k and m_k is the relevant sizing exponent. Main economic data were retrieved from the work of Hamelinck et al. (Hamelinck et al. 2005) on the techno-economic performance of lignocellulosic biorefineries producing bioethanol. The Total Investment Cost, TIC , was calculated by multiplying the bare-module cost of equipment by relevant factors (Hamelinck et al. 2005)(Seider et al. 2010).

Manufacturing costs, also referred to as Total Annual Costs, TAC , including raw materials, reactants, catalysts, utilities, labour and maintenance costs were estimated on the basis of the data reported by Humbird et al. (Humbird & Aden 2009). In particular, labour and maintenance costs are calculated as proportional to the total investment cost by a relevant factor as generally assumed in process design textbooks (e.g. Seider et al. (Seider et al. 2010)). The process revenues, Rev , are provided by

the sales of levulinic acid, ethanol, succinic acid and electricity at market price (updated to September 2014). For the case of a combined use of different seasonal biomass types, *TAC* and *Rev* are the time averaged combination of the different values resulting for each of the biomass used.

4.11 Biomass feedstocks

An hardwood biomass was chosen as a representative lignocellulosic feedstock. This feedstock is a polysaccharide-rich material, with 66%wt of carbohydrate content (Sun & Cheng 2002). Biomass composition is reported in Table 5-1. The cellulose weight fraction is about 50%wt, the hemicellulose weight fraction is about 16%wt, and the lignin one is 28%wt. Other compounds (mainly oils, proteins, ashes) which cannot be exploited in the proposed biorefinery superstructure are present at 6%wt.

Eucalyptus residues (EU), wheat straw (WS) and olive tree pruning (OP) were chosen as representative feedstock from Southern Europe, as they are significantly available in relatively concentrated regions. Eucalyptus is a typical hardwood and fast growing tree (belonging to the *Rosid* clade), wheat is the classical example of an herbaceous crop (belonging to *Commelinids* clade), whereas olive tree is a slow-growing hardwood (belonging to the *Asterid* clade). These feedstocks are polysaccharide-rich materials, reaching 57% (EU), 68% (WS) and 62% (OP) of carbohydrate content (Silva-Fernandes, Duarte, Carvalheiro, Marques, et al. 2015). Biomass compositions are reported in Table 5-1. Cellulose (the main contribution of C6 sugars) weight fraction appears in decreasing order in eucalyptus, wheat straw and olive pruning, with values of 36%, 31% and 25% respectively. Wheat straw contains more hemicellulose than other biomass types (32%), while lignin is more present in eucalyptus (27%), so this biomass kind can produce more thermal energy than the others. Other compounds (mainly oils, proteins, ashes) which cannot be exploited in the proposed biorefinery superstructure are more present in olive pruning (34%).

Chapter 4

5. Results

5.1 Base case results

The MILP consisted in 2608 continuous variables, 1323 integer variables and 8482 equality and inequality constraints.

The resulting MILP was solved by means of AMPL software with IBM CPLEX optimization solver based on the simplex method and "branch & bound" or "branch & cut" methods (Biegler L.T., Grossmann I.E. 1997). The latter methods seek the MILP solution by first searching the solution of the corresponding "relaxed" linear programming problem with all real variables and then forcing one by one all the binary variables to assume either the value 0 or the value 1. Optimization model results were obtained using a workstation with an Intel Xeon 2 GHz CPU/8GB RAM.

5.1.1 Process flowsheets, biomass allocation and product yield

The optimal process flowsheet was sought for a biorefinery fed with hardwood assuming a feedstock flow rate of 50 t/h and 7200 plant operating hours per year. The hardwood composition and the main economic parameters for the optimization analysis are reported into Table 5-1. References for the model assumptions of each process sections are reported in Tables to 3-1, 3-3, 4-1.

Table 5-1: *Main parameters for the optimization model.*

Biomass	Hardwood
Plant Life (y)	20
Feedstock (t/h)	50
Cellulose (% dry)	50
Hemicellulose (% dry)	16
Lignin (% dry)	28
Other Compounds (% dry)	6
Levulinic Acid Price (\$/kg)	5.00
Succinic Acid Price (\$/kg)	7.50
Ethanol Price (\$/kg)	0.75
Biomass Price (\$/t)	40
Discount Rate (%)	8.00
Enzyme cost (\$/kg)	5.00
H ₂ SO ₄ cost (\$/kg)	0.08
HCl cost (\$/kg)	0.30
Ammonia cost (\$/kg)	0.40
Ca(OH) ₂ (\$/kg)	0.06
Electricity cost (\$/MWhe)	150
Octanol cost (\$/kg)	5.00
Taxes (%)	40
ΔT (°C)	40
ΔT_{MIN} (°C)	20

The optimal flowsheet obtained from the superstructure by maximizing the *NPV* is reported in Figure 5-1. The first significant result is that the biorefinery produces all the three possible substances levulinic acid, ethanol and succinic acid. Biomass allocation to products (kg of biomass used to obtain a product per kg of biomass feed) and product yield (kg of obtained product per kg of biomass feed) corresponding to the optimal flowsheet of Figure 5-1 are reported in Figures 5-2 to 5-3. Biomass allocation provides the mass distribution of biomass along the different process routes, but does not account for the yield of the single process steps. Succinic acid is the main product with a biomass allocation of 64% and a product yield of 6.8%. Biomass allocation and product yield to levulinic acid are about 16% and 1.1%, respectively.

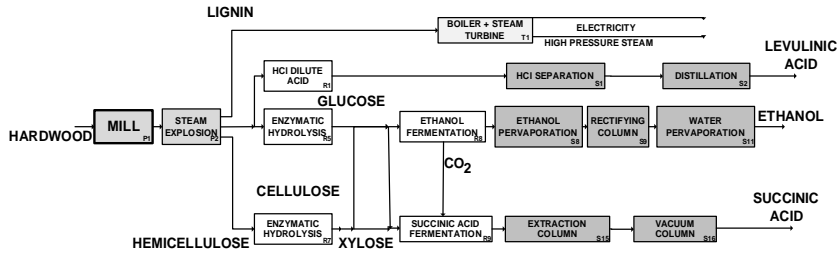


Figure 5-1: Optimal process flowsheet of the biorefinery.

Biomass allocation and product yield to ethanol are about 20% and 2.5%, respectively. These results highlight that the largest biomass allocation favours the production of the chemical with the highest selling price, succinic acid in this case. On the other hand, the production of levulinic acid turned out to be lower than that of ethanol despite levulinic acid selling price is more than five times more expensive than that of ethanol. This result can be explained considering that the maximization of NPV is not simply obtained by maximizing the revenues, but it takes into account both total annual cost and the initial total investment cost. Global yield, considering all the products, was about 10.5%.

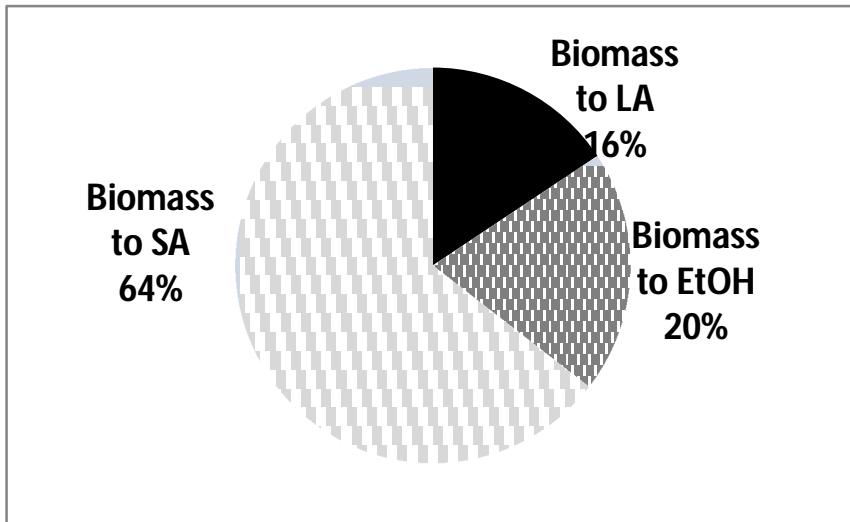


Figure 5-2: Biomass allocation for the lignocellulosic multi-product biorefinery.

A more accurate inspection of the flowsheet reported in Figure 5-1 reveals that the steam explosion (P2) was the optimal pretreatment process.

In fact, it has one of the highest yields in lignin, cellulose, and hemicellulose in spite of low capital costs. The optimal process route to levulinic acid consists in HCl acid hydrolysis (R1) of cellulose. HCl turns out to be a preferable catalyst than H_2SO_4 , because of the easier and, thus, more economical separation and recycle of the catalyst itself from levulinic acid stream. The HCl dilute acid reactor (R1) is able to perform both the reaction of cellulose to glucose and the reaction of glucose to levulinic acid at the optimal conversion. As a result, the second HCl levulinic acid reactor (R3) converting glucose to levulinic acid included in the superstructure is not present in the optimal flowsheet. Enzymatic hydrolysis (R5) and fermentation (R8-R9) were used for the production of succinic acid and ethanol. This pathway provides a mass integration solution since the CO_2 produced by the ethanol fermenter is exploited by the succinic acid fermenter. The enzymes for the enzymatic hydrolysis are purchased, because the enzyme purchase cost appear lower than the in situ manufacturing cost.

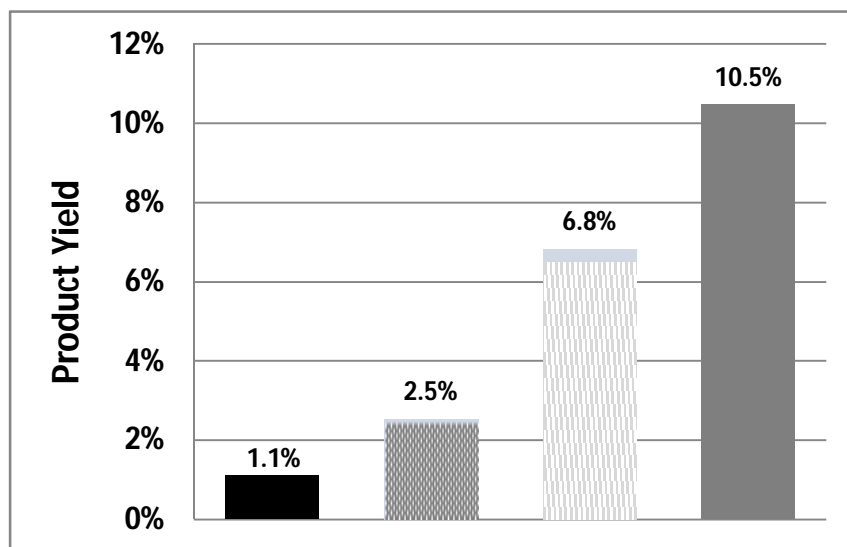


Figure 5-3: Product yields for the lignocellulosic multi-product biorefinery. Black: levulinic acid yield; Mesh grey: ethanol yield; Striped grey: succinic acid yield; Grey: total yield.

With concern to the separation and purification section, the 99%wt levulinic acid is obtained by a simple flash removing (S1)HCl catalysts and then, a distillation column (S2) separating volatile components like formic acid and water. Ethanol purification up to 99%wt is carried out by a sequence of a pervaporation membrane (S8) with water permeation, distillation column (S9)purifying ethanol up to the azeotropic composition and a pervaporation membrane (S11) with ethanol permeation. Pure succinic

acid (99% wt) was obtained by an extraction column (S15) with octanol and a purification section consisting in a vacuum distillation column (S16) and a crystallizer. This was the preferred pathways since the extraction column was less expensive than the reactive crystallization (S13) and thermal cracking pathway.

The lignin fraction optimal utilization is the burning in a traditional combustion unit (T2) with a boiler to produce high pressure steam. This result is mainly to be attributed to the higher capital costs of the alternative gasification process.

Heat integration resulted a very effective tool to minimize the utility costs of the biorefinery. The global exchanged heat in the integrated network of hot and cold process streams was about 14 MWt. This heat integration allowed to avoid about 25 t/h of LP/HP steam as hot utilities.

5.1.2 Economic and profitability analysis

Given the optimal flowsheet reported in Figure 5-1, the distribution of the total investment costs of the different plant sections is reported in Figure 5-5. In particular, the total investment of 184 M\$ is attributed for 43% to thermochemical conversion, for the 21% to hydrolysis and fermentation, for two equal portions of 17% each to pretreatment and to separations and purification, for 2% to heat integration with the heat exchanger network.

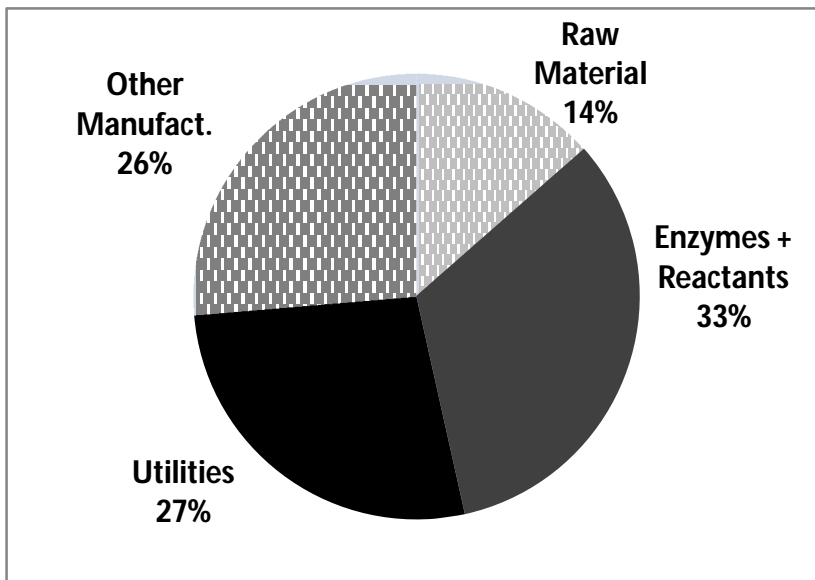


Figure 5-4: Manufacturing cost distribution for the lignocellulosic biorefinery.

The total annual cost distribution are reported in Figure 5-4. Inspection of the figure suggests that biomass raw materials, reactants and enzymes, utilities and other manufacturing costs cover 14%, 33%, 27% and 26% of the total, respectively. It appears, therefore, that reactants are the highest manufacturing costs and are mainly due to the enzymes purchase.

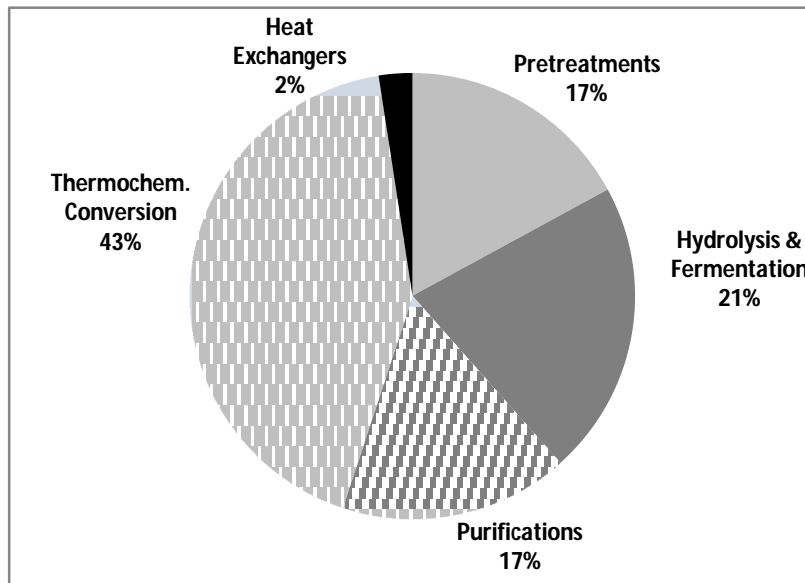


Figure 5-5: Capital cost distribution for the lignocellulosic biorefinery.

Approximate profitability measures of the investment are provided by the Return on investment, *ROI*, and the Payback period defined as follows:

$$ROI = \frac{(1 - t)(Rev - TAC)}{TIC} \quad (5-1)$$

$$PBP = \frac{TDC}{(1 - t)(Rev - TAC) + DP} \quad (5-2)$$

Where *TDC* is the total depreciable capital. Calculations provide a *ROI* of 35% and a PBP of 7 years.

More rigorous profitability measures are provided by the Net Present Value defined by equation 4-26 and representing the objective function of the optimization problem and by the Internal Rate of Return, *IRR*, given by the solution of the following equation:

$$\sum_{i=0}^{t_{fs}} \frac{CF_i}{(1+IRR)^i} = 0 \quad (5-3)$$

The maximized Net Present Value *NPV* obtained for the optimal flowsheet is 306 M\$. The corresponding *IRR* value is 29%.

5.2 Base case results with reactor modelling

The MINLP master problem included 2098 continuous variables and 23 binary variables and 1444 equality and inequality constraints. The resulting MILP after discretization consisted in 7106 continuous variables, 2092 integer variables and 11982 equality and inequality constraints.

The resulting MILP was solved by means of AMPL software with IBM CPLEX optimization solver based on the simplex method and "branch & bound" or "branch & cut" methods (Biegler L.T., Grossmann I.E. 1997). The latter methods seek the MILP solution by first searching the solution of the corresponding "relaxed" linear programming problem with all real variables and then forcing one by one all the binary variables to assume either the value 0 or the value 1. Optimization model results were obtained using a workstation with an Intel Xeon 2 GHz CPU/8GB RAM.

The optimal process flowsheet was sought for different case studies involving a biorefinery fed with hardwood and by assuming a feedstock flow rate of 50 t/h and 7200 plant operating hours per year. The hardwood composition and the main economic parameters for the optimization analysis are reported in Table 5-1. References for model assumptions regarding each process sections are reported in Tables 3-5. Firstly, the base case with the maximization of the Net Present Value was studied. Then, a sensitivity analysis was performed on the plant size and the main economic parameters. The economic parameters used in the base case are shown in Table 5-1.

5.2.1 Base case: maximization of the NPV

The optimal flowsheet obtained from the superstructure by maximizing the NPV is reported in Figure 5-6a. This flowsheet is equal to that obtained by means of the simplified model reported in the Part 1 of the paper. As a result, the biorefinery includes lines for all the three possible products, that is levulinic acid, ethanol and succinic acid. However, the distribution of the biomass allocation to products (kg of biomass in a certain product line per kg of biomass feed), reported in Table 5-2, and the product yields (kg of product per kg of biomass feed), reported in Table 5-2, are different with respect to those obtained by means of the simplified model reported the Part 1 of the paper. In particular, according to this complete model biomass allocation to levulinic acid (46%) and to succinic acid (42%) are comparable, while, as reported in Part 1, using a simplified model the allocation value of succinic acid was much higher (64%) than that of levulinic acid (20%). Considering yields, levulinic acid is the main product (8.9%), followed by succinic acid (5.7%) and ethanol (2.2%). This result can be explained considering that cellulose is the main component (50%) of the biomass and the levulinic acid process route can use only the cellulose fraction. Instead, process routes to ethanol and succinic acid exploit both glucose and xylose streams derived from cellulose and hemicellulose. Ethanol minor contribution to the revenues and thus to the maximization of the NPV causes a much lower production than the other two chemicals. Given this consideration, inspection of the flowsheet suggests that the flow rate of the produced ethanol is determined by the flow rate of the CO₂ necessary for the succinic acid fermentation. Global yield, considering all the products, is about 16.8%. This value is lower than the value of the yield to ethanol from hardwood biomass commonly found in the literature (about 24%) (Kazi et al. 2010). This discrepancy is due to lower yield values specific of the routes to succinic acid and levulinic acid.

The only significant difference in the optimal process flowsheet with respect to the application of the simplified model, presented in Part 1 of the paper, concerns the enzyme source for the enzymatic hydrolysis. In the case of the results reported in Figure 5-6a and Table 5-2, in fact, the enzymes come from a dedicated on site production section. The reason is that the local manufacturing cost turns out to be lower than the enzyme purchase cost. Instead, in the case of the simplified model of part 1 the optimal option was the purchase of the enzymes.

Heat integration resulted in a much more significant reduction of the required utilities. The global exchanged heat in the integrated network of hot and cold process streams was about 70 MWt. This heat integration allowed to avoid about 126 t/h of LP/HP steam as hot utilities.

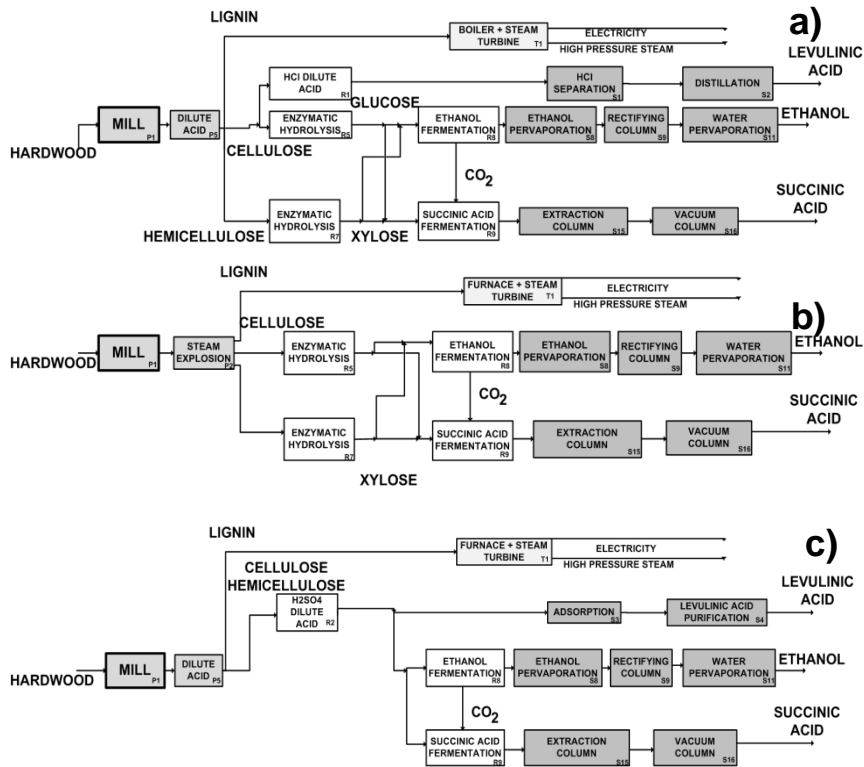


Figure 5-6: Optimal NPV flowsheets of biorefinery for base case and variants: a) base case; b) biomass feed rate 5 t/h (0.1 times the base case); c) levulinic acid selling price 7.50 \$/kg (+50% of the base case).

Figure 5-5 reports the distribution of the total investment cost (TIC) of the different plant sections corresponding to the optimal flowsheet reported in Figure 5-6. In particular, the total investment is 413.4 M\$ while it was only 184M\$ according to the simplified model reported in the Part 1 (Giuliano, Cerulli, et al. 2016). This result confirmed that rigorous reactor modelling taking into account the complete kinetic networks is necessary for the accurate design of these units and for the overall process optimization. The total investment cost is due to hydrolysis and fermentation for the 35%, to pretreatment for 26%, to thermochemical conversion for 20%, to separations and purification for 15%, to heat exchanger network for 4%. The highest cost of the hydrolysis and fermentation section includes also the enzyme production unit which contribute with about 30% of the section cost. Figure 10 reports the total annual cost distribution. Inspection of the figure suggests that biomass raw materials, reactants, utilities and other

Chapter 5

manufacturing costs cover 12%, 17%, 26% and 45% of the total, respectively.

The maximized Net Present Value *NPV* obtained for the optimal flowsheet is 677 M\$. The corresponding Internal Rate of Return, *IRR*, given by the solution of the following equation:

$$\sum_{i=0}^{t_{is}} \frac{CF_i}{(1 + IRR)^i} = 0 \quad (5-4)$$

turned out to be 25%.

5.2.2 Sensitivity analysis

5.2.2.1 Plant size

In general, the plant size and the production rate plays a significant role on the profitability of an industrial process. As a result, the effect of the plant size, in terms of the biomass feedstock rate, on the optimal flowsheet, biomass allocation and product yield was studied. The base case feedstock rate (50 t/h) was decreased and increased by a factor of 10. Biomass allocation, reported in Table 5-2, is the same for 50 and 500 t/h biomass feed rate. Instead, levulinic acid is not produced at all for a biomass feedstock rate of 5 t/h. As a result, a plant size threshold value should exist in the range 5-50 t/h to justify the existence of a levulinic acid production route. Consistently, the optimal flowsheet for the 5 t/h biomass feed rate (Figure 5-6b) does not include the process route to levulinic acid. Moreover, further inspection of the flowsheet reveals that steam explosion (P2) was selected as the most convenient pretreatment process. In fact, technologies with lower investment cost are preferred for a smaller plant size due to the effect of the economies of scale. Finally, it is worth pointing out that enzymes for the enzymatic hydrolysis (R5) are not produced in situ, but externally purchased. This difference with the flowsheet for 50 t/h biomass feed rate can be explained considering that for smaller plant size it is more convenient for the *NPV* maximization to reduce the investment cost for process units and increase the manufacturing cost.

Table 5-2 reports the results of the economic analysis as a function of the plant size. As expected, the plant size has a significant effect on the *IRR* and on the profit per mass unit of biomass. In fact, the ratio between the *NPV* and the total biomass fed to the plant during its lifetime turns out to be 26, 75 and

104 \$/t of biomass for the three plant size corresponding to biomass feed rates 5, 50 and 500 t/h. Of course, it is worth pointing out that in this analysis it was not considered at all that the biomass supply cost could vary significantly with the plant size. In fact, the larger is the amount of biomass to feed, the wider could be the geographical area of the suppliers. Thus, the mobilisation, the logistics as well as the wider and more differentiated sources could affect significantly the biomass cost depending on the scenario. This point, however, is beyond the scope of this work and deserves further studies.

5.2.2.2 Products selling price

A sensitivity on the product selling price was carried out in order to take into account the possible market fluctuations. A ± 50 % variation was considered and its effect on the optimal flowsheet, biomass allocation and product yield was assessed. Table 5-2 reports the biomass allocation for varying price of succinic acid and of levulinic acid, respectively. The values reported in Table 5-2 point out that by reducing the succinic acid price by 50%, the biomass allocation to levulinic acid increases up to about 90%. The residual 10% biomass is used for succinic acid and ethanol production. Instead, by increasing the succinic acid price by 50%, levulinic acid is not produced at all. This result is obtained also if the levulinic price decreases by 50% (Table 5-2). Instead, if the levulinic acid price increases by 50%, levulinic acid becomes the main product. This demonstrates once more that ethanol production is strictly linked to the succinic acid production for the CO₂ mass integration. The optimal flowsheet corresponding to this case is reported in Figure 5-6c. A significant difference with respect to previous flowsheet is that all the cellulose and hemicellulose are converted together in a H₂SO₄ dilute acid hydrolysis (R2). The latter produces levulinic acid for separation and purification and glucose and xylose for ethanol and succinic acid fermentation.

Table 5-2 reports also the results of the economic analysis obtained by varying the biochemicals selling prices. On the one hand, as expected the NPV increases with increasing both biochemicals price. On the other hand, the IRR increases with increasing succinic acid price and with decreasing levulinic acid price. This evidence can be explained considering that by increasing by 50% the succinic acid price, the revenues increase by about 30% while the total investment cost decreases by about 40%, due to the absence of the levulinic acid process route. Differently, by increasing by 50% the levulinic acid price, the revenues increase by about 100% while the TIC increases by more than 220%, due to the increase of the size of the levulinic acid production units.

Chapter 5

5.2.2.3 Discount rate

A sensitivity analysis was performed also on the discount rate r which is dependent on the economic scenario. As a result, the maximization of the Net Present Value was pursued for several values of r . This analysis was important for two reasons. The first was to take into account possible changes of this economic index. The second one, was to establish the dependence of objective function from this economic parameter.

The results are reported in terms of optimal NPV and corresponding IRR shown in Figure 5-7. As expected the NPV decreases with r . Differently, the IRR is not affected significantly by the discount rate for r values in the range 3-10%. While IRR increases with increasing discount rate between 12 and 15%. This result corresponds to the evidence that the optimal flowsheet turned out to be the same of the base case (Figure 5-6a) for r values in the range 3-10%. Instead, for r between 12 and 15% the optimal flowsheet does not include the production of levulinic acid as in the above mentioned cases of small plant size and of high succinic acid price. The corresponding optimal flowsheet is similar to that reported in Figure 5-6b. The levulinic acid process units were not present in the optimal solution to reduce the capital cost for the NPV maximization. In fact, the negative contribution of the TIC to the NPV is heavier for higher discount rate. On the whole, despite the NPV decreases, IRR increases due to the reduction of the TIC for r between 12 and 15%.

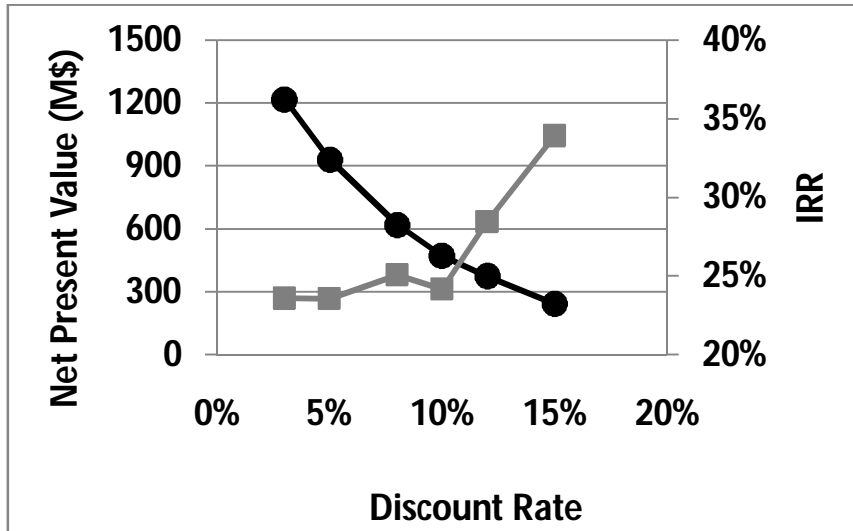


Figure 5-7: Objective function (net present value) and internal rate of return for each value of the discount rate. Net present value (●); internal rate of return (■).

5.2.3 Maximization of the IRR

In the previous section it was highlighted that the optimal flowsheet obtained by maximizing the *NPV* is affected by the discount rate, which is very dependent on the economic scenario and period. Differently, the internal rate of return *IRR* is not affected by the economic uncertainty in the long period term. As a result, in this final part of the work, the *IRR*, calculated according to Equation 5-4, was chosen as the objective function to maximize. The *IRR* maximization problem was addressed by using the iterative algorithm proposed by Pintaric and Kravanja (Pintarič & Kravanja 2006).

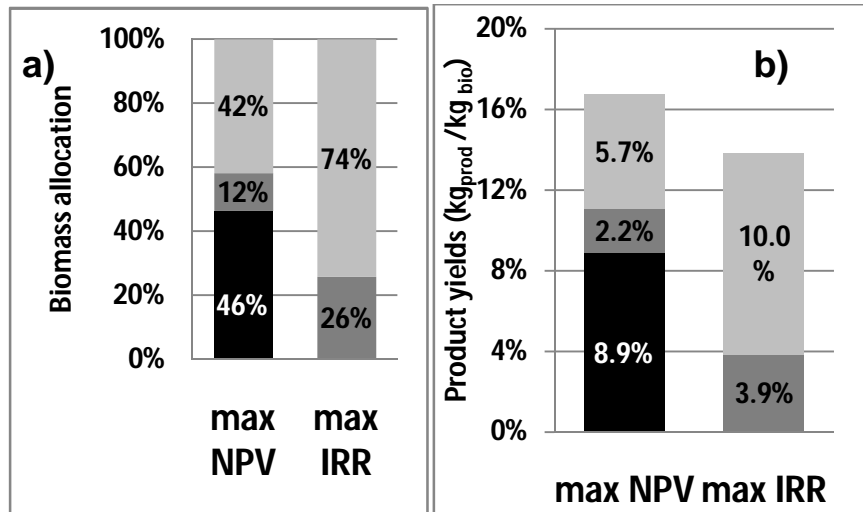


Figure 5-8: Biomass allocation (a) and product yields (b) for the base case by maximizing the net present value and the internal rate of return. Black: levulinic acid; dark grey: ethanol; light grey: succinic acid.

The optimal flowsheet obtained by maximizing the *IRR* is like that already reported in Figure 5-6b. This result corresponds to a biorefinery producing succinic acid and ethanol and no levulinic acid. As described above, the optimal flowsheet includes steam explosion (P2) for the biomass pretreatment and enzymatic hydrolysis (R5) to obtain the sugars. Enzymes are not produced in situ, but are purchased. This result can be explained considering that the *IRR* maximization provides optimal flowsheets which minimize the investment costs (Kasaš et al. 2011). As a result, parallel process routes which require additional process units are often cancelled and pathways allowing less pieces of equipment with a larger size are selected by the optimization algorithm. Thus, the most significant effect in the biorefinery flowsheet is the elimination of the levulinic acid production. Biomass allocation values and product yield values obtained by *IRR* maximization are reported in Figure 5-8 for the sake of comparison with the values obtained by *NPV* maximization. Biomass allocation to succinic acid and to ethanol is 74% and 26%, respectively (Figure 5-8a). The global product yields is 13.9% and is lower than that for maximum *NPV* (16.8%). In particular, the succinic acid yield is 10% and the ethanol yield is 3.9%. This result can be explained by considering that higher *IRR* can be obtained with lower revenues (lower productivity) and lower *TIC*.

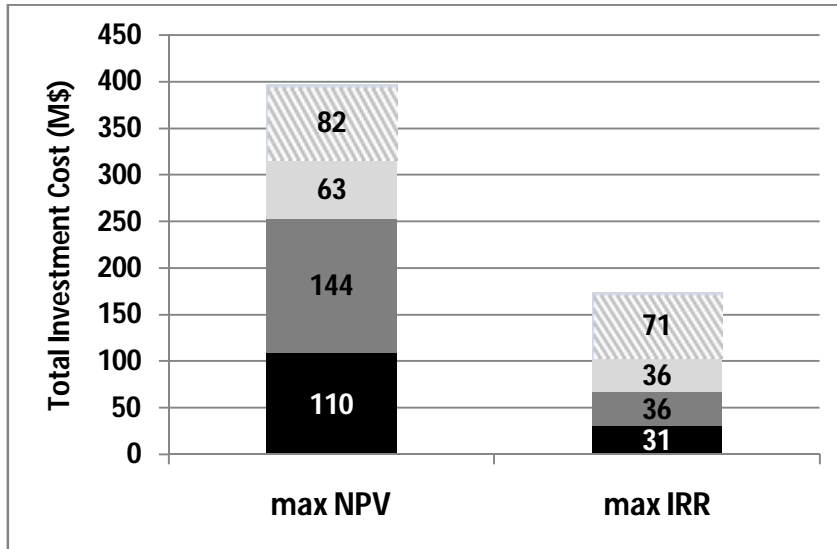


Figure 5-9: Capital cost for the lignocellulosic biorefinery by maximizing the net present value and the internal rate of return. Black: pretreatment section; dark grey: hydrolysis and fermentation section; light grey: separation and purification section; striped grey: thermochemical conversion section.

Figure 5-9 reports the *TIC* for the two economic objective functions. It is confirmed that, using the *IRR* as objective function, lower *TIC* values are obtained. This result agrees also with the general finding by Kasas et al. (2011) that the maximization of *IRR* is significantly related to the minimization of *TIC*. Conversely, the maximization of *NPV* determines a larger production plant with higher revenues and, thus, with higher *TIC*.

For the *IRR* maximization case a lower total product yield value corresponds to process units with smaller size in the pretreatment, hydrolysis and fermentation, separation and purification sections. This determines lower *TIC*. In particular, *TIC* required for the lignocellulosic biorefinery by maximizing *NPV* are 413 M\$, while less than half this value (179 M\$) was obtained by maximizing *IRR*. This significant reduction corresponds to three main differences in the process flowsheet:

- No acid hydrolysis section and levulinic acid purification section;
- Steam explosion (P2) as pretreatment instead of dilute acid (P5);
- No enzyme production section.

Table 5-2: Sensitivity results of the economic analysis on plant size and biochemicals selling price by maximizing the net present value

	No reactor sizing base case	Base case	Effect of plant size		Effect of succinic acid price		Effect of levulinic acid price	
Biomass feedstock rate(t/h)	50	50	5	500	50	50	50	50
Succinic acid Price (\$/kg)	7.50	7.50	7.50	7.50	3.75	11.25	7.50	7.50
Levulinic acid Price (\$/kg)	5.00	5.00	5.00	5.00	5.00	5.00	2.50	7.50
Biomass allocation to Levulinic acid (%)	16	46	0	46	90	0	0	86
Ethanol (%)	20	12	26	12	4	26	26	5
Succinic acid (%)	64	42	74	42	6	74	74	9
Yield to Levulinic acid (%)	1.1	8.9	0.0	8.9	13.4	0	0	22.2
Ethanol (%)	2.5	2.2	3.9	2.1	1.0	3.9	3.9	1.3
Succinic acid (%)	6.8	5.7	10.0	5.7	1.2	10.0	10.0	2.3
Total (%)	10.5	16.7	13.9	16.7	15.6	13.9	13.9	25.9
Total Investment Cost (M\$)	184	413	35	2412	338	249	231	1319
Total Annual Cost (M\$/y)	123	118	18	904	125	120	122	236
Rev (M\$/y)	231	319	28	3202	259	416	280	666
IRR (%)	29	25	14	40	20	47	31	16

NPV (M\$)	306	620	19	9036	358	1215	570	957
-----------	-----	-----	----	------	-----	------	-----	-----

Figure 5-10 reports the comparison of the total annual cost, *TAC*, distribution for the two economic objective functions. Inspection of the figure suggests that the costs for enzymes and reactants are higher for the case without levulinic acid production. In fact, enzymes used in the hydrolysis of the process routes to ethanol and succinic acid are more expensive than the acid used in the levulinic acid production. Differences in other manufacturing costs values, mainly consisting in labour and maintenance costs, are related to *TIC* different values. In particular, maintenance costs were estimated as 10% of total investment cost.

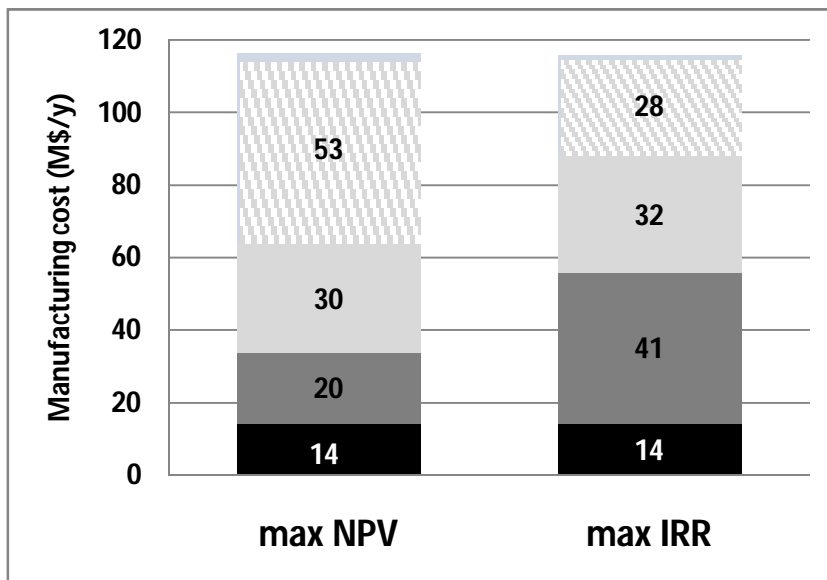


Figure 5-10: Cost distribution for the lignocellulosic biorefinery by maximizing the net present value and the internal rate of return. Black: raw material cost; dark grey: enzymes and reactants cost; light grey: utility cost; striped grey: other manufacturing cost.

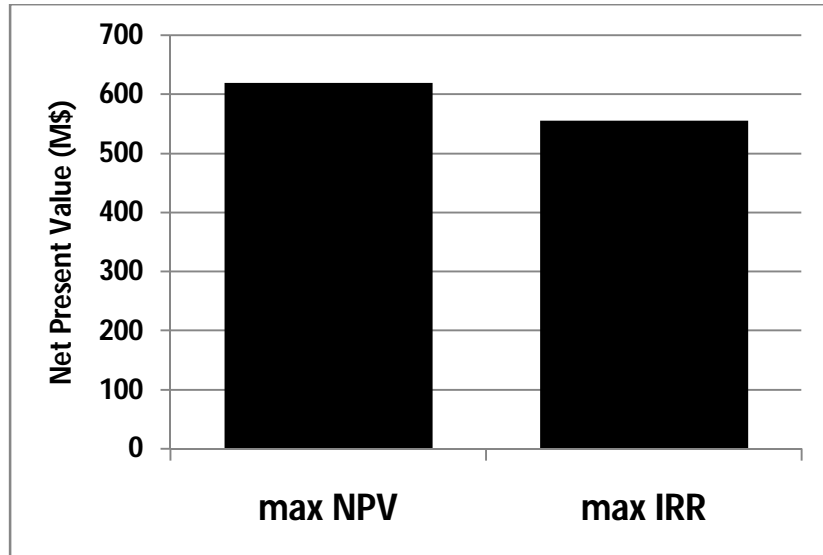


Figure 5-11: *Net present value for the lignocellulosic biorefinery by maximizing the net present value and the internal rate of return.*

Figure 5-11 reports the comparison between the *NPV* obtained for the optimal flowsheet with maximum *NPV* and the *NPV* obtained for the optimal flowsheet with maximum *IRR*. In both cases an 8% annual discount rate is applied to calculate *NPV*. In particular, the maximum *NPV* turned out to be 620 M\$, while the *NPV* for maximum *IRR* was 556 M\$. Consistently, *IRR* was 25%, and 36% by maximizing *NPV* and *IRR*, respectively.

6 Results for biomass type and seasonality

The resulting MILP was solved by means of AMPL software with IBM CPLEX optimization solver based on the simplex method and "branch & bound" or "branch & cut" methods(Biegler L.T., Grossmann I.E. 1997). These latter methods seek the MILP solution by first searching the solution of the corresponding "relaxed" linear programming problem considering all the variables (x and y) as real and then forcing one by one all the binary variables y to assume either the value 0 or the value 1. Optimization model results were obtained using a workstation with an Intel Xeon 2 GHz CPU/8GB RAM. The resulting MILP consisted in 7106 continuous variables, 2092 integer variables and 11982 equality and inequality constraints for the case studies with a single biomass feedstock and in 12198 continuous variables, 2171 integer variables and 17492 equality and inequality constraints for the case studies with a combined biomass feedstock.

Table 6-1: *Biomass price and composition (from Silvia-Fernandes et al, 2015a).*

Biomass composition (dry base mass, %)	Eucalyptus	Wheat straw	Olive pruning
Cellulose	36	31	25
Hemicellulose	24	32	19
Lignin	27	17	22
Other Compounds	13	20	34
Biomass Price (\$/t)	60	50	45

6.1 Process flowsheets, biomass allocation and product yield

The optimal process flowsheet was sought for different case studies. Firstly, the case of a biorefinery with the same biomass feedstock for the whole year was considered. Then, the tree alternative biomass types considered, namely eucalyptus, wheat straw, and olive pruning were used in the calculations. As above mentioned, these three cases were referred to as EU, WS and OP. Finally, a combined use of the three biomass types according to their seasonal availability during the year was studied. In particular, two different case studies were analyzed: in the first one it was assumed that each of the three biomass types was available for four months in a year. This case was referred to as SB. In the second one we assumed that eucalyptus was available all the year long while wheat straw and olive pruning were available four months each. Namely, eucalyptus was the only feedstock for four months in a year while a mix of eucalyptus and of a second biomass was used for the rest of the year (i.e. eucalyptus and wheat straw for four months and eucalyptus and olive pruning for four months). This case was referred to as SC. Since the relative quantities of the two biomass types used contemporarily are not fixed, the amounts of WS and of OP in the mix with EU for each of the two four months period of co-feeding are two additional degrees of freedom in the optimization problem.

For all the case studies, a feedstock of 50 t/h and 7900 plant operating hours per year were assumed. The main plant operating data and the economic parameters for the optimization analysis are reported in Table 5-1.

The optimal flowsheets obtained from the superstructure by maximizing the *NPV* are reported in Figures 6-1, 6-2 for the five case studies. Inspection of the flowsheets reveal some common features for all the cases: a) dilute acid pretreatment results to be the optimal pretreatment operation; b) in the hydrolysis and fermentation section the preferred hydrolysis is the enzymatic one and the production of succinic acid is always present with ethanol fermentation at its side for the production of the necessary CO₂; c) in the purification section succinic acid purification is treated by extraction by octanol combined with vacuum distillation and crystallization; d) in the thermochemical section lignin is thermally converted in a traditional burner with a boiler to produce high pressure steam.

6 Results for biomass type and seasonality

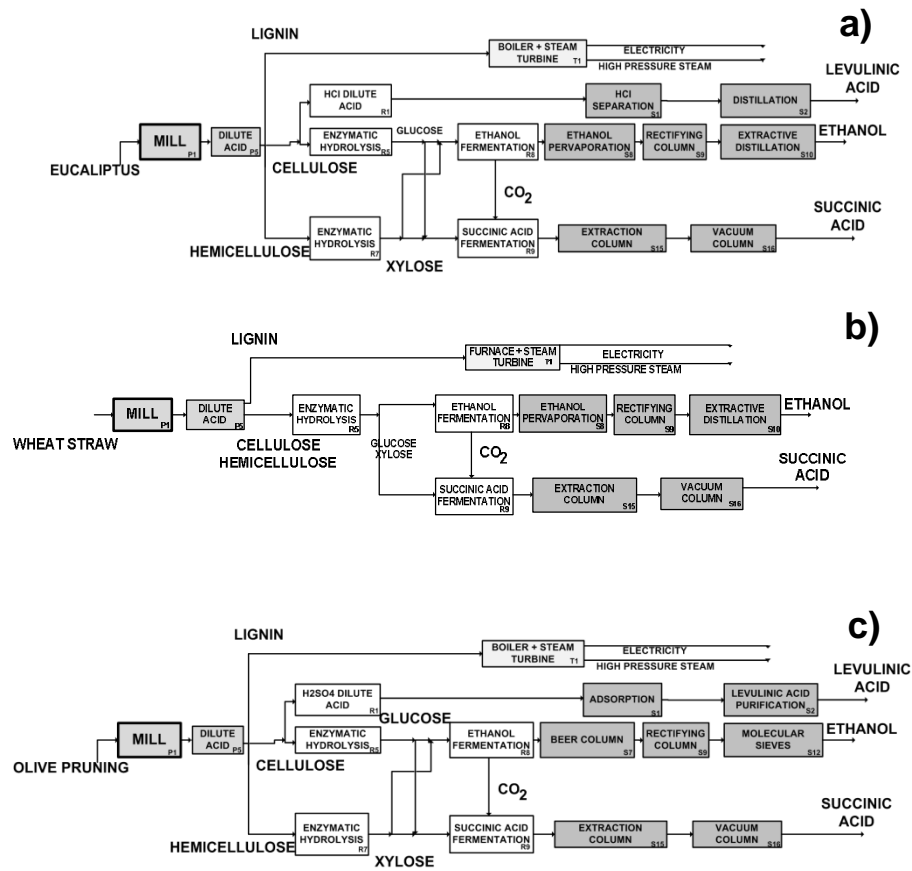


Figure 6-1: Optimal flowsheet using net present value as objective function. a) for eucalyptus; b) for wheat straw; c) for olive pruning.

The main difference between the optimal flowsheets consists in the absence of levulinic acid production for the case of wheat straw. This result is due to the higher content of hemicellulose in wheat straw and, thus, to the higher amount of obtainable xylose. In fact, the constraint on feed ratio of fermenters (glucose/xylose larger than 1) determines that all the glucose is used with the xylose in the fermentations of ethanol and succinic acid. Differently, in the other case studies with eucalyptus and olive pruning there is an excess of glucose that allows also the production of levulinic acid by means of dilute acid hydrolysis of cellulose.

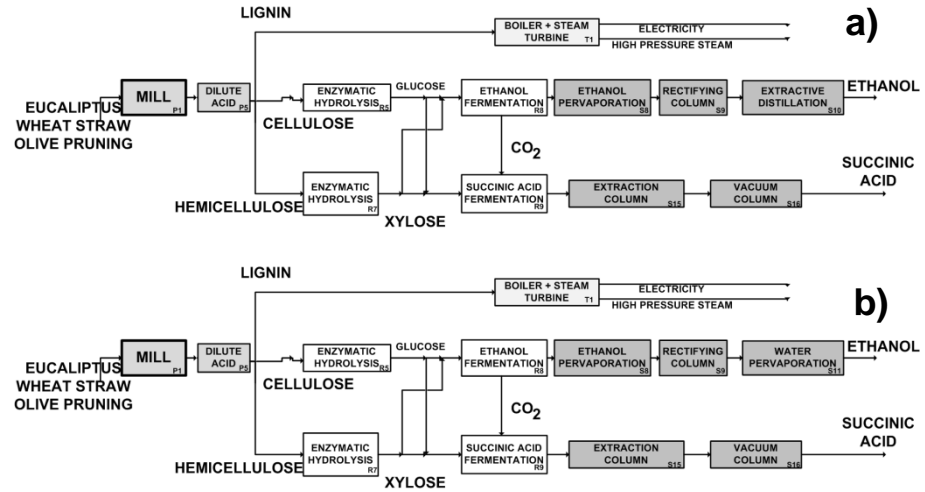


Figure 6-2: Optimal flowsheet for the season-based biorefinery using net present value as objective function. a) case SB: three periods with a single biomass feedstock each; b) case SC: 1st period with eucalyptus, 2nd period with eucalyptus and wheat straw, 3rd period with eucalyptus and olive pruning.

In the eucalyptus case we find that cellulose hydrolysis is carried out with HCl and this forces also the choice of the relevant separation steps. Instead, in the the olive pruning case, the dilute acid hydrolysis with H₂SO₄ and adsorption are the best pathway to the levulinic acid production. Another difference concerns the enzymatic hydrolysis. In particular, when the optimization results provide the same value of the glucose/xylose feed ratio to both the ethanol fermenter and the succinic acid fermenter, a single enzymatic hydrolysis unit for cellulose and hemicellulose is obtained. Instead, when different feed ratio values result for the two fermentation units, two parallel enzymatic hydrolysis units are required for cellulose and hemicellulose. In this way, in fact, the glucose/xylose ratio can be adjusted freely by splitting and mixing the separate glucose and xylose streams.

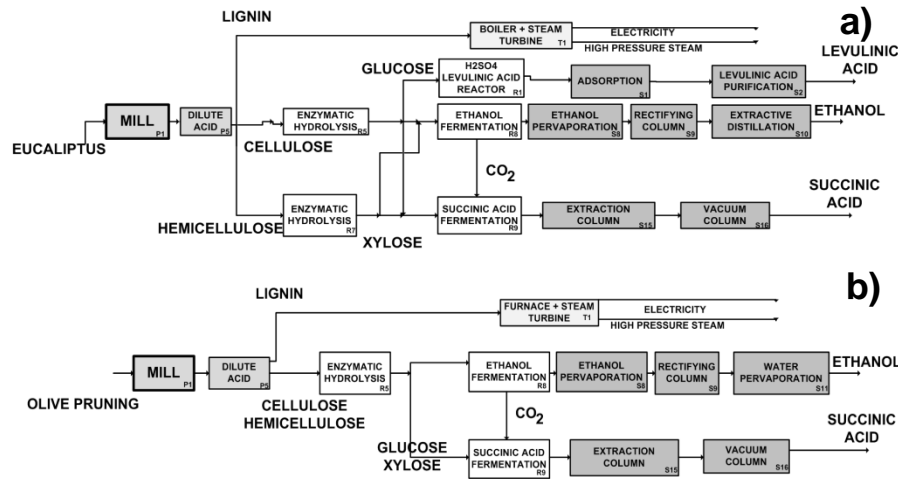


Figure 6-3: Optimal flowsheet using internal rate of return as objective function. a) for eucalyptus; b) for olive pruning.

Other differences are present in the ethanol process section. The same ethanol purification methods result for wheat straw and eucalyptus. In particular, pervaporation membranes and three distillation columns (a rectifying column and two columns for the extractive distillation) are used to reach ethanol 99%. Instead, in the olive pruning case, two distillation columns (beer column and rectifying column) are used to reach the azeotropic composition and then molecular sieves are used for the final purification. In particular, when the flowrate of ethanol is higher (for EU and for WS), pervaporation is preferred because of scale economies reducing the capital cost. Differently when the ethanol flowrate is lower (for OP) a first beer column and a second rectifying column are optimal, because the manufacturing costs are prevailing over the capital costs.

Optimization results for the cases with a single biomass type showed that the highest NPV was obtained for eucalyptus. Consequently, if we considered the mixed amount of two biomass types as a degree of freedom for the case study SC, the optimization analysis would yield 100% eucalyptus (EU). For this reason, a 50%wt amount of eucalyptus was assumed as a reasonable value to assess the effect of co-feeding on the optimal flowsheet and biomass allocation. The SB and SC case studies with a combined use of the three biomass types provide optimal flowsheets without levulinic acid production, similarly to the case WS, relative to the wheat straw as single feedstock. Both the SB and the SC case studies result to have cellulose and hemicellulose enzymatic hydrolysis in two parallel units supplying separate streams of glucose and xylose respectively similarly to the EU and OP single feedstock case studies. The only difference between

SB and SC consists in the final purification unit for the ethanol (extractive distillation for SB and pervaporation for SC). Since the ethanol concentration in the distillate stream of the rectifying column is fixed, the reason for the different purification process in the two cases should be searched in the ethanol flowrate. In fact, it ought to be recalled that, according to Equation 4-34, the size of each unit in the SB and SC cases is constrained to be the largest size value of the three required during the three four months periods. Consequently, the size of the final purification unit for the ethanol is determined by the largest ethanol flowrate during the year. According to the results of product yield reported in Figures 6-4 and 6-5, the largest ethanol flowrate is obtained during the first period with total EU feed for both SB and SC cases. In particular, the ethanol yield in this condition is 4.1%, corresponding to 2.05 t/h ethanol flowrate, for the SB case and 3.8%, corresponding to 1.9 t/h ethanol flowrate, for the SC case. As a result, this difference in the ethanol flowrate determines the more economically convenient unit operation for the final purification between extractive distillation and membrane pervaporation for the SB and the SC cases.

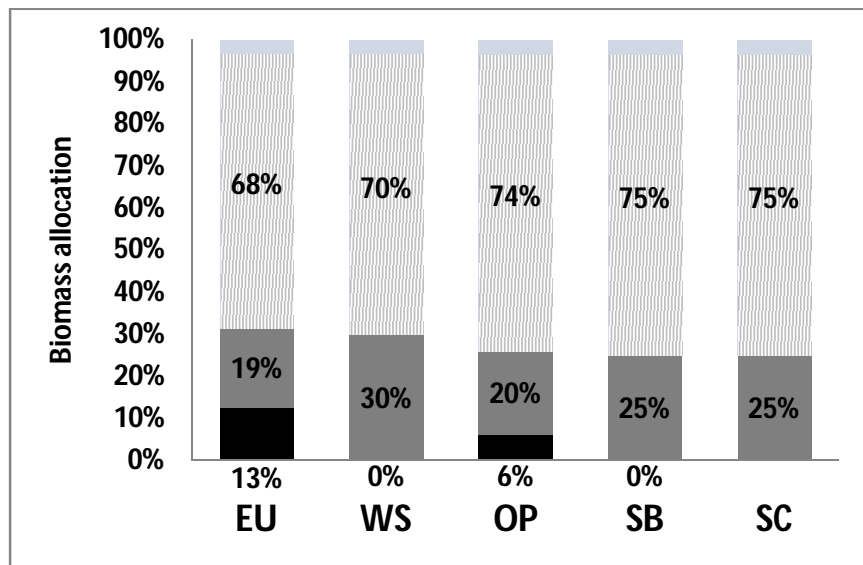


Figure 6-4: Biomass allocation (kg of biomass used to obtain a product / kg of biomass feed) using net present value as objective function. Black: biomass to levulinic acid; Grey: biomass to ethanol; Striped: biomass to succinic acid.

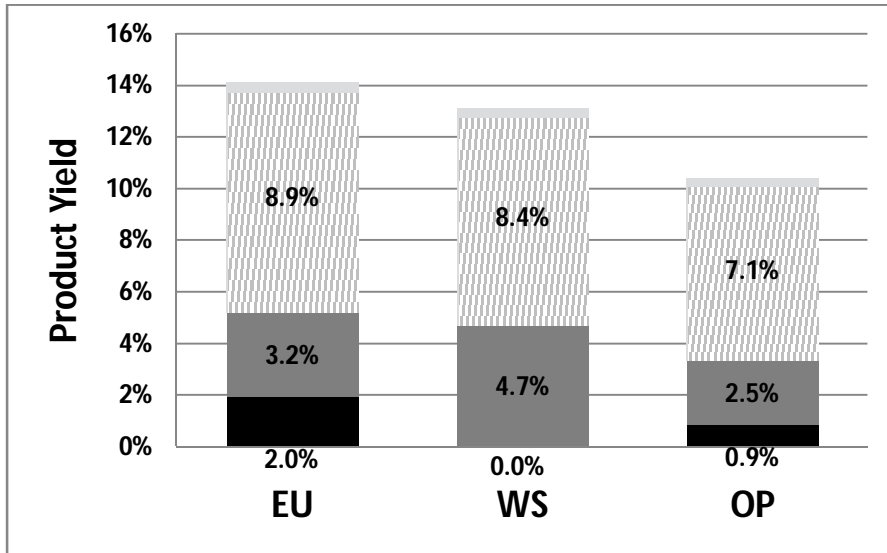


Figure 6-5: Product yields using the net present value as objective function. Black: levulinic acid yield; Grey: ethanol yield; Striped: succinic acid yield.

The biomass allocation to products (kg of biomass used to obtain a product per kg of biomass feed) and product yield (kg of obtained product per kg of biomass feed) corresponding to the optimal flowsheets of Figures 6-1 and 6-2 are reported in Figure 6-4, 6-5. It is worth noting that the biomass allocation provides the mass distribution of biomass along the different process routes, but, differently from product yield, does not account for the yield of the single process steps. Succinic acid is the main product for all the case studies with a biomass allocation between 68% and 75% (Figure 6-4) and a product yield between 7.1% and 9.4% (Figures 6-5, 6-6, 6-7). This is due to the higher value of succinic acid than of the other products. The biomass allocation and the product yield to ethanol vary between 19% and 30% and between 2.5% and 4.7%, respectively. Lower biomass allocation (between 6% and 13%) and product yield (between 0.9% and 2%) to levulinic acid are obtained for olive pruning and eucalyptus. For the wheat straw case study, levulinic acid is not produced at all. The overall product yield, calculated as the sum of the product yield to ethanol, succinic acid and levulinic acid, is 14.1% for eucalyptus, 13.1% for wheat straw, 10.5% for olive pruning. These values are related to the cellulose and hemicellulose content of the biomass.

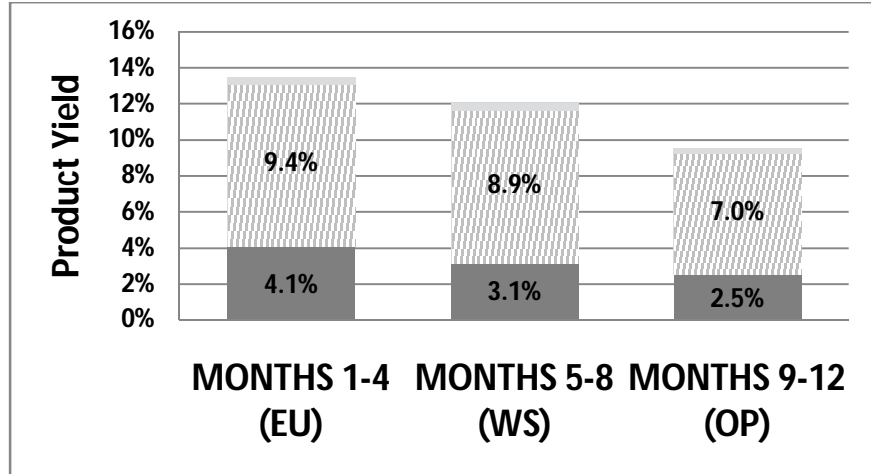


Figure 6-6: Product yields using the net present value as objective function for the case with a single biomass feedstock. Black: levulinic acid yield; Grey: ethanol yield; Striped: succinic acid yield.

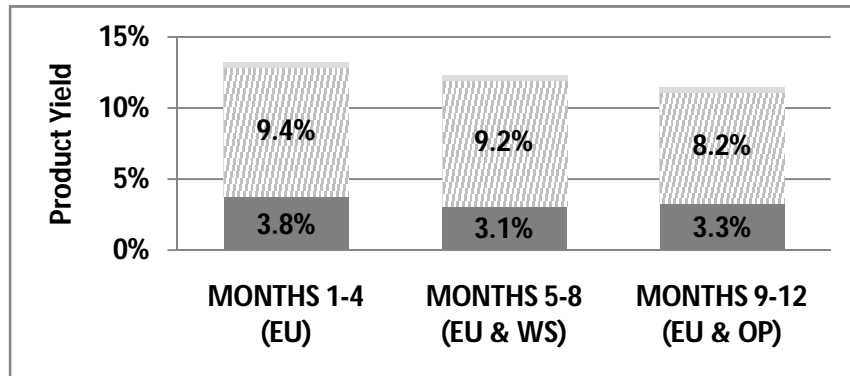


Figure 6-7: Product yields using the net present value as objective function for 1st period with eucalyptus, 2nd period with eucalyptus and wheat straw, 3rd period with eucalyptus and olive pruning. Black: levulinic acid yield; Grey: ethanol yield; Striped: succinic acid yield.

For the combined SB and SC case studies the product yield distribution obtained for each period of the year is reported in Figures 6-6 and 6-7. These figures show that, coherently with the flowsheets of Figures 6-1 and 6-2 in the SB and SC case only succinic acid and ethanol are produced as in the single biomass case with wheat straw. The yields to succinic acid and to ethanol with the same optimal flowsheet are different in the three periods of the year depending on the used biomass feedstock. As a result, the overall productivity of the plant varies during the three periods provided a constant

biomass feed rate. In particular, the highest product yields were obtained for the period with EU and the lowest values for the period with OP. These results are in qualitative agreement with those obtained for the three case studies with a single biomass feedstock for the whole year (Figure 6-5), but the yield values are different. This can be explained considering that the product yield is a function of both the biomass composition and the process flowsheet. In fact, the optimal flowsheets of the three cases with a single biomass (Figure 6-1) are different from that of the combined case SB (Figure 6-2a).

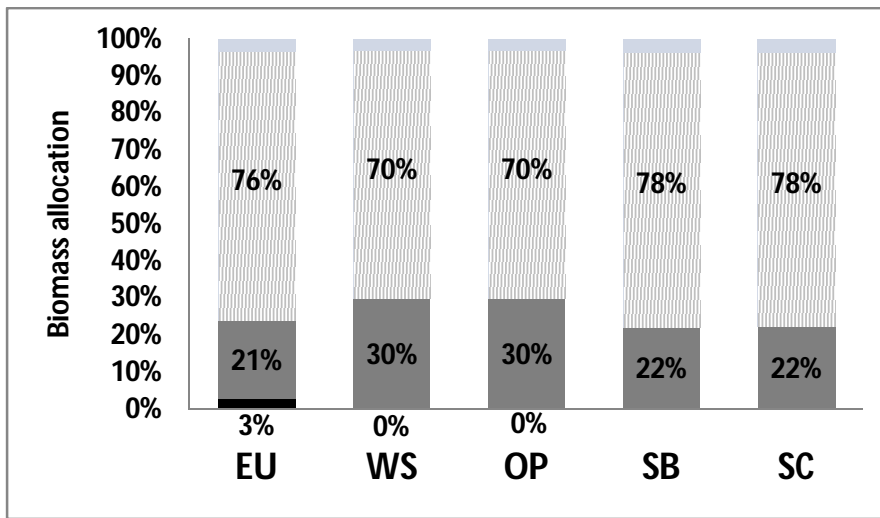


Figure 6-8: Biomass allocation (kg of biomass used to obtain a product / kg of biomass feed) using the internal rate of return as objective function. Black: biomass to levulinic acid; Grey: biomass to ethanol; Striped: biomass to succinic acid.

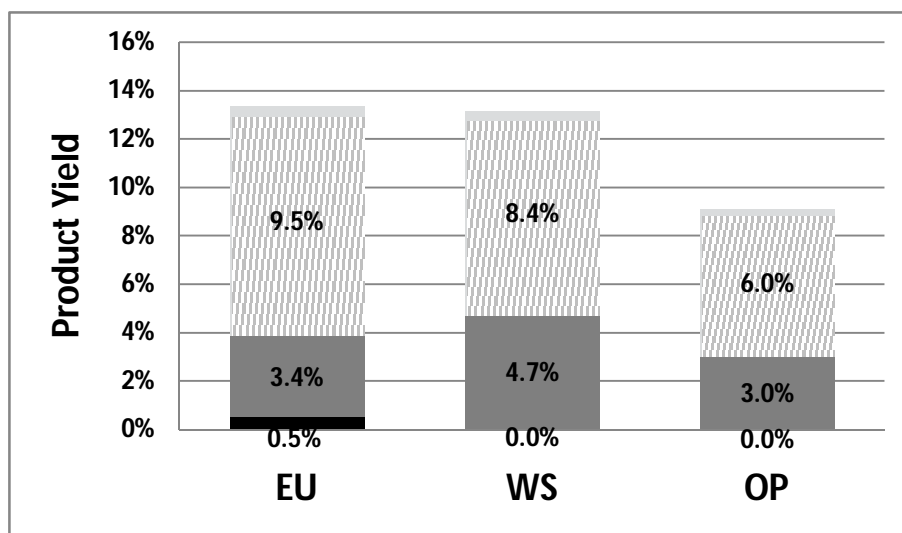


Figure 6-9: Product yields using the internal rate of return as objective function. Black: levulinic acid yield; Grey: ethanol yield; Striped: succinic acid yield.

Optimization with the internal rate of return as the objective function gives an optimal flowsheet which minimizes the investment costs (Kansas et al., 2011). As a result, parallel process routes which require additional process units are often cancelled and pathways allowing less pieces of equipment with a larger size are selected by the optimization algorithm. The most significant effect in the biorefinery flowsheet (Figure 6-3) is the reduction or even the elimination of the levulinic acid production. In fact, the biomass allocation to levulinic acid for maximum *IRR* (reported in Figure 6-8) indicates the decrease of the value for eucalyptus from 13% to 3% and for olive pruning from 6% to 0%. Figure 6-3a and 6-3b reports the optimal flowsheets maximizing *IRR* for eucalyptus and olive pruning, respectively. For the eucalyptus case study a comparison between Figure 6-1a and 6-3a reveals that by maximizing the *IRR* the dilute acid hydrolysis disappears and the much smaller levulinic acid stream is produced by a dedicated reactor converting glucose. This change is due to a forced decrease of the capital costs in the *IRR* optimized solution for which capital cost has a larger weight, than in the *NPV* optimized solution. As discussed above, this is due to the higher interest rates resulting in the *IRR* optimum than in the *NPV* optimum. Similar considerations can be made for the olive pruning case study, with reference to which, the comparison between Figure 6-1c and 8b suggests that the optimal flowsheet for a maximum *IRR* has a single

enzymatic hydrolysis unit for cellulose and hemicellulose (as in the wheat straw case study Figure 6-1b) and does not have any process pathway to levulinic acid. Also in this case this result is forced by a need of reduction of the investment costs. The single enzymatic hydrolysis unit for cellulose and hemicellulose is the only change for the SB case study when the maximum *IRR* is sought. The optimal process flowsheet with maximum *IRR* for wheat straw and for SC case studies are equal to those with maximum *NPV* reported in Figure 6-1b and Figure 6-2b respectively. Finally, inspection of Figures 6-9, 6-10, 6-11 reporting the product yields for maximum *IRR* reveals a general decrease of the values obtained for this parameter. This result can be explained by considering that maximum *IRR* can be obtained with lower revenues and lower total investment costs than with the maximum *NPV*.

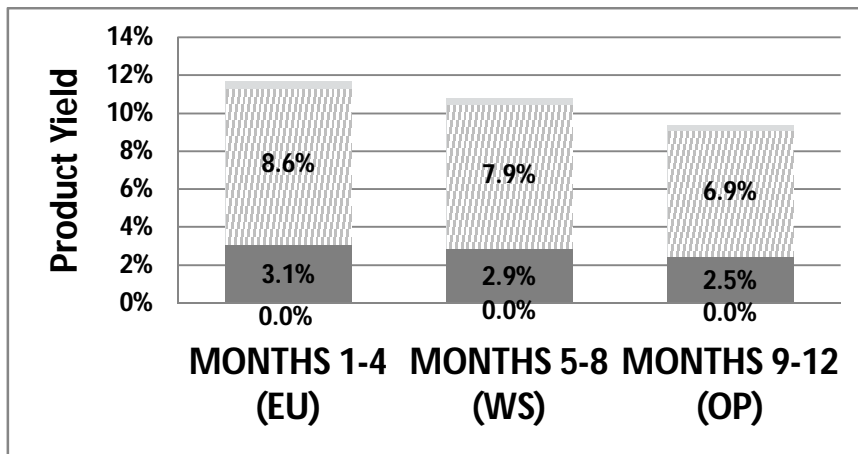


Figure 6-10: *Product yields using the internal rate of return as objective function for the case with a single biomass feedstock. Black: levulinic acid yield; Grey: ethanol yield; Striped: succinic acid yield.*

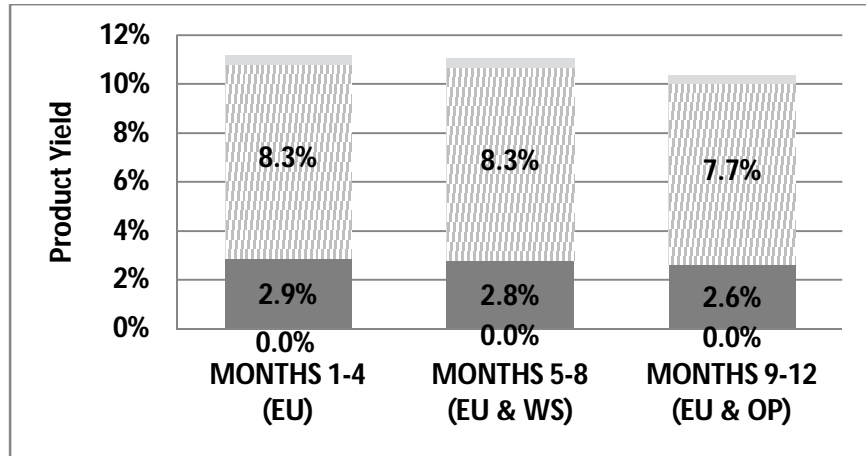


Figure 6-11: Product yields using the internal rate of return as objective function for 1st period with eucalyptus, 2nd period with eucalyptus and wheat straw, 3rd period with eucalyptus and olive pruning. Black: levulinic acid yield; Grey: ethanol yield; Striped: succinic acid yield.

6.2 Economic and profitability analysis

Figure 6-12 reports the total investment costs resulting for the five case studies with the two economic objective functions. It is confirmed that, using the *IRR* as the objective function, lower *TIC* values are obtained. This result agrees also with the general finding by Kansas et al. (2011) that the maximization of *IRR* is significantly related to the minimization of *TIC*, conversely the maximization of *NPV* implies larger production plants with higher revenues and, thus, with larger *TIC*. Further inspection of Figure 6-12 reveals that maximizing *NPV* lower *TIC* are recorded for wheat straw. This is mainly due to the lower lignin content of wheat straw which implies lower investment cost of the thermal process section. Differently, by maximizing *IRR* the lowest *TIC* are obtained for olive pruning. In this case, a lower total product yield value, as reported in Figures 6-9, 6-10, 6-11, corresponds to process units with smaller size in the sections of pretreatment, hydrolysis and fermentation, separation and purification. This determines lower *TIC*. Higher *TIC* values are obtained for the SB and SC case studies since the larger size value is assumed for each unit processing different biomass types over the year periods as formulated by the inequality constraints 4-34.

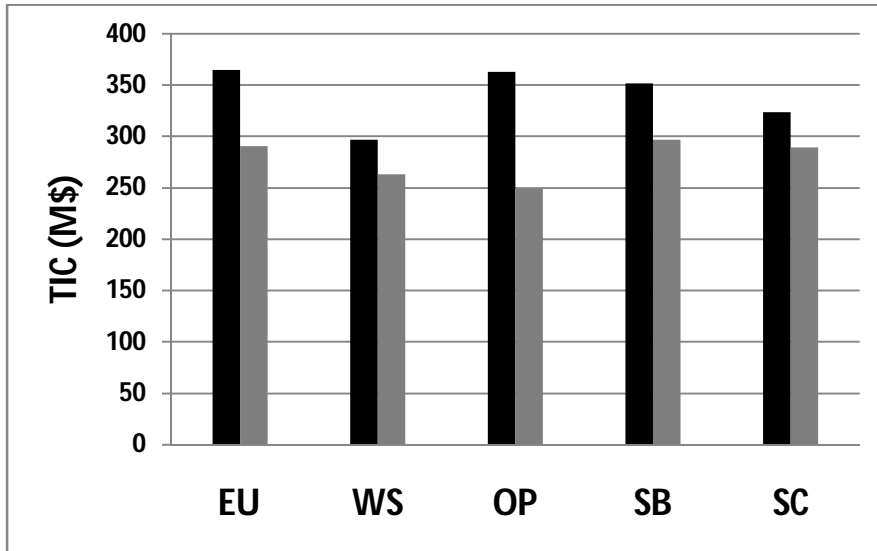


Figure 6-12: Total investment cost using as objective function: net present value (black bar), internal rate of return (grey bar).

Figure 6-13 reports the total annual cost distribution for the five case studies with maximum NPV. Inspection of the figure suggests that the costs for enzymes and reactants are higher for the cases without levulinic acid production, namely WS, SB and SC. In fact, enzymes used in the hydrolysis of the process routes to ethanol and succinic acid are more expensive than the acid used in the levulinic acid production. External utility costs are higher for wheat straw due to the lower lignin content which provides thermal energy used by the biorefinery. Differences in other manufacturing costs values, mainly consisting in labour and maintenance costs, are related to different values of the TIC.

Figure 6-14 shows the comparison between the net present value obtained for the optimal flowsheets with maximum NPV and the net present value obtained for the optimal flowsheets with maximum IRR. In both cases an 8% annual discount rate is applied to calculate NPV. The ranking of single biomass kinds based on the obtained NPV yields in increasing order olive pruning, wheat straw and eucalyptus. For the combined use of the three seasonal biomass the highest NPV is obtained for the SC case study in which eucalyptus is processed all over the year and the other two biomass on a seasonal basis. This NPV is comparable to that obtained for the biorefinery processing eucalyptus only. The largest difference between the NPV for maximum NPV and the NPV for maximum IRR is observed for olive pruning).

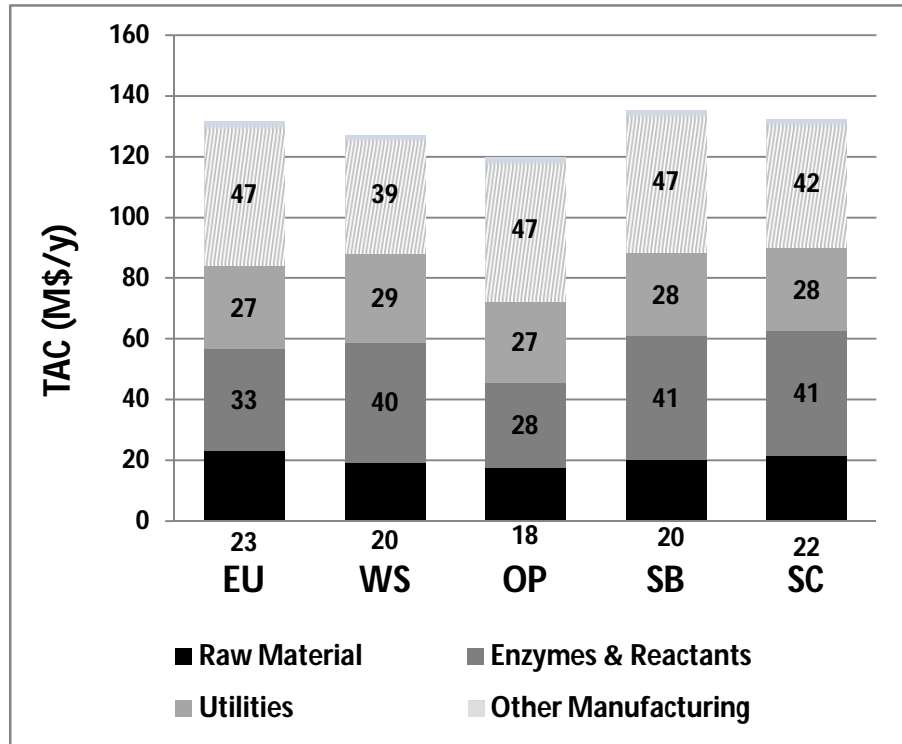


Figure 6-13: Total annual cost distribution using the net present value as objective function.

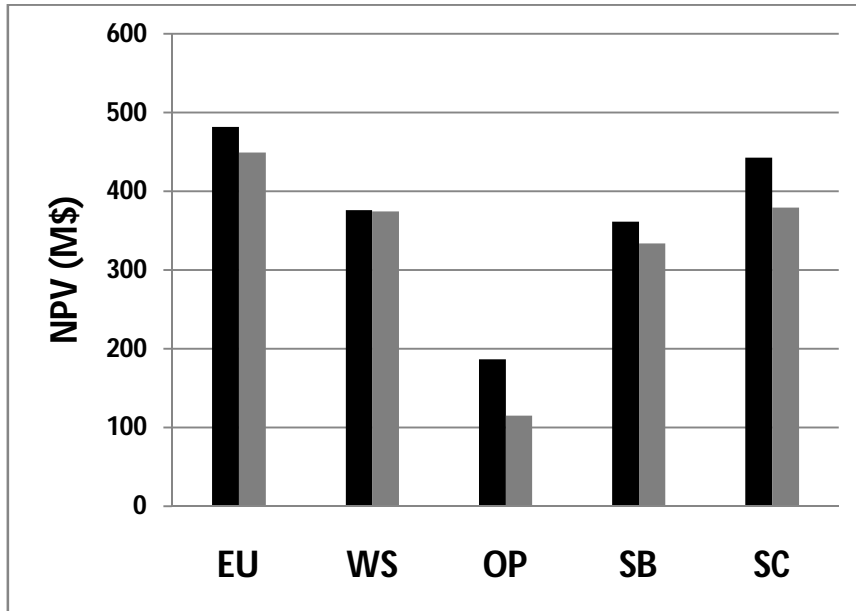


Figure 6-14: Net present value using as objective function: net present value (black bar), internal rate of return (grey bar)

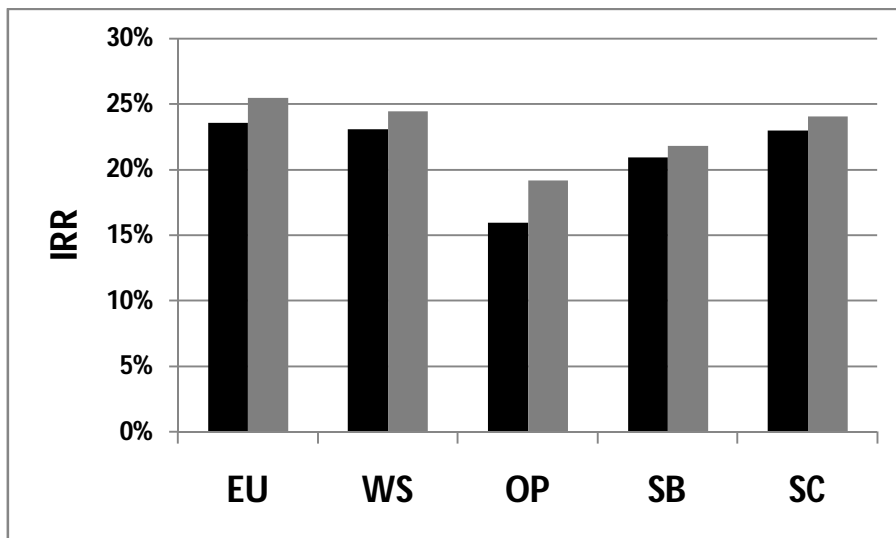


Figure 6-15: Internal rate of return using as objective function: net present value (black bar), internal rate of return (grey bar).

Figure 6-15 shows the comparison between the internal rate of return obtained for the optimal flowsheets with maximum *NPV* and the internal rate of return obtained for the optimal flowsheets with maximum *IRR*. Obtained *IRR* values vary between 16% (olive pruning with max *NPV*) and 25%

Chapter 6

(eucalyptus with max *IRR*). The ranking of single biomass and of combined biomass biorefineries based on the obtained *IRR* provides with similar results to the ranking based on *NPV*. Differences between the *IRR* values obtained with different objective functions do not exceed 3%. The largest difference, 3%, is found for olive pruning again due to the effect of the objective function on the *TIC* value.

7. Process synthesis of the biorefinery

In order to obtain an optimal process design for the lignocellulosic biorefinery, an iterative algorithm optimization process has been considered (Figure 7-1).

The algorithm consists of 8 step:

- construction of the superstructure of the biorefinery;
- construction of kinetic models of reactors and fermenters by MATLAB modeling software;
- implementation of the literature data and the process yields for all sections of the biorefinery, less reactors and fermenters;
- process optimization by ampl, obtaining the optimal biomass allocation and the optimal flowsheet;
- process simulation of the optimal flowsheet by the process simulation software Aspen Plus, addressing more rigorously to the separation and purification section;
- implementation in ampl of yields of the separation and purification sections, obtained using a more rigorous approach by Aspen Plus;
- process optimization by ampl obtaining a new optimal flowsheet and a new biomass allocation;

- When the optimum flowsheet obtained from ampl is the same as the previous iteration got a design of optimal process.

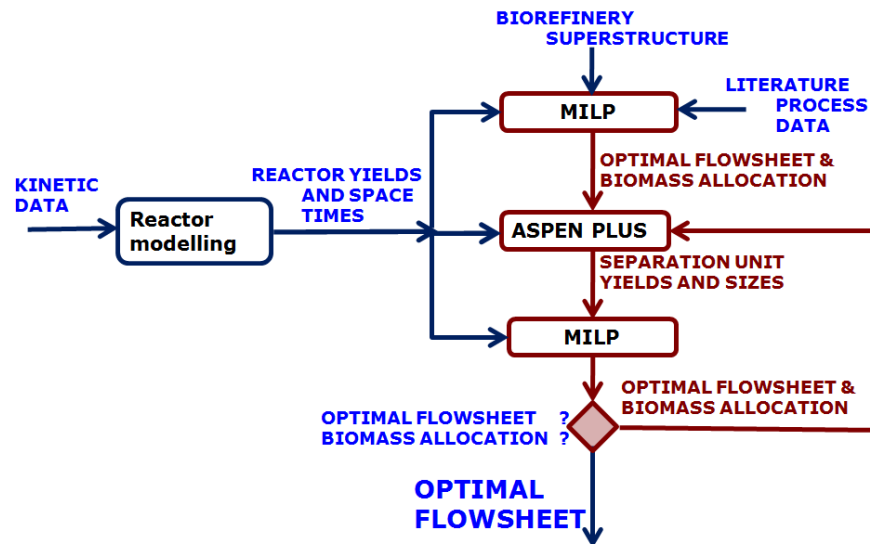


Figure 7-1: Process optimization algorithm to obtain the optimal process design.

The process simulation software Aspen Plus was used to simulate more rigorously the biorefinery and to optimize the operating conditions of each process unit of the flowsheet derived from the MILP solution. As a result, process simulations were expected to provide more precise values of the process yields and of the equipment size with respect to those obtained with the MILP analysis.

The flowsheet resulting from the process optimization of the lignocellulosic biorefinery in the base case is shown in Figure 7-2.

Biomass allocation coming from the optimization of the superstructure was used to split the pretreated biomass streams to the different process pathways of the flowsheet: 46 % of biomass fed to levulinic acid, 42 % to succinic acid, 12 % to ethanol.

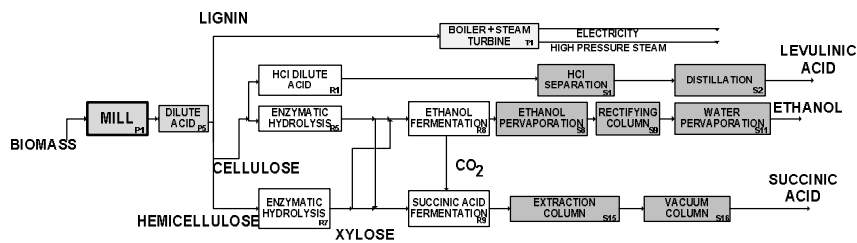


Figure 7-2: Optimal flowsheet for the base case of the multi-product biorefinery.

For the process simulation by Aspen Plus RSTOIC blocks (stoichiometric reactors) were used in pretreatment and hydrolysis and fermentation sections to set the conversions. Dilute acid pretreatment, using H_2SO_4 , was necessary to separate cellulose and hemicellulose. A neutralization reactor was used to neutralize H_2SO_4 using NH_3 . The solid fraction of cellulose and lignin essentially was sent to hydrolysis and fermentation section, while liquid fraction of hemicellulose, xylose and other soluble compounds were sent to enzymatic hydrolysis of hemicellulose. In the hydrolysis and fermentation section, part of the solid fraction was sent to levulinic acid reactor, in which the glucose converts to levulinic acid and formic acid at 200 °C and 30 bar with HCl as catalyst. RSTOIC block was used in this stage and the conversions derived from Shen and Wyman (2012). Enzymatic hydrolysis was used to convert cellulose to glucose and to convert hemicellulose to xylose (Kadam et al. 2004). The glucose and xylose from hydrolysis reactors were mixed with the glucose rich stream from levulinic purification section. This mixed stream was separated in a stream sent to ethanol fermentation and in a stream sent to succinic acid fermentation.

Ethanol fermenter performance was derived from Leksawasdi et al. (2001) and the beer stream was sent to a flash, at 32 °C and 1 bar, to separate the CO_2 gas. This CO_2 rich stream was sent to succinic acid fermentation section. Here glucose and xylose react with CO_2 to form succinic acid and oxygen. These reactions were simulated using a RSTOIC block assuming conversions derived from Song et al. (2008).

The purification section of the three products consists in several distillation and extraction columns. In this section the thermodynamic model used for the simulation was the NRTL. In the ampl model all separation yields of separation columns were assumed from data available in the literature. Instead, using the process simulator Aspen Plus it was possible to

Chapter 7

obtain more accurate separation yields for these equipment accounting for the system thermodynamics. Furthermore, it was also possible to optimize the operating conditions to minimize operating and capital costs using a rigorous multistage vapour-liquid equilibrium approach (RADFRAC block). Levulinic acid purification consisted in a flash in order to separate volatile HCl catalysts and in a distillation column to obtain levulinic acid 98.0 %wt from the bottom (Rackemann & Doherty 2011). A sequence of three units were used to purify the ethanol. The first was a pervaporation membrane (O'Brien et al. 2000), the second a distillation column to reach to azeotropic composition and the third a pervaporation membrane in order to obtain ethanol 99.5 %wt (Alvarez et al. 2008). Succinic acid at 99.0 % was obtained by separating solids and then using an extraction column with octanol as solvent (Huh et al. 2006). This unit was necessary in order to remove other fermentation acids (formic acid, acetic acid, lactic acid). A vacuum distillation column was used to separate octanol from succinic acid. The last step was the crystallization of succinic acid. Process heat integration was performed by means of Aspen Energy Analyzer in order to obtain the required utilities and the size of the heat exchangers. Economic analysis of flowsheet was carried out as well. The capital expenditure was evaluated by scaling factors and cost index. The latter economic parameters relevant to biorefinery sections were taken from Hamelinck et al. (2005). Manufacturing costs, including reactants, catalysts and utilities, were assessed from data available in Humbird et al. (2011). The total investment cost (TIC) and the total annual costs (TAC) were derived. Finally, a profitability analysis based on the discounted cash flow method assuming a plant lifetime of 20 years was performed to derive the return on investment (ROI) and the internal rate of return (IRR).

Table 7-1: Reactors yields used for RSTOIC block in Aspen Plus.

Reactor	Temp. (°C)	Yield (kg _{product} /kg _{reactant})
Reactor to convert cellulose/glucose to levulinic acid HCl as catalyst (R1)	150	Glucose: 1% Levulinic acid: 33%
Enzymatic reactor to produce glucose and xylose (R5)	45	Glucose: 52% Xylose: 66%
Enzymatic reactor to convert hemicellulose to xylose (R7)	45	Xylose : 65%
Fermenter to produce ethanol (R8)	30	Ethanol: 47%
Fermenter to produce succinic acid (R9)	40	Succinic acid: 33%

7.1 1° iteration results

The comparison between results of optimization using the mathematical programming (black bar) and results of process simulation (light bar) is reported in Figure 7-3. Products yields in terms of mass flow of products per unit mass flow of biomass do not vary significantly for levulinic acid and ethanol in both cases. The yield of succinic acid, instead, obtained from process simulation is 58.0 % of that calculated from the mathematical programming. This result is significantly affected by the simulation results of the extraction column of succinic acid using octanol as solvent. The process simulation regarding the extraction with octanol did not give the same results assumed in the optimization model in *AMPL*. This because of the difficult modeling of the extraction column with an organic solvent, or, because of a too optimistic estimate of the performance of the extraction in the *AMPL* model from literature data.

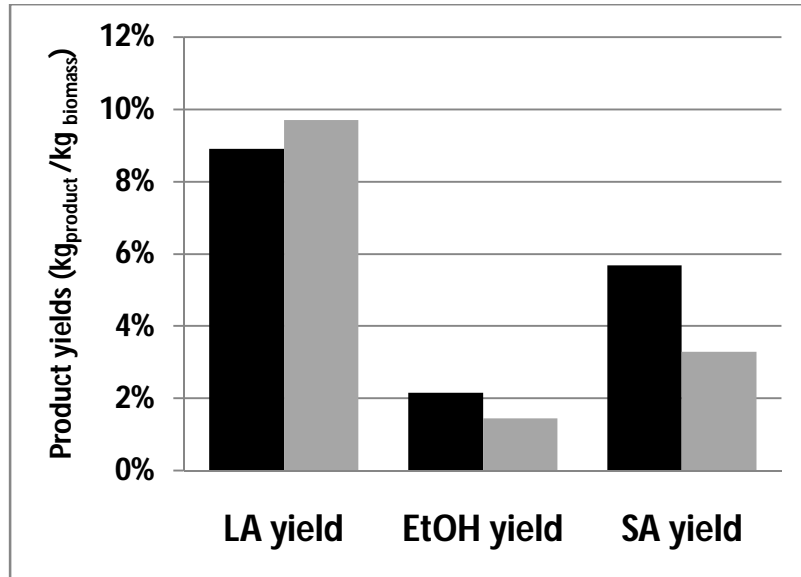


Figure 7-3: Product yields for the MILP model (dark bar) and for process simulation (light bar).

The NPV is equal to 620 M\$ for the MILP and 338 M\$ for the process simulation (Figure 7-3). This difference is mainly due to the lower revenues of the succinic acid for the second case.

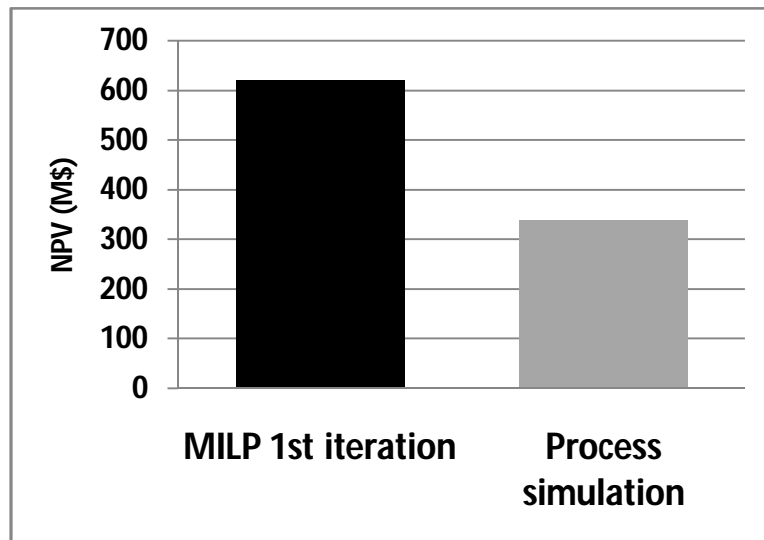


Figure 7-4: NPV obtained with the MILP model (dark bar) and with process simulation (light bar).

7.1 2° iteration results

The process yields and the equipment design obtained were used to carry out the second iteration of process optimization by ampl.

The yield results to succinic acid obtained using Aspen Plus process simulation software, have greatly influenced the second iteration in the MILP model.

The first result of the process optimization relates to a new distribution of the raw material, the biomass allocation (Figure 7-4). The lower yield of succinic acid decreases the biomass used for the production of succinic acid (21%) and, then, ethanol (9%). The biomass allocation to levulinic acid increases (70%), consequently.

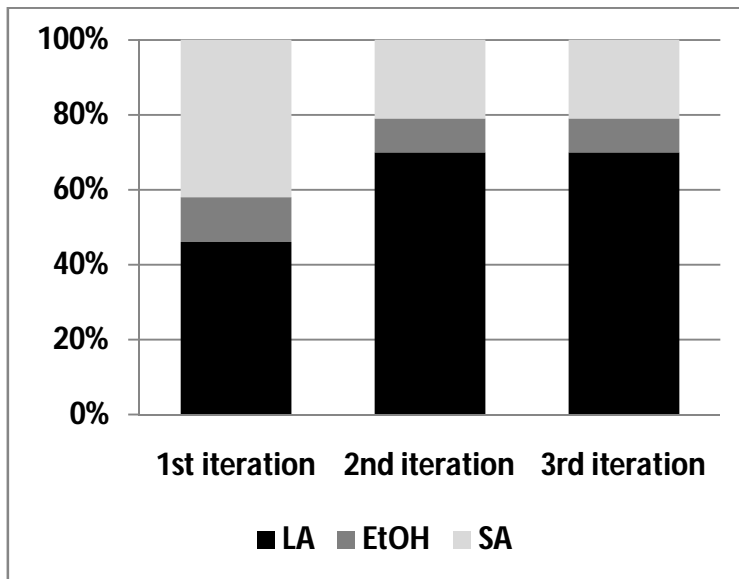


Figure 7-5: Biomass allocation for all iterations.

For the second iteration also the optimal flowsheet changes compared to the previous optimal flowsheet (Figure 7-5).

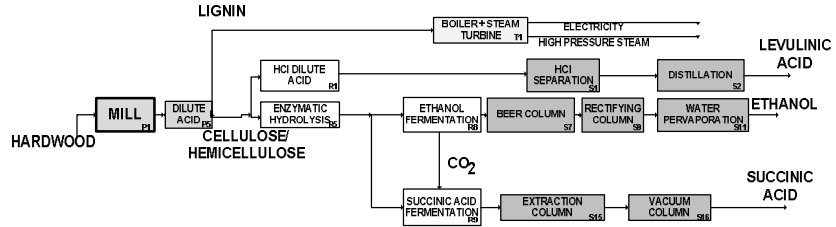


Figure 7-6: *Optimal flowsheet for the second iteration by ampl.*

The lower production of ethanol implies that, because of economies of scale, the first ethanol separation step from the beer stream is not using the pervaporation membranes, but a distillation column was used. This is because the latter one has higher operating costs and lower investment costs, becoming more convenient with lower flowrates.

Another variation of the optimal flowsheet regards the hydrolysis section. In the second iteration, cellulose hydrolysis and hemicellulose hydrolysis take place in the same reactors (R1/R5). This is because succinic acid production and ethanol production are less convenient. So, the amount of cellulose that is sent to the enzymatic hydrolysis reactor is lower, consequently, to occur the hydrolysis of the hemicellulose alone in a separate reactor is not convenient.

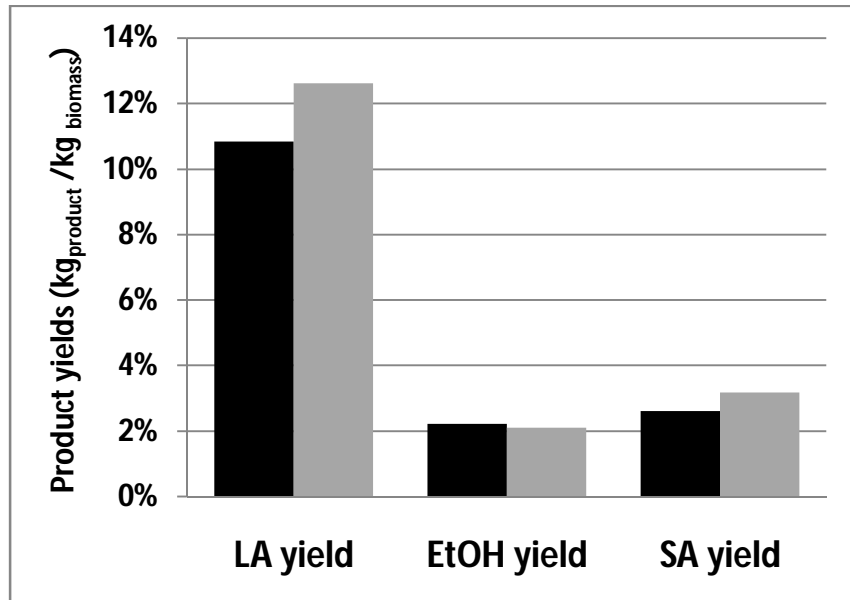


Figure 7-7: Product yields for the MILP model (dark bar) and for process simulation (light bar) for the second iteration.

The levulinic acid yield increases because of the increased allocation biomass to levulinic acid (11%). Yields to succinic acid and to ethanol decrease: 3% and 2% respectively.

For the second iteration also the beer column was accurately simulated in Aspen Plus. Differences are due to non-ideality of the ethanol-water mixture. In the MILP model could not be described because of the simplified method by Biegler et al. (1997). The result consists in two columns with a number of plates equal to 30.

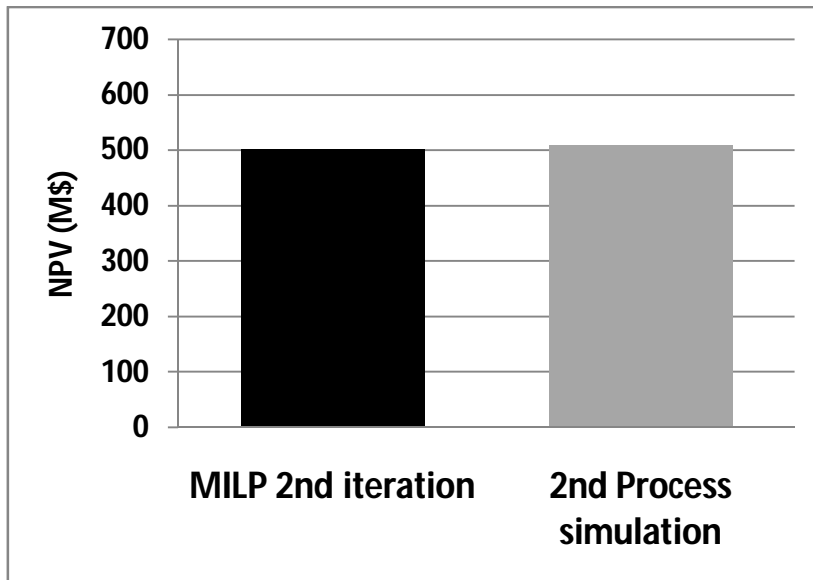


Figure 7-8: NPV obtained with the MILP model (dark bar) and with process simulation (light bar) for the second iteration.

The Net Present Value of the investment turns out to be for the second iteration equal to 502 M\$, similar value to 503 M\$, obtained by the process simulation (Figure 7-7).

7.2 3^o iteration results

The process yields and the equipment design obtained for the second iteration were used to carry out the third iteration of process optimization by ampl.

Chapter 7

Figure 7-4 shows the optimal biomass allocation for the third iteration is the same of the second iteration. Consequently, the algorithm is get to convergence. So, the third one is the last iteration of the algorithm.

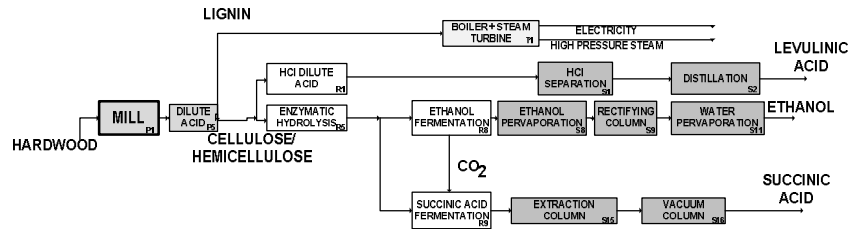


Figure 7-9: *Optimal flowsheet for the final process optimization.*

The final optimal process flowsheet is shown in Figure 7-8. Only one difference is present in the third optimal flowsheet: the ethanol pervaporation of beer stream. Using a more accurate model for the beer column the results in term of investment cost was higher than pervaporation membranes.

8. Conclusions

In this work a mathematical model was developed for the process optimization of a biorefinery co-producing succinic acid, levulinic acid and ethanol from a lignocellulosic biomass. The considered superstructure included several alternative process routes to convert cellulose and hemicellulose to the product chemicals and the thermochemical pathways for the thermal exploitation of lignin.

In a first case, fixed values of the yield to product of the hydrolysis and of the fermentation reactors were assumed. The optimal flowsheet obtained from the superstructure by solving a MILP for a maximized Net Present Value consists in a biorefinery producing all the three possible chemicals: levulinic acid, ethanol and succinic acid. The biomass allocation for this solution consisted in a 64% biomass dedicated to succinic acid production, 20% to ethanol production and 16% to levulinic acid production. The global yield of the biorefinery, considering all the products (about 10.5%), was lower than the common yield to ethanol from hardwood biomass (about 24%) (Kazi et al. 2010). This discrepancy is due to lower yield values to succinic acid and levulinic acid. Inspection of the optimal flowsheet highlights that the enzymatic hydrolysis is the preferred conversion pathway to produce the glucose and the xylose amounts necessary for the subsequent fermentation to ethanol and succinic acid. Instead, dilute acid hydrolysis turns out to be the optimal route for the direct conversion to levulinic acid. The Net Present Value obtained for the optimal flowsheet is 306 M\$ and the corresponding *IRR* value is 25%.

The technical and economic performances of the biorefinery are significantly dependent on the optimal design of the hydrolysis and fermentation reactors. In the second part of the work, the optimal design of

8. Conclusions

reactors is taken into account in the maximization procedure of the overall economic objective function. The optimal design depends on the economic scenario and on the plant scale. A sensitivity analysis of the effect of these parameters on the solution of the process optimization problem is also reported in the work. The process optimization of a multi-product biorefinery was carried out by a model embedding the design optimization of the hydrolysis and fermentation reactors by means of rigorous kinetics modeling. This work demonstrated that the coupling of the reactor modeling results with the overall process superstructure modeling can be successfully performed by a discretization procedure. In particular, this method allowed to reduce the MINLP master problem to a MILP problem and to successfully approach it by a linear optimization solver. Despite the increase by a factor of 100 of the binary variables and by a factor of 8 of the constraints due to the adopted discretization procedure, a reasonable computational time for the search of the optimal solution was required. The optimal flowsheet obtained from the superstructure by maximizing the *NPV* consists in a biorefinery producing all the three possible chemicals, levulinic acid, succinic acid and ethanol. Comparable biomass allocation values were obtained for levulinic acid and succinic acid (more than 40% each). As expected, ethanol has the lowest biomass allocation due to its significantly lower price. In particular, the flow rate of the produced ethanol was determined by the flow rate of CO₂ necessary for the succinic acid fermentation. The global yield of the biorefinery, considering all the products, (about 16.8%) was lower than the common yield to ethanol from hardwood biomass. This discrepancy is due to lower yield values to succinic acid and levulinic acid. The results of the sensitivity analysis highlighted that the optimal flowsheet and the relevant technical and economic performances are significantly dependent on the economic scenario (chemical products selling price, discount rate) and on the plant scale. In particular, threshold values of the high value chemicals price, levulinic acid and succinic acid, can be derived for the biomass allocation distribution and process flowsheet. As expected process optimization achieved by maximizing two different economic objective functions, *NPV* and *IRR*, provided different optimal flowsheets and biomass allocation to chemical products. The maximization of *NPV* determined a larger production plant with higher product yields and revenues, but also higher *TIC*. *IRR* maximization provided optimal flowsheets which minimize the investment costs. For the present multiproduct biorefinery case, this resulted in the elimination of the process route to levulinic acid, the reduction of the biorefinery global product yield and productivity.

The third part of the work highlighted that the biomass composition has a significant effect on the optimal flowsheet of a multi-product lignocellulosic biorefinery. In particular, the total content of cellulose and hemicellulose and their ratio affects the biomass allocation to products and the choice of the

process routes to obtain them. Analysis of the considered case studies with eucalyptus, wheat straw and olive pruning indicated that the levulinic acid process pathway was not convenient when 1) cellulose and hemicellulose had comparable amounts in the biomass feedstock, 2) the minimization of the total investment cost was sought to maximize the internal rate of return. A methodology to take into account the seasonal availability of different biomass types in the MILP process optimization problem was successfully applied to two different case studies: 1) each of the three biomass types was available for four months in a year, 2) a biomass kind was available all the year long while the other two were available four months each. This methodology can be applied to other superstructure process optimization problems with seasonal feedstock and co-feeding options as well. Optimization results on the season-based biorefineries provided total process yields to products comparable to those obtained for single biomass biorefineries. However, product yield distribution and overall productivity of the plant varies during the different periods provided a constant biomass feed rate. On the whole, competitive profitability indicators values (net present value and internal rate of return) were obtained from the economic analysis. These findings encourage the development and the optimization of multi-product biorefineries with multiple seasonal biomass feedstock. Further studies should address important factors not considered in this paper like the optimal processing capacity and location, the collection costs, the market prices volatility.

Finally, it was developed and tested an iterative optimization algorithm to obtain an optimal flowsheet. The algorithm is based on the MILP optimization model, described in the early chapters, and on the use of a process simulation software to model more rigorously the optimal process pathways.

This algorithm has been considered for the base case and showed that in three iterations is reached the convergence, obtaining an optimal process flowsheet and an optimal process design.

References

- Aden, a et al., 2002. Lignocellulosic Biomass to Ethanol Process Design and Economics Utilizing Co-Current Dilute Acid Prehydrolysis and Enzymatic Hydrolysis for Corn Stover. *Other Information PBD 1 Jun 2002*, (June), p.Medium: ED; Size: 154 pages. Available at: <http://www.osti.gov/bridge/servlets/purl/15001119-zb17aV/native/>.
- Alvarez, M.E.T. et al., 2008. Development of a mathematical model for studying bioethanol–water separation using hydrophilic polyetherimide membrane. *Journal of Applied Polymer Science*, 107(4), pp.2256–2265. Available at: <http://doi.wiley.com/10.1002/app.27311>.
- Arantes, V. & Saddler, J.N., 2011. Cellulose accessibility limits the effectiveness of minimum cellulase loading on the efficient hydrolysis of pretreated lignocellulosic substrates. *Biotechnology for Biofuels*, 4(1), p.3. Available at: <http://www.biotechnologyforbiofuels.com/content/4/1/3>.
- Ayoub, 2008. Process for the reactive extractive extraction of levulinic acid.
- Balat, M., 2011. Production of bioethanol from lignocellulosic materials via the biochemical pathway: A review. *Energy Conversion and Management*, 52(2), pp.858–875. Available at: <http://linkinghub.elsevier.com/retrieve/pii/S0196890410003791>.
- Balat, M. & Ayar, G., 2005. Biomass Energy in the World, Use of Biomass and Potential Trends. *Energy Sources*, 27(10), pp.931–940.
- Biegler L.T., Grossmann I.E., W.A.W., 1997. *Systematic Methods of Chemical Process Design*, Prentice-Hall.
- Bischi, A. et al., 2014. A detailed MILP optimization model for combined cooling, heat and power system operation planning. *Energy*, 74, pp.12–26. Available at: <http://linkinghub.elsevier.com/retrieve/pii/S0360544214001765>.
- Bozell, J.J. & Petersen, G.R., 2010. Technology development for the production of biobased products from biorefinery carbohydrates—the US Department of Energy’s “Top 10” revisited. *Green Chemistry*,

References

12(4), p.539.

- Cardona, C.A. & Sanchez, O.J., 2007. Fuel ethanol production: process design trends and integration opportunities. *Bioresource technology*, 98(12), pp.2415–2457. Available at: <http://www.ncbi.nlm.nih.gov/pubmed/17336061>.
- Chang, V.S., Nagwani, M. & Holtzapple, M.T., 1998. Lime pretreatment of crop residues bagasse and wheat straw. *Applied Biochemistry and Biotechnology*, 74(3), pp.135–159.
- Cheali, P. et al., 2014. Uncertainty Analysis in Raw Material and Utility Cost of Biorefinery Synthesis and Design.
- Cheali, P. et al., 2015. Upgrading of lignocellulosic biorefinery to value-added chemicals: Sustainability and economics of bioethanol-derivatives. *Biomass and Bioenergy*, 75, pp.282–300. Available at: <http://www.sciencedirect.com/science/article/pii/S0961953415000665>.
- Cherubini, F. & Strömman, A.H., 2010. Production of biofuels and biochemicals from lignocellulosic biomass: Estimation of maximum theoretical yields and efficiencies using matrix algebra. *Energy and Fuels*, 24(4), pp.2657–2666.
- Dimian, A.C. & Bildea, C.S., 2008. *Chemical Process Design*, Weinheim, Germany: Wiley-VCH Verlag GmbH & Co. KGaA. Available at: <http://doi.wiley.com/10.1002/9783527621583>.
- Duran, M.A. & Grossmann, I.E., 1986. Simultaneous optimization and heat integration of chemical processes. *AIChE Journal*, 32(1), pp.123–138.
- Eggeman, T. & Elander, R.T., 2005. Process and economic analysis of pretreatment technologies. *Bioresource Technology*, 96(18 SPEC. ISS.), pp.2019–2025.
- Errico, M. et al., 2013. Optimal synthesis of distillation systems for bioethanol separation. Part 1. Extractive distillation with simple columns. *Industrial and Engineering Chemistry Research*, 52(4), pp.1612–1619.
- Farone, I.W.A., John, E. & Ana, S., 2000. Method for the production of levulinic acid and its derivatives. *US006054611A*, 36.

- FitzPatrick, M. et al., 2010. A biorefinery processing perspective: Treatment of lignocellulosic materials for the production of value-added products. *Bioresource Technology*, 101(23), pp.8915–8922. Available at: <http://dx.doi.org/10.1016/j.biortech.2010.06.125>.
- Flores-Sánchez, A., Flores-Tlacuahuac, A. & Pedraza-Segura, L.L., 2013. Model-based experimental design to estimate kinetic parameters of the enzymatic hydrolysis of lignocellulose. *Industrial and Engineering Chemistry Research*, 52, pp.4834–4850.
- Floudas, C. a., 1995. *Nonlinear and Mixed-Integer Optimization* N. Y. Oxford & O. U. PRESS, eds.,
- Gabriel, K.J. & El-Halwagi, M.M., 2013a. Modeling and optimization of a bioethanol production facility. *Clean Technologies and Environmental Policy*, 15(6), pp.931–944.
- Gabriel, K.J. & El-Halwagi, M.M., 2013b. Modeling and optimization of a bioethanol production facility. *Clean Technologies and Environmental Policy*, 15(6), pp.931–944. Available at: <http://link.springer.com/10.1007/s10098-013-0584-8>.
- Geraili, a., Sharma, P. & Romagnoli, J. a., 2014. Technology analysis of integrated biorefineries through process simulation and hybrid optimization. *Energy*, 73, pp.145–159. Available at: <http://www.sciencedirect.com/science/article/pii/S0360544214006951>.
- Girisuta, B. et al., 2008. Experimental and kinetic modelling studies on the acid-catalysed hydrolysis of the water hyacinth plant to levulinic acid. *Bioresource Technology*, 99(17), pp.8367–8375.
- Girisuta, B., Janssen, L.P.B.M. & Heeres, H.J., 2007. Kinetic Study on the Acid-Catalyzed Hydrolysis of Cellulose to Levulinic Acid. *Industrial & Engineering Chemistry Research*, 46(6), pp.1696–1708. Available at: <http://pubs.acs.org/doi/abs/10.1021/ie061186z>.
- Giuliano, A., Cerulli, R., et al., 2016. Flowsheet optimization of a multi-product lignocellulosic biorefinery - PART 1: MILP approach for a reference economic scenario. *Ind. Eng. Chem. Res.*
- Giuliano, A. et al., 2014. Optimization of a Multiproduct Lignocellulosic

References

- Biorefinery using a MILP Approximation. , pp.1423–1428. Available at: <http://linkinghub.elsevier.com/retrieve/pii/B9780444634559500726>.
- Giuliano, A., Poletto, M. & Barletta, D., 2016. Flowsheet Optimization of a Multi-product Lignocellulosic Biorefinery. Part 2: Effect of Reaction Yield and of Economic Parameters. *Ind. Eng. Chem. Res.*
- Gnansounou, E. & Dauriat, A., 2010. Techno-economic analysis of lignocellulosic ethanol: A review. *Bioresource Technology*, 101(13), pp.4980–4991. Available at: <http://www.sciencedirect.com/science/article/pii/S0960852410002804>.
- González-García, S., Moreira, M.T. & Feijoo, G., 2010. Comparative environmental performance of lignocellulosic ethanol from different feedstocks. *Renewable and Sustainable Energy Reviews*, 14(7), pp.2077–2085. Available at: <http://linkinghub.elsevier.com/retrieve/pii/S1364032110000973>.
- Gupta, Omprakash K., Ravindran, A., 1985. BRANCH AND BOUND EXPERIMENTS IN CONVEX NONLINEAR INTEGER PROGRAMMING. , 31(12), pp.15333–1546.
- Hallac, B.B. & Ragauskas, A.J., 2011. Analyzing cellulose degree of polymerization and its relevancy to cellulosic ethanol. *Biofuels, Bioproducts and Biorefining*, 5(2), pp.215–225. Available at: <http://doi.wiley.com/10.1002/bbb.269>.
- Hamelinck, C.N., Van Hooijdonk, G. & Faaij, a. P.C., 2005. Ethanol from lignocellulosic biomass: Techno-economic performance in short-, middle- and long-term. *Biomass and Bioenergy*, 28(4), pp.384–410.
- Huang, H.-J. et al., 2009. Effect of biomass species and plant size on cellulosic ethanol: A comparative process and economic analysis. *Biomass and Bioenergy*, 33(2), pp.234–246. Available at: <http://linkinghub.elsevier.com/retrieve/pii/S0961953408001396>.
- Huang, H.-J. et al., 2010. Process modeling and analysis of pulp mill-based integrated biorefinery with hemicellulose pre-extraction for ethanol production: A comparative study. *Bioresource Technology*, 101(2), pp.624–631. Available at: <http://linkinghub.elsevier.com/retrieve/pii/S0960852409010402>.

- Huh, Y.S. et al., 2006. Effective purification of succinic acid from fermentation broth produced by *Mannheimia succiniciproducens*. *Process Biochemistry*, 41, pp.1461–1465.
- Humbird, D. & Aden, A., 2009. Biochemical Production of Ethanol from Corn Stover: 2008 State of Technology Model Biochemical Production of Ethanol from Corn Stover. , (August).
- de Jong, E. et al., 2012. Product developments in the bio-based chemicals arena. *Biofuels, Bioproducts and Biorefining*, p.n/a–n/a. Available at: <http://doi.wiley.com/10.1002/bbb.1360>.
- Kadam, K.L., Rydholm, E.C. & McMillan, J.D., 2004. Development and validation of a kinetic model for enzymatic saccharification of lignocellulosic biomass. *Biotechnology Progress*, 20(3), pp.698–705.
- Kalitventzeff, B., 1991. Mixed integer non-linear programming and its application to the management of utility networks. *Engineering Optimization*, 18(1-3), pp.183–207. Available at: <http://www.tandfonline.com/doi/abs/10.1080/03052159108941021>.
- Kamm, B., Gruber, P.R. & Kamm, M., 2007. Biorefineries - Industrial Processes and Products. In *Ullmann's Encyclopedia of Industrial Chemistry*. Weinheim, Germany: Wiley-VCH Verlag GmbH & Co. KGaA. Available at: http://doi.wiley.com/10.1002/14356007.i04_i01.
- Kasaš, M., Kravanja, Z. & Novak Pintarič, Z., 2011. Suitable modeling for process flow sheet optimization using the correct economic criterion. *Industrial and Engineering Chemistry Research*, 50, pp.3356–3370.
- Kazi, F.K., Fortman, J. & Anex, R., 2010. Techno-Economic Analysis of Biochemical Scenarios for Production of Cellulosic Ethanol. *National Renewable Energy Laboratory-NREL*, (June), p.102.
- Kim, S.B., Park, C. & Kim, S.W., 2014. Process design and evaluation of production of bioethanol and β -lactam antibiotic from lignocellulosic biomass. *Bioresource Technology*, 172, pp.194–200. Available at: <http://linkinghub.elsevier.com/retrieve/pii/S0960852414012826>.
- Knauf, M. & Moniruzzaman, M., 2004. Lignocellulosic biomass processing: a perspective. *International Sugar Journal*, 106(1263), pp.147–150.

References

- Kocis, G.R. & Grossmann, I.E., 1989. A modelling and decomposition strategy for the minlp optimization of process flowsheets. *Computers & Chemical Engineering*, 13(7), pp.797–819.
- Kokossis, A.C., Tsakalova, M. & Pyrgakis, K., 2015. Design of integrated biorefineries. *Computers & Chemical Engineering*, 81, pp.40–56. Available at: <http://linkinghub.elsevier.com/retrieve/pii/S0098135415002021>.
- Kwiatkowski, J.R. et al., 2006. Modeling the process and costs of fuel ethanol production by the corn dry-grind process. *Industrial Crops and Products*, 23(3), pp.288–296. Available at: <http://linkinghub.elsevier.com/retrieve/pii/S0926669005000944>.
- Lee, Y.Y., Wu, Z. & Torget, R.W., 2000. Modeling of countercurrent shrinking-bed reactor in dilute-acid total-hydrolysis of lignocellulosic biomass. *Bioresource Technology*, 71(1), pp.29–39.
- Leksawasdi, N., Joachimsthal, E.L. & Rogers, P.L., 2001. Mathematical modelling of ethanol production from glucose/xylose mixtures by recombinant *Zymomonas mobilis*. *Biotechnology Letters*, 23(13), pp.1087–1093. Available at: <http://link.springer.com/10.1023/A:1010599530577>.
- Linnhoff, B., 1993. Pinch analysis: a state of the art overview. *Chemical Engineering Research and Design*, 71, pp.503–522.
- Linnhoff, B. & Hindmarsh, E., 1983. The pinch design method for heat exchanger networks. *Chemical Engineering Science*, 38(5), pp.745–763. Available at: <http://linkinghub.elsevier.com/retrieve/pii/0009250983801857>.
- Luo, L., van der Voet, E. & Huppes, G., 2010. Biorefining of lignocellulosic feedstock – Technical, economic and environmental considerations. *Bioresource Technology*, 101(13), pp.5023–5032. Available at: <http://linkinghub.elsevier.com/retrieve/pii/S0960852409018070>.
- M. Douglas J., 1988. *Conceptual design of chemical processes* New York: McGraw-Hill, ed.,
- Mani, S., Tabil, L.G. & Sokhansanj, S., 2004. Grinding performance and

- physical properties of wheat and barley straws, corn stover and switchgrass. *Biomass and Bioenergy*, 27, pp.339–352.
- Martín, M. & Grossmann, I.E., 2014. Optimal simultaneous production of i-butene and ethanol from switchgrass. *Biomass and Bioenergy*, 61, pp.93–103. Available at: <http://linkinghub.elsevier.com/retrieve/pii/S0961953413004972>.
- Menon, V. & Rao, M., 2012. Trends in bioconversion of lignocellulose: Biofuels, platform chemicals & biorefinery concept. *Progress in Energy and Combustion Science*, 38(4), pp.522–550. Available at: <http://www.sciencedirect.com/science/article/pii/S036012851200007X>.
- Mosier, N., 2005. Features of promising technologies for pretreatment of lignocellulosic biomass. *Bioresour. Technol.*, 96(6), pp.673–686. Available at: [http://linkinghub.elsevier.com/retrieve/pii/S0960-8524\(04\)00253-6](http://linkinghub.elsevier.com/retrieve/pii/S0960-8524(04)00253-6).
- O'Brien, D.J., Roth, L.H. & McAloon, A.J., 2000. Ethanol production by continuous fermentation–pervaporation: a preliminary economic analysis. *Journal of Membrane Science*, 166(1), pp.105–111. Available at: <http://linkinghub.elsevier.com/retrieve/pii/S0376738899002550>.
- Pan, X. et al., 2007. Pretreatment of lodgepole pine killed by mountain pine beetle using the ethanol organosolv process: Fractionation and process optimization. *Industrial and Engineering Chemistry Research*, 46(8), pp.2609–2617.
- Peplow, M., 2014. Cellulosic ethanol fights for life. *Nature*, 507, pp.152–153.
- Pintarič, Z. & Kravanja, Z., 2006. Selection of the economic objective function for the optimization of process flow sheets. *Industrial & engineering chemistry*, pp.4222–4232. Available at: <http://pubs.acs.org/doi/abs/10.1021/ie050496z>.
- Poliakoff, M. & Licence, P., 2007. Sustainable technology: Green chemistry. *Nature*, 450(7171), pp.810–812. Available at: <http://www.nature.com/doi/abs/10.1038/450810a>.
- Ponce-Ortega, J.M. et al., 2012. A disjunctive programming formulation for

References

- the optimal design of biorefinery configurations. *Industrial and Engineering Chemistry Research*, 51, pp.3381–3400.
- Quaglia, A. et al., 2012. Integrated business and engineering framework for synthesis and design of enterprise-wide processing networks. *Computers & Chemical Engineering*, 38, pp.213–223. Available at: <http://linkinghub.elsevier.com/retrieve/pii/S0098135411003486>.
- Rackemann, D.W. & Doherty, W.O., 2011. The conversion of lignocellulosics to levulinic acid. *Biofuels, Bioproducts and Biorefining*, 5(2), pp.198–214. Available at: <http://doi.wiley.com/10.1002/bbb.267>.
- Ramaswamy, S., Huang, H.-J. & Ramarao, B. V., 2013. *Separation and Purification Technologies in Biorefineries*, Chichester, UK: John Wiley & Sons, Ltd. Available at: <http://doi.wiley.com/10.1002/9781118493441>.
- Rudd, D.F., Powers, G.J. & Siirola, J.J., 1973. *Process synthesis*, Prentice-Hall., Englewood Cliffs NJ:
- Sammons, N.E. et al., 2008. Optimal biorefinery product allocation by combining process and economic modeling. *Chemical Engineering Research and Design*, 86(7), pp.800–808. Available at: <http://linkinghub.elsevier.com/retrieve/pii/S0263876208000798>.
- Scott, F. et al., 2013. Process design and sustainability in the production of bioethanol from lignocellulosic materials. *Electronic Journal of Biotechnology*, 16(3), pp.1–16. Available at: <http://www.ejbiotechnology.info/index.php/ejbiotechnology/article/view/1420>.
- Seider, W.D. et al., 2010. *Product and process design principles: synthesis, analysis, and evaluation*,
- Shen, J. & Wyman, C.E., 2012. Hydrochloric acid-catalyzed levulinic acid formation from cellulose: data and kinetic model to maximize yields. *AIChE Journal*, 58(1), pp.236–246. Available at: <http://doi.wiley.com/10.1002/aic.12556>.
- Silva-Fernandes, T., Duarte, L.C., Carvalheiro, F., Marques, S., et al., 2015.

- Biorefining strategy for maximal monosaccharide recovery from three different feedstocks: Eucalyptus residues, wheat straw and olive tree pruning. *Bioresource Technology*, 183, pp.203–212. Available at: <http://linkinghub.elsevier.com/retrieve/pii/S0960852415001650>.
- Silva-Fernandes, T., Duarte, L.C., Carvalheiro, F., Loureiro-Dias, M.C., et al., 2015. Hydrothermal pretreatment of several lignocellulosic mixtures containing wheat straw and two hardwood residues available in Southern Europe. *Bioresource Technology*, 183, pp.213–220. Available at: <http://linkinghub.elsevier.com/retrieve/pii/S0960852415000796>.
- Solomon, S. et al., 2007. Contribution of working group 1 to the fourth assessment report of the intergovernmental panel on climate change. *Cambridge, United Kingdom and New York, NY, USA: Cambridge University Press*.
- Song, H. et al., 2008a. Modeling of batch fermentation kinetics for succinic acid production by *Mannheimia succiniciproducens*. *Biochemical Engineering Journal*, 40(1), pp.107–115. Available at: <http://linkinghub.elsevier.com/retrieve/pii/S1369703X07004457>.
- Song, H. et al., 2008b. Modeling of batch fermentation kinetics for succinic acid production by *Mannheimia succiniciproducens*. *Biochemical Engineering Journal*, 40(1), pp.107–115.
- Song, H. et al., 2007. Recovery of succinic acid produced by fermentation of a metabolically engineered *Mannheimia succiniciproducens* strain. *Journal of Biotechnology*, 132(4), pp.445–452.
- Sun, Y. & Cheng, J., 2002. Hydrolysis of lignocellulosic materials for ethanol production : a review q. *Bioresource technology*, 83(1), pp.1–11. Available at: <http://www.ncbi.nlm.nih.gov/pubmed/12058826>.
- T. Werpy. & G. Petersen., 2004. Top Value Added Chemicals from Biomass Volume I — Results of Screening for Potential Candidates from Sugars and Synthesis Gas Top Value Added Chemicals From Biomass Volume I : Results of Screening for Potential Candidates. , 1.
- Tippkötter, N. et al., 2014. Enzymatic hydrolysis of beech wood lignocellulose at high solid contents and its utilization as substrate for

References

- the production of biobutanol and dicarboxylic acids. *Bioresource Technology*, 167, pp.447–455. Available at: <http://linkinghub.elsevier.com/retrieve/pii/S0960852414008967>.
- Trespalacios, F. & Grossmann, I.E., 2014. Review of Mixed-Integer Nonlinear and Generalized Disjunctive Programming Methods. *Chemie Ingenieur Technik*, 86(7), pp.991–1012. Available at: <http://doi.wiley.com/10.1002/cite.201400037>.
- Wang, B., Gebreslassie, B.H. & You, F., 2013. Sustainable design and synthesis of hydrocarbon biorefinery via gasification pathway: Integrated life cycle assessment and techno-economic analysis with multiobjective superstructure optimization. *Computers & Chemical Engineering*, 52, pp.55–76. Available at: <http://linkinghub.elsevier.com/retrieve/pii/S0098135413000033>.
- Westerberg, A.W., 2004. A retrospective on design and process synthesis. *Computers & Chemical Engineering*, 28(4), pp.447–458. Available at: <http://www.sciencedirect.com/science/article/pii/S0098135403002564>.
- Westerlund, T. et al., 1998. An extended cutting plane method for a class of non-convex MINLP problems. *Computers & Chemical Engineering*, 22(3), pp.357–365. Available at: <http://linkinghub.elsevier.com/retrieve/pii/S0098135497000008>.
- Yedur, S. et al., 2001. Succinic acid production and purification.
- Yee, T.F., Grossmann, I.E. & Kravanja, Z., 1990. Simultaneous optimization models for heat integration—I. Area and energy targeting and modeling of multi-stream exchangers. *Computers & Chemical Engineering*, 14, pp.1151–1164.
- Yue, D., You, F. & Snyder, S.W., 2014. Biomass-to-bioenergy and biofuel supply chain optimization: Overview, key issues and challenges. *Computers & Chemical Engineering*, 66, pp.36–56. Available at: <http://linkinghub.elsevier.com/retrieve/pii/S0098135413003670>.
- Zhou, Z. et al., 2012. Impacts of equipment off-design characteristics on the optimal design and operation of combined cooling; heating and power systems. *Computers & Chemical Engineering*, 48(0), p.-. Available at:

<http://www.sciencedirect.com/science/article/pii/S0098135412002670?v=s5>.

Zimbardi, F., Ricci, E. & Braccio, G., 2002. Technoeconomic study on steam explosion application in biomass processing. *Applied biochemistry and biotechnology*, 98-100, pp.89–99.

Zondervan, E. et al., 2011. Optimal design of a multi-product biorefinery system. *Computers and Chemical Engineering*, 35(9), pp.1752–1766. Available at: <http://dx.doi.org/10.1016/j.compchemeng.2011.01.042>.

Abbreviations and symbols

ABBREVIATIONS

CF Cash Flow

IRR Internal Rate of Return

MILP Mixed Integer Linear Programming

MINLP Mixed Integer Non Linear Programming

NPV Net Present Value

TAC Total Annual cost, \$/y

TIC Total Investment Cost, \$

SYMBOLS

A vector matrices of non linear functions of the continuous variables x^N

b vector of coefficients

B matrix of coefficients

C vector matrices of non linear functions of the continuous variables x^N

c_i molar concentration of component i

c_{i0} initial concentration of component i

D matrix of coefficients

F stream mass flow rate, t/h

F_p^{OUT} product p outlet flowrate

F_r^{IN} reactant r inlet flowrate

F_p^{IN} product p inlet flowrate

Abbreviations and symbols

$F_{r,i}^{IN}$	additional linear variables
g	design specification functions
h	mass and energy balances
n_{comp}	number of components
n_d	number of discrete values
n_r	number of reactions
n_j	number of discrete values assumed for the non linear variable
p	product -
r	reactant
r_j	reaction rate of component i in reaction j
R_j	reaction rate of component i in reaction j
t_{ls}	Mixed Integer Non Linear Programming
UB	upper bound
V	volume of PFR and CSTR, m ³
w_i	mass concentration of component i
w_{i0}	initial mass concentration of component i
x^N	vector of continuous non linear variables
x^L	vector of continuous linear variables
$x_{k,i}^L$	additional linear variables
y	vector of binary variables
y_i^d	binary variables of the discretization

Abbreviations and symbols

y_{ji}^d	binary variables of the discretization
z	economic objective function
$A, B, \Gamma, \Delta, E, H$	matrices of coefficients
$\alpha, \beta, \gamma, \delta, \varepsilon$	vectors of coefficients
$a(x^N)$	vector of non linear functions of the continuous variables x^N
ζ_i	vector of possible values of the variable
$\zeta_{j,i}$	discrete values assumed for the non linear variable x_j^N
α_{ij}	discrete values of the function $a_j(x_j^N)$
η_p	overall product yield of product p
$\bar{\eta}_{p,i}$	discrete values of the function $\eta_p(\tau)$
τ	residence time in the reactor, min
$\bar{\tau}_i$	discrete values assumed for τ
$\nu_{i,j}$	stoichiometric coefficient for component i in reaction j
ρ	stream average density, t/m ³
$\psi_{i,j}$	ratio between the molecular weight of component i and the molecular weight of the component on which the reaction rate R_j is calculated

Appendix

Appendix

Reactor modeling

Dilute acid hydrolysis with HCl (R1/R3) (Shen & Wyman 2012):

r_1, H^+, k_1	r_2, H^+, k_2	r_4, H^+, k_4	r_6, H^+, k_6
$C_6H_{10}O_5$ Cellulose	$C_6H_{12}O_6$ Glucose	$C_6H_6O_3$ HMF Humins	$C_5H_8O_3 + C_2H_2O$ LA FA Humins Decomposition product
	r_3, H^+, k_3	r_5, k_5	

$\frac{dC}{dt} = -k_1 C$ $\frac{dG}{dt} = k_1 C - (k_2 + k_3) G$ $\frac{dM}{dt} = k_2 G - (k_4 + k_5) M$ $\frac{dL}{dt} = k_4 M - k_6 L$ $k_i = k_i' H = A_i H \exp\left(-\frac{E_a}{RT}\right)$	$C = C_0 \exp(-k_1 t)$ $G = \frac{k_1 C_0}{k_2 + k_3 - k_1} \{ \exp(-k_1 t) - \exp[-(k_2 + k_3)t] \}$ $M = \frac{k_1 k_2 C_0}{k_2 + k_3 - k_1} \left\{ \frac{\exp(-k_1 t)}{k_4 + k_5 - k_1} - \frac{\exp[-(k_2 + k_3)t]}{k_4 + k_5 - k_2 - k_3} \right\} + \frac{k_1 k_2 C_0 \exp[-(k_4 + k_5)t]}{(k_4 + k_5 - k_1)(k_4 + k_5 - k_2 - k_3)}$ $L = \frac{k_1 k_2 k_4 C_0}{k_2 + k_3 - k_1} \left\{ \frac{\exp(-k_1 t) - \exp(-k_6 t)}{(k_4 + k_5 - k_1)(k_6 - k_1)} - \frac{\exp[-(k_2 + k_3)t] - \exp(-k_6 t)}{(k_4 + k_5 - k_2 - k_3)(k_6 - k_2 - k_3)} \right\} + \frac{k_1 k_2 k_4 C_0 \{ \exp[-(k_4 + k_5)t] - \exp(-k_6 t) \}}{(k_4 + k_5 - k_1)(k_4 + k_5 - k_2 - k_3)(k_6 - k_4 - k_5)}$
--	---

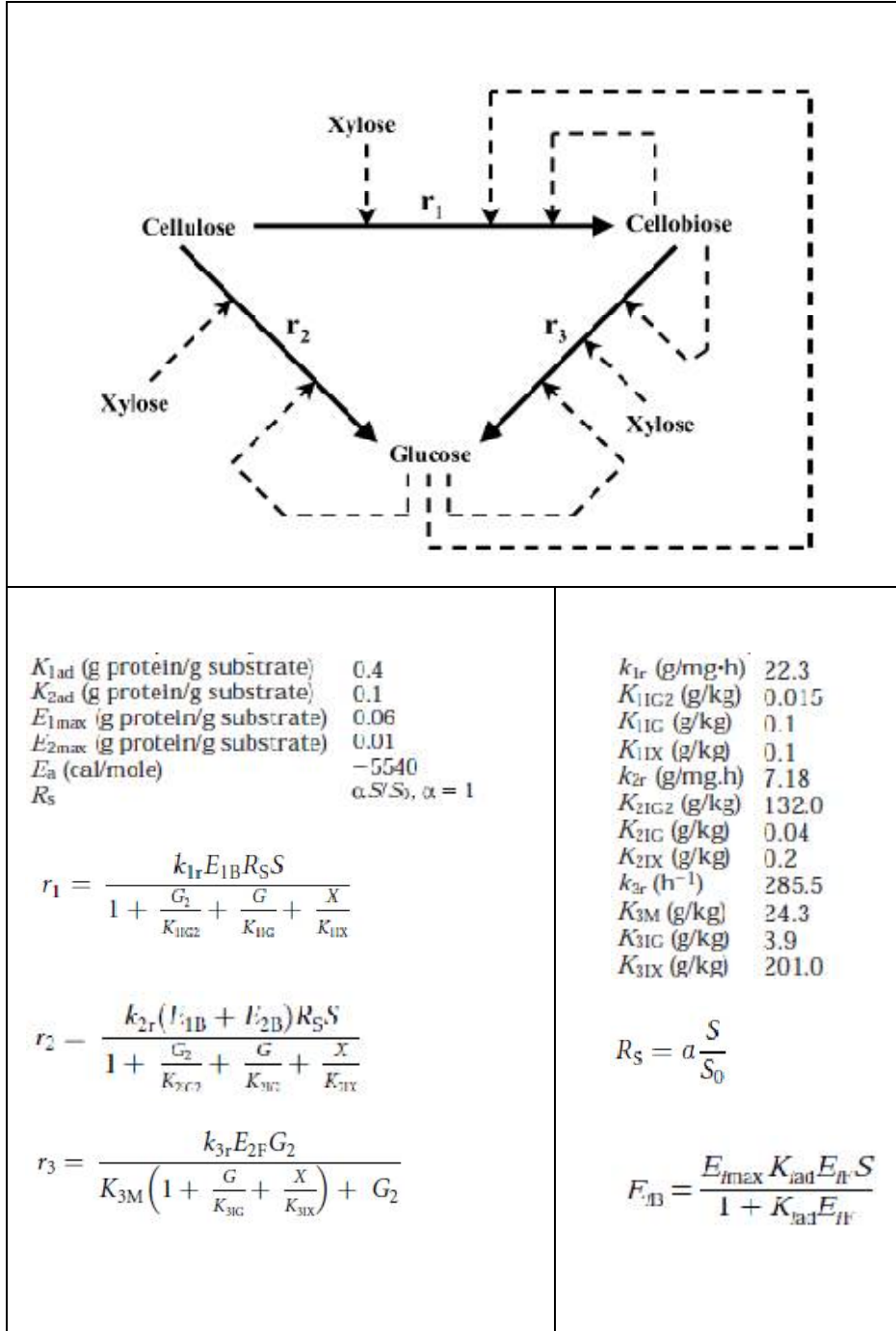
Appendix

Dilute acid hydrolysis with H₂SO₄ (R2/R4) (Girisuta et al. 2008):

$\begin{array}{c} \text{Cellulose} \xrightarrow{R_{1C}} \text{Glucose} \xrightarrow{R_{1G}} \text{HMF} \xrightarrow{R_{1H}} \text{Levulinic Acid} + \text{Formic Acid} \\ \downarrow R_{2C} \qquad \qquad \downarrow R_{2G} \\ \text{Decomposed} \qquad \text{Decomposed} \\ \text{Compounds} \qquad \text{Compounds} \end{array}$	
$\frac{dC_{\text{CEL}}}{dt} = -R_{1C} - R_{2C}$	a_C 0.98 ± 0.02 b_C 1.01 ± 0.08 α_C 0.96 ± 0.02 β_C 0.94 ± 0.07 E_{1C} (kJ mol ⁻¹) 151.5 ± 1.2 E_{2C} (kJ mol ⁻¹) 174.7 ± 1.4 k_{1RC} ^a (M ^{1-α_C-β_C min⁻¹) 0.410 ± 0.018 k_{2RC} ^a (M^{1-b_C-β_C min⁻¹) 0.065 ± 0.014}}
$\frac{dC_{\text{GLC}}}{dt} = R_{1C} - R_{1G} - R_{2G}$	a_H 0.88 ± 0.01 b_H 1.23 ± 0.03 α_H 1.38 ± 0.02 β_H 1.07 ± 0.04 E_{1H} (kJ mol ⁻¹) 110.5 ± 0.7 E_{2H} (kJ mol ⁻¹) 111.3 ± 2.0 k_{1RH} ^a (M ^{1-α_H-β_H min⁻¹) 0.340 ± 0.010 k_{2RH} ^a (M^{1-b_H-β_H min⁻¹) 0.117 ± 0.008}}
$\frac{dC_{\text{HMF}}}{dt} = R_{1G} - R_{1H} - R_{2H}$	a_G 1.09 ± 0.01 b_G 1.30 ± 0.02 α_G 1.13 ± 0.01 β_G 1.13 ± 0.02 E_{1G} (kJ mol ⁻¹) 152.2 ± 0.7 E_{2G} (kJ mol ⁻¹) 164.7 ± 0.6 k_{1RG} ^a (M ^{1-α_G-β_G min⁻¹) 0.013 ± 0.001 k_{2RG} ^a (M^{1-b_G-β_G min⁻¹) 0.013 ± 0.001}}
$\frac{dC_{\text{LA}}}{dt} = R_{1H}$	
$R_{1C} = k_{1C}(C_{\text{CEL}})^{a_C}$	C_{GLC} = glucose concentration, M C_{HMF} = HMF concentration, M
$R_{2C} = k_{2C}(C_{\text{CEL}})^{b_C}$	C_{LA} = levulinic acid concentration, M
$R_{1G} = k_{1G}(C_{\text{GLC}})^{a_G}$	C_{CEL} = cellulose concentration, M
$R_{2G} = k_{2G}(C_{\text{GLC}})^{b_G}$	
$R_{1H} = k_{1H}(C_{\text{HMF}})^{a_H}$	

Appendix

Enzymatic hydrolysis (R5) (Kadam et al. 2004):

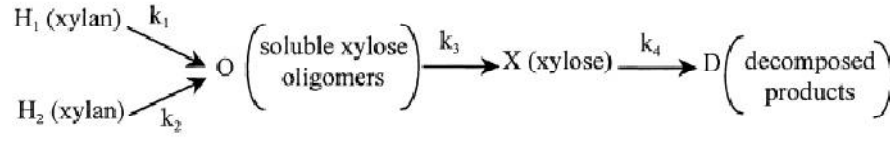


Appendix

cellulose:	$\frac{dS}{dt} = -r_1 - r_2$
cellobiose:	$\frac{dG_2}{dt} = 1.056r_1 - r_3$
glucose:	$\frac{dG}{dt} = 1.111r_2 + 1.053r_3$
enzyme:	$E_{Tl} = E_{Fl} + E_{Bl}$
G	glucose concentration (g/kg)
G_2	cellobiose concentration (g/kg)
X	xylose concentration (g/kg)
S	substrate concentration (g/kg)

Appendix

Acid hydrolysis of hemicellulose (R6) (Lee et al. 2000):

			
\bar{r}	$k_{i0} \text{ min}^{-1}(\text{wt}\%)^{-n_i}$	n_i	$E_i \text{ kcal/g mol}$
1	1.458×10^{15}	1.0	30.9
2	1.300×10^{14}	0.5	30.0
3	6.372×10^{10}	1.5	21.0
4	1.618×10^{12}	0.8	27.5
$\frac{d(vC_H)}{dx} - K_H C_H = 0$ $\epsilon u \frac{dC_O}{dx} - K_H C_H + \epsilon k_3 C_O = 0,$ $\frac{dC_X}{dx} - k_3 C_O + k_4 C_X = 0,$ $K_H = F^* k_1 + (1 - F)^* k_2.$ $k_i = k_{i0} (C_A)_{in} \exp(-E_i/RT)$			

Appendix

Ethanol fermentation (R8) (Leksawasdi et al. 2001):

$q_{p,max}$ – overall maximum specific ethanol production rate μ_{max} – maximum overall specific growth rate (1 h ⁻¹) p – ethanol concentration (g l ⁻¹) s – substrate concentration (g l ⁻¹) x – biomass concentration (g l ⁻¹)			
$\mu_{max,1}$	0.31	$\mu_{max,2}$	0.1
$K_{sx,1}$	1.45	$K_{sx,2}$	4.91
$P_{mx,1}$	57.2	$P_{mx,2}$	56.3
$K_{ix,1}$	200	$K_{ix,2}$	600
$P_{ix,1}$	28.9	$P_{ix,2}$	26.6
$q_{p,max,1}$	5.12	$q_{p,max,2}$	1.59
$K_{sp,1}$	6.32	$K_{sp,2}$	0.03
$P_{mp,1}$	75.4	$P_{mp,2}$	81.2
$K_{ip,1}$	186	$K_{ip,2}$	600
$P_{ip,1}$	42.6	$P_{ip,2}$	53.1
$q_{s,max,1}$	10.9	$q_{s,max,2}$	3.27
$K_{ss,1}$	6.32	$K_{ss,2}$	0.03
$P_{ms,1}$	75.4	$P_{ms,2}$	81.2
$K_{is,1}$	186	$K_{is,2}$	600
$P_{is,1}$	42.6	$P_{is,2}$	53.1
$r_{x,1} = \mu_{max,1} \left(\frac{s_1}{K_{sx,1} + s_1} \right) \times \left(1 - \frac{p - P_{ix,1}}{P_{mx,1} - P_{ix,1}} \right) \left(\frac{K_{ix,1}}{K_{ix,1} + s_1} \right)$		$\frac{dx}{dt} = [\alpha r_{x,1} + (1 - \alpha) r_{x,2}] x$	
$r_{x,2} = \mu_{max,2} \left(\frac{s_2}{K_{sx,2} + s_2} \right) \times \left(1 - \frac{p - P_{ix,2}}{P_{mx,2} - P_{ix,2}} \right) \left(\frac{K_{ix,2}}{K_{ix,2} + s_2} \right)$		$\frac{ds_1}{dt} = -\alpha q_{s,max,1} \left(\frac{s_1}{K_{ss,1} + s_1} \right) \times \left(1 - \frac{p - P_{is,1}}{P_{ms,1} - P_{is,1}} \right) \left(\frac{K_{is,1}}{K_{is,1} + s_1} \right) x$	
$r_{p,1} = q_{p,max,1} \left(\frac{s_1}{K_{sp,1} + s_1} \right) \times \left(1 - \frac{p - P_{ip,1}}{P_{mp,1} - P_{ip,1}} \right) \left(\frac{K_{ip,1}}{K_{ip,1} + s_1} \right)$		$\frac{ds_2}{dt} = -(1 - \alpha) q_{s,max,2} \left(\frac{s_2}{K_{ss,2} + s_2} \right) \times \left(1 - \frac{p - P_{is,2}}{P_{ms,2} - P_{is,2}} \right) \left(\frac{K_{is,2}}{K_{is,2} + s_2} \right) x$	

Appendix

$r_{p,2} = q_{p,\max,2} \left(\frac{s_2}{K_{sp,2} + s_2} \right) \times$ $\left(1 - \frac{p - P_{ip,2}}{P_{mp,2} - P_{ip,2}} \right) \left(\frac{K_{ip,2}}{K_{ip,2} + s_2} \right)$	$\frac{dp}{dt} = [\alpha r_{p,1} + (1 - \alpha)r_{p,2}]x$
--	---

Appendix

Succinic acid fermentation (R9) (Song et al. 2008a):

$r_{SA} = \alpha_{SA}r_X + \beta_{SA}X$	$\mu = \frac{\mu_{max}S}{(S + K_S + (S^2/K_I))}$
$r_{AA} = \alpha_{AA}r_X + \beta_{AA}X$	$\mu = \frac{\mu_m S}{(S + K_S + (S^2/K_I))} \times \left(1 - \frac{P}{P_{CRIT}}\right)^i$
$r_{FA} = \alpha_{FA}r_X + \beta_{FA}X$	$r_X = \left[\frac{\mu_m S}{(S + K_S + (S^2/K_I))} \times \left(1 - \frac{P}{P_{CRIT}}\right)^i \right] X,$
$r_{LA} = \alpha_{LA}r_X + \beta_{LA}X$	$-r_S = \frac{1}{Y_X}r_X + \frac{1}{Y_{SA}}r_{SA} + \frac{1}{Y_{AA}}r_{AA} + \frac{1}{Y_{FA}}r_{FA} + \frac{1}{Y_{LA}}r_{LA} + m_S X$
μ_m (h ⁻¹) 1.324	S substrate concentration (g L ⁻¹)
m_s (h ⁻¹) 0.061	X biomass concentration (g L ⁻¹)
i (dimensionless) 1.301	P product concentration (g L ⁻¹)
Y_{AA} (g g ⁻¹) 0.999	
Y_{FA} (g g ⁻¹) 1.532	
Y_{LA} (g g ⁻¹) 0.999	
Y_{SA} (g g ⁻¹) 1.310	
Y_X (g g ⁻¹) 0.765	
K_d (h ⁻¹) 0.010	
K_S (g L ⁻¹) 1.123	
K_I (g L ⁻¹) 88.35	
P_{CRIT} (g L ⁻¹) 17.23	
α_{AA} (g g ⁻¹) 0.626	
α_{FA} (g g ⁻¹) 0.665	
α_{LA} (g g ⁻¹) 0	
α_{SA} (g g ⁻¹) 1.619	
β_{AA} (h ⁻¹) 0.124	
β_{FA} (h ⁻¹) 0.105	
β_{LA} (h ⁻¹) 0.210	
β_{SA} (h ⁻¹) 0.355	

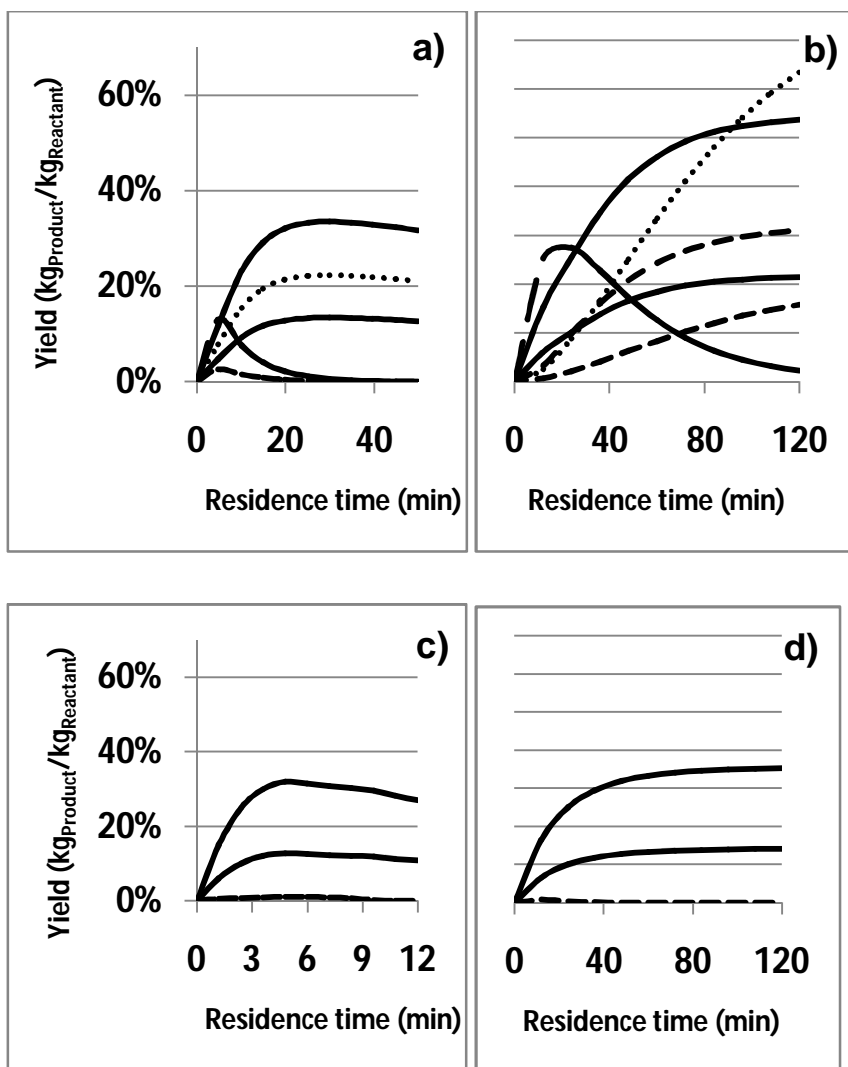


Figure A-1: Product yields as a function of residence time in PF reactors operating: a) a dilute acid hydrolysis with HCl; b) a dilute acid hydrolysis with H₂SO₄; c) levulinic acid production with HCl; d) a levulinic acid production with H₂SO₄. Product legend: — — —, glucose; - - - -, HMF; — — —, levulinic acid; •••••, xylose; - - - -, furfural; — •• —, formic acid.

Appendix

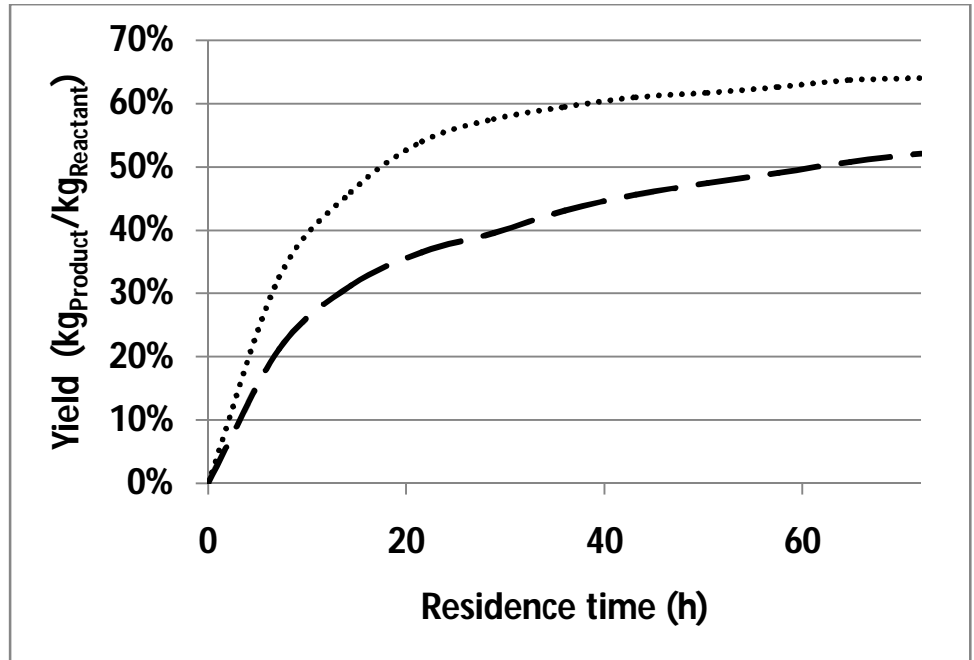


Figure A-2: Product yields in an enzymatic hydrolysis CST reactor.
Product legend: — — —, glucose; - - -, xylose;

Appendix

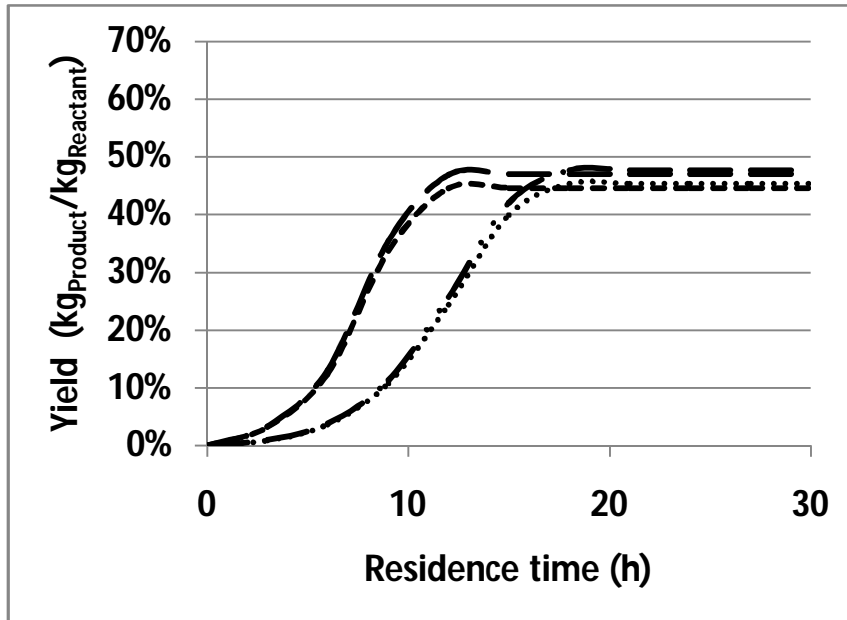


Figure A-3: Product yields in a batch fermenter for ethanol production. Product legend: — — —, ethanol from glucose; — •• —, ethanol from xylose; — — —, CO₂ from glucose; •••••, CO₂ from xylose.

Appendix

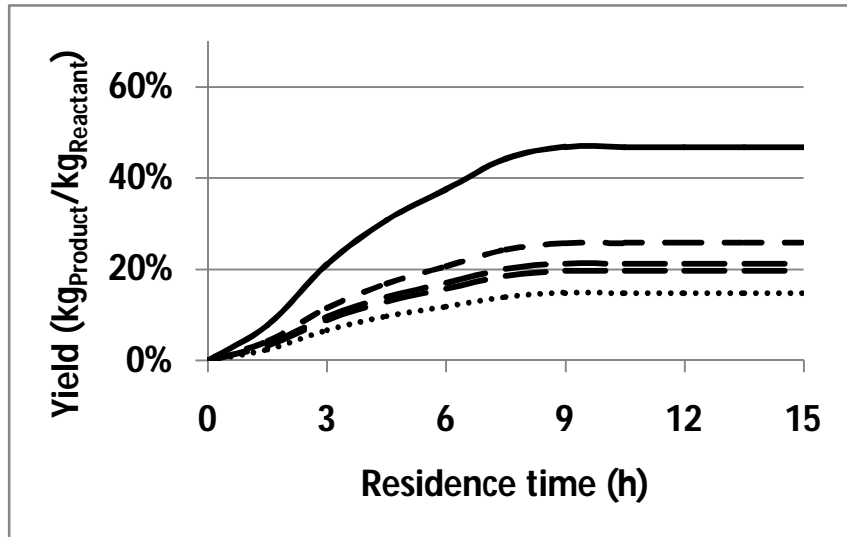


Figure A-4: Product yields in a batch fermenter for succinic acid production. Product legend: —, succinic acid from glucose; ---, succinic acid from xylose; -.-, acetic acid; •••••, lactic acid, -••-, formic acid.